Chapter 5
Preparation, optimization and characterization of nanoparticles

Preparation, optimization and characterization of nanoparticles

5.1 Introduction

Pulmonary drug and gene delivery are of considerable interest due to the variety of lung diseases that can be addressed by this approach. Diseases like cystic fibrosis, asthma, chronic obstructive pulmonary disease, lung cancer and more could be treated by high-level and long-term expression of the corresponding gene of interest (1-4).

Gene delivery in humans includes the transfer DNA into the nuclei of target cells. These carriers must be efficient in transfection, safe for human use, protect the DNA from degradation before arriving at the target cell and possibly hold targeting qualities for the specific delivery of the gene to the required cells or tissue. The two approaches have been used for gene delivery are viral and non-viral systems. Although very efficient in transfection, viral gene delivery systems still face safety issues for human use and due to their inherent immunogenicity, are problematic when repeated doses with the same carrier are required. Non-viral delivery systems are generally synthetic agents that are much safer, however, their transfection efficiency in-vivo is limited (5, 6).

Over the last decade, biodegradable polymeric nanoparticles (NPs) have gained increasing interest due to their many advantages in therapeutics delivery. These include protection of the therapeutics against degradation and deleterious biological interactions, improved bioavailability, solubility, retention time and intracellular penetration (7). Thus NPs are a promising for the delivery of therapeutics such as hydrophilic and hydrophobic drugs, vaccines, pDNA, proteins and biological macromolecules. Much attention have been given to the NPs based on poly(dl-lactide-co-glycolide) (PLGA) due to their biodegradable and bio compatible nature, small particle size, favorable safety profile, and ability to provide sustained release (8). They are approved for human use by the Food and Drug Administration and several PLGA-based formulations and are available in worldwide market (9). These nanoparticulate systems are rapidly endocytosed by cells followed by release of their therapeutic payload by both passive diffusion and slow matrix degradation (10, 11). These properties rendered PLGA NPs as potential polymer for sustained release therapeutics.

Lipophilic drugs can be encapsulated easily into hydrophobic PLGA matrix; however, encapsulation of low molecular weight hydrophilic drugs in PLGA matrix presents a great challenge (12). Barichello et al. reported low entrapment efficiency of hydrophilic drugs in

PLGA NPs when compared with lipophilic drugs (13). The major reason was the poor affinity between the hydrophilic drug and PLGA, which promotes drug diffusion into the external aqueous medium resulting in low entrapment efficiency (13). Thus, attempts have been made to enhance the entrapment of hydrophilic drugs into PLGA hydrophobic matrix by nanoprecipitation (14), single emulsification (15), W/O/W double emulsification (15, 16), and in the case of PLGA NPs, by use of reverse micelles (17). Nevertheless, the application of PLGA NPs for entrapping hydrophilic drugs remains limited.

The efficiency of such nanoparticulate delivery systems can also be enhanced by the attachment of functional ligands to the surface of NP. Potential ligands include, cationic moieties, small molecules, cell-penetrating peptides (CPPs), targeting peptides, antibodies or aptamers (18-20). Attachment of these moieties to NPs promote intracellular uptake, endosome disruption, and delivery of the therapeutics pay load to the nucleus. There have been numerous methods employed to tether ligands to the particle surface. One approach is direct covalent attachment to the functional groups on PLGA NPs (21). Another approach utilizes amphiphilic conjugates like avidin palmitate to secure biotinylated ligands to the NP surface (22, 23).This approach produces particles with enhanced uptake into cells, but reduced pDNA release and gene transfection, which is likely due to the surface modification occluding pDNA release (23). In a similar approach, lipid-conjugated poly ethylene glycol (PEG) is used as a multivalent linker of penetratin, a CPP, or folate (24). These methods can be combined to tune particle function and efficacy.

In present study we used Netilmicin sulfate (NS) a aminoglycoside antibiotics as a model drug to treat *P. aeruginosa* infections in cystic fibrosis due to their concentration-dependent antibacterial activity and long post-antibiotic effect (25, 26). Moreover they penetrate into the sputum of CF patients poorly and their activity is reduced due to binding with sputum components such as glycoproteins and cations (27, 28). Consequently high systemic doses of antibiotics are needed to achieve effective concentrations of the drug at the infection site (29). High doses can result in nephrotic and ototoxic effects, triggering permanent renal insufficiency and auditory nerve damage, with deafness, dizziness and unsteadiness, reducing the therapeutic window (30). While CFTR gene is used for the correction of the CFTR defect in cystic fibrosis. Though various viral and non-viral vectors have been used for gene delivery but long term, persistent correction of the

defect is achieved on repeated administration only. Thus there is need of such delivery system which enable prolong expression of CFTR gene (31).

Also, it was found that, *P. aeruginosa* could invade and replicate within cells. Internalized *P. aeruginosa* may play an important role in the pathogenesis of infection and that, by allowing greater internalization into epithelial cells, mutant CFTR results in an increased susceptibility of bronchial infection with this microbe [5]. By considering this, currently available CF therapies focus on attenuating disease progression and delaying the onset of irreversible damage in the respiratory system and other organs. However, better clinical outcomes of CF therapies is depend upon the concentration of the antibiotic at the site of infection as well as the extent of penetration of the drug into lung-lining fluids and bronchial mucosa and thus reach to the cell [3, 6].

However highly hydrophilic nature of these therapeutics make them challengeable to incorporate into hydrophobic PLGA matrix. Recently it has been demonstrated that nanoparticulate drug delivery is a promising approach to deliver antibiotics and gene (32-35). Previous reports have been shown that PLGA NPs are safe and efficient carriers for the delivery of plasmid DNA. Also in case of antibiotics, NPs can provide controlled antibiotic release, maintaining a constant plasma concentration above the minimum inhibitory concentration (MIC) for a prolonged duration. This maximizes the therapeutic effect while minimizing antibiotic resistance, and improves patient compliance (36). However, attempts to use NPs for the delivery of for these therapeutics have shown little drug entrapment in the PLGA hydrophobic core (16, 34, 35, 37, 38). Thus more efficient formulation techniques are needed.

The aim of the present study was to investigate the effects of important process and formulation parameters on the encapsulation of the highly water soluble therapeutic moiety in PLGA hydrophobic matrix to improve bioavailability and provide sustained release of drug& gene, and thus reduce the dosing frequency and side effects associated with the system.

5.2 Formulation and development of Netilmicin sulfate loaded NPs

5.2.1 Materials

Netilmicin Sulfate was provided as a gift sample by Samarth Life Sciences Pvt. Ltd., Mumbai, India. Poly (DL-lactic-co-glycolic acid) (PLGA, 50:50) (Mw=17 kDa) was received as a gift sample from PuracBiochem, Netherlands. Dextran sulfate sodium (DS, M_r=5,000) was purchased from Himedia, Mumbai, India. Pluronic® F68 (Poloxamer 188), sodium dodecyl sulfate, MTT, ethyl acetate, and sucrose were purchased from Sigma-Aldrich, India. DSPE-PEG

2000 was a generous gift from Lipoid, Switzerland. Amicon Ultra 15 filtration units were purchased from Millipore.

5.2.2 Development of drug-loaded NPs

NPs were prepared by a (w/o/w) double emulsion solvent evaporation method as previously described with some modifications (39). Briefly, water in oil emulsion was prepared by adding 0.15 to 0.35 mL of an internal aqueous phase (W_1) containing Netilmicin sulfate (NS) in double-distilled water to 0.5mL ethyl acetate (organic phase, O) containing PLGA polymer (10-30 mg/mL) by means of probe sonication (Sartorius Labsonic) at 60 amplitude for 90 sec on ice bath. Then primary (W_1/O) emulsion was added drop-wise to 2 mL 1.5% w/v of Pluronic® F68 solution (external aqueous phase, W_2), and further emulsified by sonication for another 30sec by mean of probe sonication at 60 amplitude (on ice bath) to form a W_1/O/W_2 double emulsion. The resulting double emulsion was further diluted with 5 mL of 1.5% (w/v) Pluronic® F68 solution and stirred magnetically for 4 h at room temperature to evaporate the ethyl acetate. The remaining organic solvent and free drug were removed by washing the NPs 3 times with double-deionized water using an Amicon Ultra-15 centrifuge filter (10-kDa) (Milli-pore), then re-suspended in double-distilled water to obtain the desired final concentration.

To examine the effect of helper hydrophilic polymer dextran sulfate (DS) on the EE of NS, NPs were prepared using the same procedure but with DS in the internal aqueous phase of the emulsion (with different charge-to-drug ratios). The blank PLGA NPs were also prepared using the same procedure without adding NS. Various factors affecting the entrapment of the drug in the polymer were evaluated by using the factorial design as explained bellow.

5.2.3 Experimental design

To elucidate the effect of different process conditions on the entrapment of NS in PLGA NPs and particle size of NPs, experiments were performed using a routine in the JMP 10.02 software (SAS, Cary, NC, USA). A preliminary screen was carried out to determine which process parameters have the most significant effects on the NPs. Results of the preliminary study suggested that five factors can influence the characteristics of the NPs. The chosen independent process parameters included: the volume ratio between the inner water phase and the oil phase (V_{w1}/V_O) (X1), the PLGA concentration (mg/mL) (C_{PLGA}) (X2), the surfactant concentration (%) ($C_{Pluoronic\ F68}$) (X3), the NS-to-DS charge ratio (DS:NS Charge ratio) (X4), and the sonication time (sec) of the primary emulsion ($t_{sonication}$) (X5).

Table 5.1: Actual and coded values of the formulation parameters

Variables	Factors	Unit	Levels		
			Low level (-1)	Central level (0)	High Level (+1)
X1	V_{w1}/V_O	ratio	0.3	0.5	0.7
X2	C_{PLGA}	mg/ml	10	20	30
X3	$C_{Pluoronic\ F68}$	%	0.5	1	1.5
X4	DS:NS Charge ratio	ratio	0.5	1.5	2.5
X5	$t_{sonication}$	sec	30	60	90

Table 5.2: Effects of the independent variables on two response variables: encapsulation efficiency and the particle size

Run	X1	X2	X3	X4	X5	% EE	Particle size (nm)
1	1	1	-1	1	-1	81.45 ± 1.5	140.79± 3.5
2	1	-1	1	-1	1	50.55 ± 2.3	127.44± 2.9
3	1	-1	-1	1	1	62.76± 1.7	134.55± 1.7
4	1	1	1	-1	-1	54.76± 1.1	137.36± 2.3
5	-1	-1	-1	-1	1	46.65± 1.4	121.43± 1.4
6	0	0	0	0	0	65.44± 2.5	133.23± 1.8
7	1	1	-1	-1	1	59.76± 3.1	137.94± 0.9
8	-1	1	-1	1	1	81.87± 1.0	138.33± 1.6
9	-1	1	1	1	-1	79.23± 1.3	134.43± 1.4
10	1	-1	-1	-1	-1	52.76± 0.7	130.27± 1.3
11	1	-1	1	1	-1	65.34± 2.9	125.34± 1.6
12	1	1	1	1	1	93.23± 2.7	140.83± 2.4
13	-1	1	-1	-1	-1	66.87± 1.6	139.55± 2.9
14	-1	-1	-1	1	-1	43.98± 0.7	133.33± 3.5
15	0	0	0	0	0	66.85± 2.6	132.43± 1.6
16	-1	-1	1	1	1	73.88± 1.5	126.43± 2.9
17	-1	1	1	-1	1	63.45± 1.3	133.94± 0.8
18	-1	-1	1	-1	-1	41.54± 1.5	130.45± 2.2

A 2^{5-1} fractional factorial design (FFD) was then created in SAS-JMP 10.02 and used to determine the effect of these process parameters on NP characteristics. Each process parameter was evaluated at the two levels; low and high levels assigned by (−1) and (+1), respectively as listed in Table 5.1. The levels were chosen in such a way that they provided a maximal design space and enabled feasible processing of the NPs. In addition, two center points were included to evaluate the curvature of the statistical model. The effects of the independent variables on two response variables: EE of the NS (Y1) and the particle size (Y2), are given in Table 5.2. The applied 2^{5-1} FFD is of resolution V, which indicated that the main effects are confounded with four-factor interactions, and two-factor interactions are confounded with three-factor interactions. The main effects and the two-factor interactions are comprised in the statistical model stated in Eq. (1):

$$Y = \beta_0 + \sum \beta_i X_i + \sum \beta_{ij} X_i X_j + \varepsilon \quad (1)$$

Where, Y is the measured response, β_0 is the arithmetic mean response, β_{ij} is the interaction term β_i, β_j are the estimated parameters, X is the coded value of the independent parameter and ε is the residual error. The effects of the main factors and the two-factor interactions were analyzed by analysis of variance. Statistical analysis was considered significant when the p values were lower than 0.05. The coefficients in Eq. (1) were calculated using coded values of the independent parameters using Eq. (2):

$$x_i = \frac{X_i - (X_{i,high} + X_{i,low})/2}{(X_{i,high} - X_{i,low})/2} \quad (2)$$

Where X_i is the coded value of the independent variable X_i, and $X_{i,\,high}$ and $X_{i,\,low}$ are the high and low levels of the independent variable X_i. Statistical models were accepted when there was no lack of fit, no correlation in the residual plots and the residuals were normally distributed.

Further, the obtained optimized formulation was PEGylated using DSPE-PEG. PEGylated NPs were prepared by using DSPE-PEG in secondary aqueous phase during formation of the secondary emulsion at a 3 % w/w lipid to-polymer ratio (40). Non-tethered DSPE-PEG was removed during wash steps. The blank PLGA NPs were also prepared as the same procedure without adding NS. Fluorescently-labelled NPs (Rhodamine B-loaded NPs) were prepared in a same way by replacing NS with Rhodamine B (1.425 mg/ mL in inner aqueous phase) in optimized formulation conditions for *in-vitro*/*in-vivo* deposition studies.

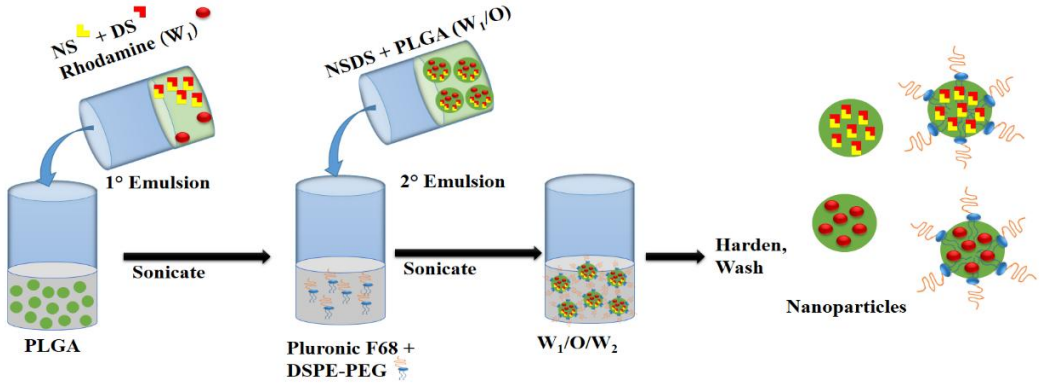

Figure 5.1: Nanoparticulate formulation with varying charge ratio of DS & NS and different concentrations of PLGA were formulated using a double emulsion/solvent evaporation technique. Particles were either encapsulated with NS or with Rhodamine B.

5.2.4 Nanoparticle characterization

5.2.4.1 Particle size

NPs size (diameter, nm) and polydispersity index were determined by differential light scattering using a Malvern Zetasizer Nano ZS (Malvern Instruments, UK). The NPs suspensions were diluted suitably with filtered double-distilled water to avoid multi-scattering phenomena and placed in a disposable sizing cuvette. The polydispersity index was also evaluated to investigate the narrowness of the particle size distribution. All the analyses were carried out in triplicate.

5.2.4.2 Zeta potential

Zeta (ζ) potential measurements of samples were made with a Malvern Zetasizer Nano ZS (Malvern Instruments, UK). Zeta potential was calculated by Smoluchowski's equation from the electrophoretic mobility. Measurements were taken after 10 fold dilution of the NPS suspension with filtered, double-distilled water in a disposable zeta cuvette. All the analyses were carried out in triplicate.

5.2.4.3 Determination of encapsulation efficiency (EE)

Encapsulation efficiency of NS in NPs was determined by both direct and indirect methods. In case of indirect method, to determine the drug incorporation efficiency, NS loaded NPs were centrifuge filtered in a 10-kDa Amicon Ultra-15 centrifuge filter for 4000 g at 4 °C to remove free drug. Filtrate was collected and analyzed for NS by using Shimadzu spectrophotometer (UV

1800, Shimadzu, Japan) after derivatization with OPA at 60°C for 15 min at 335 nm as discussed in chapter 4 to determine the amount of unentrapped NS.

For the determination of loaded NS in NPs, 200 µl NP suspension was dissolved in acetonitrile/phosphate buffer (2:1, v/v) by sonication for 30 min. The obtained solution was then centrifuged, and an aliquot of was analyzed for NS after suitable dilution by using Shimadzu spectrophotometer (UV 1800, Shimadzu, Japan) at 335 nm after derivatization with OPA at 60°C for 15 min. The EE was calculated from following equation. All the analyses were carried out in triplicate.

$$\text{Encalsulation efficiency (\%)} = \frac{\text{Amount of drug loaded in NP}}{\text{Initial amount of drug used in formulation}} \times 100$$

Total amount of rhodamine B entrapped in PLGA NPs was determined after dissolving NPs in Chloroform: Methanol (1:1). The amount of rhodamine B in resulting solution was then determined by fluorimetry using a Spectrofluorometer (RF-5301PC, Shimadzu) at excitation and emission wavelengths of 560 and 595 nm, respectively as mentioned in previous chapter.

5.2.4.4 Transmission electron microscopy (TEM)

The TEM study was conducted to examine the morphology of NPs. The observations were conducted by using a transmission electron microscope (Hitachi H-7500, 120 kV). A suspension of NPs was coated on a copper grid, air dried and stained with 2% (w/v) phospho-tungstic acid. Air-dried samples of NPs were then examined directly under the transmission electronic microscope.

5.2.4.5 Differential scanning calorimetry (DSC)

DSC analysis was carried out to evaluate possible interactions between the NS and the excipients used, and to evaluate the nature of NS within the NPs. DSC analysis of samples (NS, PLGA, blank NPs, and NS loaded NPs, NS loaded PEGylated NPs) was performed using a TA-60WS Thermal Analyzer (Shimadzu, Japan). The samples were sealed hermetically into an aluminum pan and heating curves were recorded at a scan rate of 10 °C/min from 20 to 350°C in an inert atmosphere, which was maintained by purging dry nitrogen at a flow rate of 40 mL/min.

5.2.4.6 FTIR studies

FTIR spectroscopy was used to characterize functional groups. A FTIR Spectrophotometer (BRUKER ALPHA FT-IR Spectrometer, Germany) was used to obtain the FTIR spectrogram of NS, PLGA, physical mixture, NS loaded NPs, NS loaded PEGylated NPs. The samples were

mixed with potassium bromide (1:100 ratio) and compressed into a pellet. Then pellet was scanned under the FTIR spectroscope.

5.2.4.7 In vitro drug release studies

Drug release from the NPs was studied in phosphate buffer pH 7.4 and simultaneous lung fluid (SLF). SLF was prepared carefully following the preparation instructions dictated by Moss (41). Briefly, 20 mg of NPs were dispersed in 1mL release medium and incubated at 37^{o}C in a shaking incubator. At specific time intervals, samples were centrifuged at 13,000 rpm for 5 min at 4°C to isolate NPs; 0.2 mL of medium were withdrawn and replaced by the same amount of fresh medium. The withdrawn medium was analyzed for NS content by UV spectrophotometric analysis after derivatization with OPA as described above. Experiments were performed in triplicate.

5.2.4.8Antibacterial susceptibility testing

The minimum inhibitory concentration (MIC) is the lowest antibiotic concentration that inhibits a visible planktonic bacterial growth. The MIC of free NS and NS-loaded NPs were determined by the broth microdilution method in 96-well microplates (42). An optical density measurement at 600nm was used to examine the visible bacterial growth in which OD 600<0.1 indicated zero bacterial growth. Briefly, *P. aeruginosa* was grown in Trypticase soy broth (TSB) at 37°C to obtain an optical density (OD) of ~1 at 600nm (~1×10^{8} CFU/mL). The bacterial cell suspension was then further diluted by 100-fold. Free NS and NS-loaded NPs were serially diluted in 100µL TSB in such way that a final NS concentration ranging from 50 µg/mL to 0.2 µg/mL (calculated from % drug loading) will be obtain in a total volume of 200µL. Then, 100µl of diluted *P. aeruginosa* inoculum were added to each well containing free NS and NS-loaded NPs in 100µL TSB and the samples were incubated at 37°C for 12h. The MIC endpoints were determined by reading the OD of the plate wells at 600 nm and confirmed by visual inspection. The lowest concentration that yielded OD≤0.1 was determined as the MIC.

Minimum bactericidal concentration (MBC) is the drug concentration where no visible growth appears on agar plates. NS and NS-loaded NPs treated bacterial cultures showing growth or no growth in the MIC tests were used for this test. Bacterial cultures that were used for the MIC test were inoculated onto the agar and incubated at 37°C for 12h. Microbial growth was assessed by counting colonies. The minimal concentration of the NS and NS-loaded NPs that abolished colony growth was determined as the MBC.

Control NPs were evaluated for possible antibacterial activity against *P. aeruginosa*. Bacteria were cultivated in a 96 well plate following the same procedures used above to determine the MIC/MBC. A bacterial suspension were exposed to the blank NPs (1 to 5% w/v) and incubated overnight at 37°C, then the number of Colony-Forming Units (CFU) was determined using the agar plate method.

To mimic *in-vivo* conditions, human bronchial epithelial cells (CFBE41o-) were incubated with free NS or NS-loaded NPs, and antimicrobial activity was tested every 24h for 5 days. The cells were seeded in 12 mm Transwell® inserts (250,000cells/well, 12wells, 0.4µm-pore Polyester membrane, Costar 3460)**.** Culture medium was removed from apical surface on the 3rd day after plating and particles were added apically in 500 µL of EMEM without serum. 50 µL apical medium was then collected every 24h for 5 days. Samples were stored at 4°C. Standard inocula of *P. aeruginosa* were incubated overnight with shaking at 37°C in 2mL of TSB. Bacteria were diluted to 0.5x10^6 cells/50 µL and added to the 50 µL of collected samples and incubated overnight at 37°C. The bacteria-sample mixture was then diluted and plated onto agar plates and CFU were counted. To evaluate the effect of NP on cell integrity TEER was recorded with help of EVOM chopstick electrodes (World Precision Instruments; New Haven, USA).

5.2.4.9 Mucus penetration study

The penetration of fluorescent NPs trough artificial mucus was evaluated by the method suggested by Yang et al with some modification (43). Briefly, 50 mL of artificial mucus was prepared adding 500 mg of DNA, 250 µL of sterile egg yolk emulsion, 250 mg of mucin, 0.295 mg DTPA, 250 mg NaCl, 110 mg KCl, 1 mL of RPMI to 50 mL of water. The pH was adjusted to 7 pH using a sterile NaOH solution.

1 mL of 10% (w/v) gelatin solution was placed in each well of a 24-well plate, hardened at room temperature and stored at 4 °C until use. 1 mL of artificial mucus was placed on the hardened gelatin gel. Then, 500 µL of a water dispersion of Rhodamine-loaded NPs (1mg/mL) were placed on the artificial mucus layer and maintained at closed humid chamber, emulating the humid environment of the airways (44). After 8, 12, 24 h, the NP-containing artificial mucus was withdrawn, gelatin plates washed three times with water and subsequently melted at 60 °C. The Rhodamine B amount in gelatin was evaluated using a microplate reader (Synergy™ MxMonochromator-Based Multi-Mode Microplate Reader; BioTek Instruments, Winooski, VT, USA) at excitation and emission wavelengths of 545 and 577 nm, respectively. Results are

reported as percentage of Rhodamine B penetrated through artificial mucus (amount of Rhodamine B in gelatin plates/total amount of Rhodamine B in NPs × 100) ± SD.

5.2.4.10 Cell Culture

CFBE41o- cells were kindly provided by Dr. Dieter Gruenert (California Pacific Medical Center Research Institute and Department of Laboratory Medicine, University of California, San Francisco CA) and were cultured in Eagle's minimum essential medium with Earls salt (EMEM) (Wisent, St-Bruno, QC, Canada) containing 10% fetal bovine serum (FBS), 1% penicillin/streptomycin, 2mM L-Glutamine. Cells were maintained in a humidified incubator with 5% CO_2 at 37°C ± 2°C.

5.2.4.11 Safety studies

5.2.4.11.1 Cell viability

The viability of CFBE41o- cells after exposure to NPs was evaluated using MTT (3-(4,5-dimethylthiazol-2-yl)-2,5-diphenyltetrazolium bromide). Briefly, CFBE41o- cells were seeded into 96 well plates (Falcon 3072) at density 4×10^4 cells/well in EMEM containing 10 % FBS and 1% antibiotic and incubated at 37°C, 5% CO_2 for 24h. After 24h, the cells were exposed to different concentration of NPs (0.5mg/mL to 5mg/mL) in EMEM for 24h. Cells treated with EMEM and 0.1% sodium dodecyl sulfate (SDS) were used as negative and positive controls, respectively. After 24h treatment, cells were rinsed thoroughly with phosphate buffer saline (PBS), treated with 100µL MTT solution, and incubated for 4h. After 4h of incubation, the medium with MTT was replaced with a solubilization solution (100µL DMSO) to dissolve the formazan crystals formed after internalization of MTT by live cells. The resulting colored solution was analyzed using a microplate reader (Synergy Mix, Biotek) at 570 nm. Cell viability was expressed as the percentage of absorbance of test samples relative to that of cells treated with EMEM (n=3).

5.2.4.11.2 Transepithelial electrical resistance (TEER) analysis

Transepithelial electrical resistance (TEER) analysis was performed on CFBE41o- cells to determine the integrity of the cell monolayer upon exposure to NPs suspension. The cells were seeded onto Transwell® clear permeable filter inserts as described above. 500 µL of medium was added to the apical side of the cell monolayer and 1,500 µL were added to the basolateral side. TEER across the insert was measured using an ohm meter using chopstick electrodes. TEER was measured from days 1 to 3 to ensure that the monolayer was confluent, and this was confirmed

by light microscopy. The resistance of an insert lacking cells was subtracted from all measurements to correct for the resistance of the Transwell. On day 3, the apical medium was replaced with fresh medium containing the NPs (1 mg/mL) and TEER was measured immediately and again after 1, 2, 3, 4 and 5 days.

5.2.4.12 Cell uptake study

CFBE41o- cells ($1x10^6$ cells) were seeded in FluoroDish FD35-100 (Tissue culture dish with cover glass bottom, Dish: 0.35mm, glass: 0.23 mm) EMEM with 10% FBS, 1% 20 mM glutamine and 1% penicillin/ streptomycin and incubated at 37 °C, 5% CO_2 for 24 hour. After 24 hour, the EMEM was replaced and cells were washed three times with PBS. Then cells were treated with rhodamine B NPs and incubated for 24 h at 37°C. After 24 hour incubation, cells were washed three times with PBS. The nuclei were finally labeled with a Hoechst dye for 10 min at room temperature and observed under confocal microscope (Carl Zeiss, Confocol LSM 510 META, ×63, NA 1.4, oil immersion) at excitation and emission wavelengths of 570 and 595 nm, respectively.

The uptake amount of rhodamine B loaded NPs were further quantified for more exact comparison. Briefly, CFBE41o- cells were seeded into 96 well plates (Falcon 3072) at density 4×10^4 cells/well in EMEM containing 10 % FBS and 1% antibiotic and incubated at 37°C, 5% CO_2 for 24 h. After 24 h, the cells were treated with rhodamine B NPs and incubated for 24 h at 37◦C.After 24 h the incubation was terminated by the addition of ice-cold PBS (100 µL), and then PBS was removed. This process was repeated twice to remove NPs that were not taken up by the cells. Then cell membrane was then lysed with 50 µL of 0.5% triton X-100 solution in 0.2 N NaOH, and 20 µl of the cell lysate from each well was used to determine the total cell protein content using the Pierce® BCA protein assay kit (Thermo Scientific BioRad Protein Assay) with bovine serum albumin as protein standard. (The amount of protein in the supernatant was determined, after a suitable dilution). The remaining cell lysates were used for the analysis of rhodamine B. Rhodamine B from the NPs was extracted with 150 µL of chloroform: methanol (1:1) at 37 °C for 4 h with shaking. The concentration of rhodamine B was determined using a microplate reader (Synergy™ MxMonochromator-Based Multi-Mode Microplate Reader; BioTek Instruments, Winooski, VT, USA) at excitation and emission wavelengths of 485 and 535 nm, respectively. The uptake of NPs was calculated from the standard curve and expressed as the amount of NPs (µg) taken up per mg cell protein.

5.2.4.13 Stability study

To determine in vitro stability, the NPs were suspended in saline (0.9% sodium chloride solution), 10% fetal bovine serum and simulated lung fluid (prepared as described by Moss et al. and incubated at 37 ^{o}C for 48 h. Particle size was measured every 1, 2, 3, 6, 12, 24, 48 h. DLS was used to measure particle size at each interval.

5.2.4.14 Statistical analysis

The experiments were performed in triplicate, unless otherwise stated. All data were expressed as mean ± standard deviation. The statistical significance of the results was determined using a Student's t-test where $P<0.05$ as minimum level of significance.

5.3 Formulation and development of plasmid loaded NPs

5.3.1 Materials

Poly (DL-lactic-co-glycolic acid) (PLGA, 50:50) (Mw=17 kDa) was a generous gift from Purac Biochem, Netherlands. Polyethylenimine (25 kD), Pluronic® F68 (Poloxamer 188), and chloroform were purchased from Sigma-Aldrich, India. Tris – HCl, EDTA DNase-free RNase-A were purchased from Himedia, Mumbai, India. DSPE-PEG 2000 was a generous gift from Lipoid, Switzerland. Amicon Ultra 15 filtration units were purchased from Millipore. piRIS2-EGFP CFTR plasmid (10 kb) & *p*CDNA-3 LUC-WT plasmid (7.4 kb) were obtained as gift samples from Prof. John Hanrahan, Mcgill University. piRIS2-EGFP CFTR plasmid & *p*CDNA-3 LUC-WT plasmid were isolated and purified as discussed earlier.

5.3.2 Development of pDNA loaded NPs

The NPs were produced by the double emulsion solvent evaporation method as reported previously (23), but with a few minor changes. In brief, 250 µg plasmid DNA (*p*CDNA-3 LUC-WT Luciferase plasmid or piRIS2-EGFP CFTR plasmid) in 250 µL Tris EDTA buffer (10 mMTris-Cl, 1 mM EDTA, pH 8) was added to 500 µL chloroform (oil phase) containing varying w/w ratio of PEI to PLGA (0- 12.5% w/w). The total concentration of PLGA was kept constant at 100 mg/ml. The mixture was sonicated on ice using probe sonicator (Sartorius Labsonic) at 20 amplitude for 30 sec to obtain water in oil (w/o) emulsion. Then this primary emulsion was added to 1 mL 1.5 % (w/v) Pluronic F-68 solution and again sonicated on ice using probe sonicator at 20 amplitude for 30 sec to obtain water-in-oil-in-water ($w_1/o/w_2$) double emulsion. This double emulsion subsequently diluted with 5 mL of 1.5 % (w/v) PF-68 solution and stirring overnight to evaporate chloroform. The obtained NPs were centrifuge filtered in a 30-kDa

Amicon Ultra-15 centrifuge filter for 30 minutes at 4000 RPM at 4 °C to remove surfactant and free PEI. Centrifugation and re-dispersion of the NPs pellet was repeated three times to ensure removal of surfactant and free PEI before further characterization.

Large T Antigen was added along with pCDNA-3 LUC-WT Luciferase plasmid (1:10 ratio) as it requires for the expression of plasmid. Large T antigen induces replication of plasmids bearing the SV40 origin of replication (SV40 ori) within mammalian cells. The fluorescent NPs were prepared by adding 6-coumarin (2 mg/mL) in polymer solution. PEGylation of particles was done by using DSPE-PEG at 3 % w/w to polymer concentration.

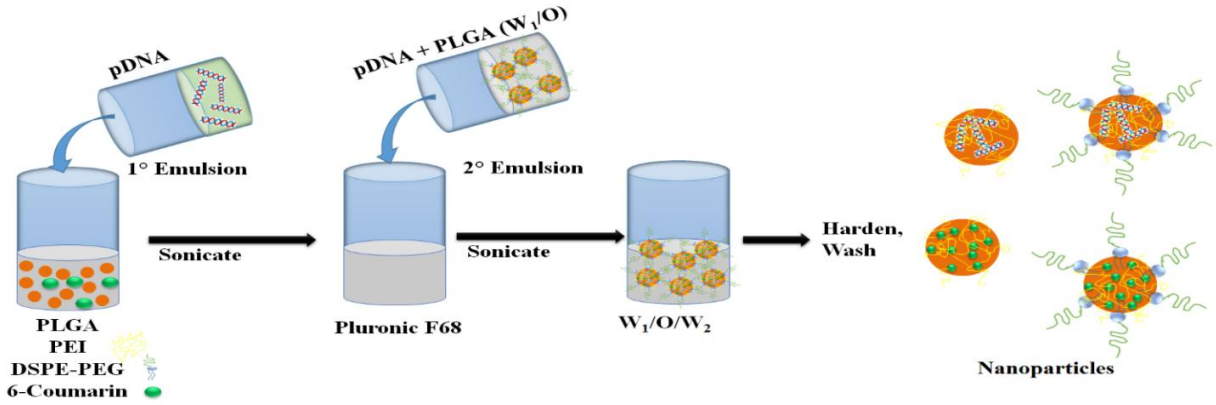

Figure 5.2: Nanoparticulate formulation with varying w/w ratio of PEI to PLGA were formulated using a double emulsion/solvent evaporation technique encapsulated with pDNA or 6-coumarin.

5.3.3 Nanoparticle characterization

5.3.3.1 Determination of encapsulation efficiency

The pDNA was extracted from the NPs matrix by dissolving a known fraction of the NPs suspension, corresponding to approximately 1 mg of NPs in 500µl chloroform followed by the addition of 500µl TE buffer. The mixture was rotated end-over-end for 90 min to facilitate the extraction of DNA from the organic phase and into the aqueous phase. After incubation, the two phases were separated by centrifugation at 13,000 rpm for 15 min at 4 °C. The aqueous supernatant was collected and DNA concentration in the supernatant was measured by the QuantiFluor™ dsDNA System (Promega). Each sample was assayed in triplicate. The encapsulation efficiency was defined as the amount of DNA recovered from the NPs relative to the initial amount of DNA used.

$$\text{Encapsulation efficiency (\%)} = \frac{\text{Amount of pDNA loaded in NPs}}{\text{Initial amount of pDNA used in formulation}} \times 100$$

Total amount of 6-coumarinentrapped in NPs was determined after dissolving NPs in Chloroform: Methanol (1:1). The amount of 6-Coumarin in resulting solution was then determined by fluorimetry using a Spectrofluorometer (RF-5301PC, Shimadzu) at excitation and emission wavelengths of 430 and 485 nm, respectively as mentioned in previous chapter.

5.3.3.2 Particle size

NPs size (diameter, nm) and polydispersity index were determined by differential light scattering using a Malvern Zetasizer Nano ZS (Malvern Instruments, UK). The NPs suspensions were diluted suitably with filtered double-distilled water to avoid multi-scattering phenomena and placed in a disposable sizing cuvette. The polydispersity index was also evaluated to investigate the narrowness of the particle size distribution. All the analyses were carried out in triplicate.

5.3.3.3 Zeta potential

Zeta (ζ) potential measurements of samples were made with a Malvern Zetasizer Nano ZS (Malvern Instruments, UK). Zeta potential was calculated by Smoluchowski's equation from the electrophoretic mobility. Measurements were taken after 10 fold dilution of the NPS suspension with filtered, double-distilled water in a disposable zeta cuvette. All the analyses were carried out in triplicate.

5.3.3.4 Transmission electron microscopy

The TEM study was conducted to examine the morphology of NPs. The observations were conducted by using a transmission electron microscope (Hitachi H-7500, 120 kV). A suspension of NPs was coated on a copper grid, air dried and stained with 2% (w/v) phospho-tungstic acid. Air-dried samples of NPs were then examined directly under the transmission electronic microscope.

5.3.3.5 FTIR studies

FTIR spectroscopy was used to characterize functional groups. A FTIR Spectrophotometer (BRUKER ALPHA FT-IR Spectrometer, Germany) was used to obtain the FTIR spectrogram of PEI, PLGA NPs, PLGA PEI NPs. The samples were mixed with potassium bromide (1:100 ratio) and compressed into a pellet. Then pellet was scanned under the FTIR spectroscope.

5.3.3.6 Structural integrity of the encapsulated pDNA

The integrity of the encapsulated plasmid was analyzed by agarose gel electrophoresis. For this, 1 mg of NPs was dissolved in 1 mL of chloroform and diluted in 250 µL TE buffer (10 mM Tris-Cl, 1 mM EDTA, pH 8). The samples were agitated in shaking incubator at 37ºC for 3 h at room temperature. The extracted DNA was collected by centrifugation (13000 rpm, 15 min) and stored at -20 ºC. Samples of control and recovered pDNA were diluted 5 times with loading dye and electrophoresis was carried out with 0.8% agarose gel containing ethidium bromide (EtBr) at a constant voltage of 150 V for 20 min in TBE buffer (1M Tris–base, 0.01M sodium EDTA, 0.9 M boric acid). The gel was visualized under UV illumination using a camera Gel doc 2000, Bio-Rad, USA.

5.3.3.7 In vitro release study

To investigate the in vitro pDNA release, 20 mg of PLGA NP , PEI-PLGA NP, PEG PEI-PLGA NPs (n=6) were incubated in 1 ml of PBS buffer (pH 7.4), in a microcentrifuged tube in shaking incubator at 37ºC. After incubation for 24 h, half of the samples (n=3) were transferred to acetate buffer (pH 5.0) to simulate acidification of the endolysosome of the cell. At various time point's particles were pelleted (13,000 rpm, 15 min) and the 100 µL supernatant was removed and stored for analysis. An equal volume of fresh buffer was added to replace the supernatant and particles were resuspended and returned to the shaker. This process continued for 10 days. At the end of 10 days, the remaining particle pellets were added to Chloroform and the DNA still remaining in the particles was extracted into TE buffer to determine total loading. Samples were analyzed for DNA content using a QuantiFluor™ dsDNA System (Promega).

5.3.3.8 Cell Culture

CFBE41o- cells were kindly provided by Dr. Dieter Gruenert (California Pacific Medical Center Research Institute and Department of Laboratory Medicine, University of California, San Francisco CA) and were cultured in Eagle's minimum essential medium with Earls salt (EMEM) (Wisent, St-Bruno, QC, Canada) containing 10% fetal bovine serum (FBS), 1% penicillin/streptomycin, 2mM L-Glutamine. Cells were maintained in a humidified incubator with 5% CO_2 at 37°C.

5.3.3.9 In-vitro bioactivity

5.3.3.9.1 Luciferase expression

The CFBE 41o- cells were seeded in 96 well plate (Falcon, Cell Growth Area: 0.16 cm²) at a density of 20000 cells / well in 100 µl of MEM with Earle's salts and L-glutamine, and containing 10 % (v/v) FBS, 1 % L-glutamine 20mM and 1% Penicillin–Streptomycin. After 24 h, the culture medium was replaced with fresh MEM medium (serum free) containing NPs having the quantity of pDNA (LUC WT) constant (500 ng). After 24 h of incubation of the NPs were removed and the cells were washed with PBS pH 7.4 and were replaced with complete media. In all the experiments, naked pDNA transfected cells were used as negative control and the Lipofectamine plus (Invitrogen) transfected cells were used as a positive control. After 48, 96,120h of the post transfection luciferase detection was performed on the transfected cells using a chemiluminescent assay (Promega, USA). Tests were carried out as described by the manufacturer. After two rinses in PBS 1X, cells were lysed with 40 µL lysis buffer (Promega) for 10 min. Then lysate were centrifuged at 13000 rpm for 15 min at 4 °C. The 20 µL supernatant was then added into the luminometer tubes containing 100 µL of the Luciferase Assay Reagent. The tube was vortexed and Luciferase activity in the supernatant was quantified in relative light units (RLU) using TD-20/20 Luminometer, version 2, Turners designs, CA. Results were normalized to total cell protein using Pierce® BCA protein assay kit (Thermo Scientific BioRad Protein Assay) with bovine serum albumin as protein standard. (The amount of protein in the supernatant was determined, after a suitable dilution).

5.3.3.9.2 Western blot analysis

The CFBE 41o- cells were seeded in 6 well plate (Falcon, Cell Growth Area: 0.16 cm²) at a density of 250000 cells / well in 1000 µl of MEM with Earle's salts and L-glutamine, and containing 10 % (v/v) FBS, 1 % L-glutamine 20mM and 1% Penicillin–Streptomycin. After 24 h, the culture medium was replaced with fresh EMEM medium (serum free) containing NPs containing the pDNA (piRIS2-EGFP CFTR). After 24 h of incubation of the NPs were removed and the cells were washed with PBS pH 7.4 and were replaced with complete media. After 144 hr cells were observed under confocal microscope for GFP expression. Cells were washed with cold PBS two times and cells were scrapped with scrapper. Then cells were lysed by using cold Radio-Immunoprecipitation Assay (RIPA) Buffer (1% Triton X 100, 0.1% sodium dodecyl sulfate (SDS), 150 nM NaCl, 0.1 % Deoxycholic sodium, 10mM TrisHCl, 2% protease inhibitor

cocktail), homogenized well and stored at for 30 min. Cells were then centrifuged at 13000 rpm for 15 min at 4 °C. The supernatants were collected as lysate samples. The protein content in cell lysate was measured by using Pierce BCA Protein Assay Kit and the samples were stored at –80°Cuntil needed. In each well of the sodium dodecylsulfate-polyacrylamide gel electrophoresis (SDS-PAGE, 8%) gel, 50 µg of total protein was loaded. The samples were separated electrophoretically by 8%SDS-PAGE at 100 V for 2 hr. After electrophoresis, the proteins were transferred to nitrocellulose membrane (BioRad Laboratories, Hercules, CA, USA) at 90 V for 1 h. The membrane was blocked with 7% milk in TTBS (1.05g milk + 15 mL TTBS (0.1% tween in Tris buffer saline pH 7.5) at room temperature for 40 min. Discard the blocking solution and quickly rinse membrane 3 time with TTBS and 1 time TBS. Then the membrane was incubated overnight at 4 °C with primary anti-CFTR 23C5 antibody (mouse) (1:100 dilution in TBS with 0.5 % BSA and 0.01 % NaN_3). The blot was quickly rinsed 3 time with TTBS and 1 time TBS for 15 min each at room temperature with agitation. Immunoreactivity was detected with anti-sodium pump secondary antibody (mouse) (1:200dilution in TBS with 0.5 % milk) using an enhanced chemiluminescence (ECL) detection kit (Amersham Biosciences).The relative intensity of each CFTR glycol form (band B or C) was estimated by densitometry using Image J software and reported as a percentage of wild-type CFTR after normalization to the amount of sodium potassium ATPase in the same lane.

5.3.3.10 Safety studies

5.3.3.10.1 Cell viability

The viability of CFBE41o- cells after exposure to NPs was evaluated using MTT (3-(4,5-dimethylthiazol-2-yl)-2,5-diphenyltetrazolium bromide). Briefly, CFBE41o- cells were seeded into 96 well plates (Falcon 3072) at density 4×10^4 cells/well in EMEM containing 10 % FBS and 1% antibiotic and incubated at 37°C, 5% CO_2 for 24 h. After 24 h, the cells were exposed to different concentration of NPs (0.5mg/mL to 5mg/mL) in EMEM for 24 h. Cells treated with EMEM and 0.1% sodium dodecyl sulfate (SDS) were used as negative and positive controls, respectively. After 24 h treatment, cells were rinsed thoroughly with phosphate buffer saline (PBS), treated with 100 µL MTT solution, and incubated for 4 h. After 4 h of incubation, the medium with MTT was replaced with a solubilization solution (100 µL DMSO) to dissolve the formazan crystals formed after internalization of MTT by live cells. The resulting colored solution was analyzed using a microplate reader (Synergy Mix, Biotek) at 570 nm. Cell viability

was expressed as the percentage of absorbance of test samples relative to that of cells treated with EMEM (n=3).

5.3.3.10.2 TEER analysis

Transepithelial electrical resistance (TEER) analysis was performed on CFBE41o- cells to determine the integrity of the cell monolayer upon exposure to NPs suspension. The cells were seeded onto Transwell® clear permeable filter inserts as described above. 500µL of medium was added to the apical side of the cell monolayer and 1,500 µL were added to the basolateral side. TEER across the insert was measured using an ohm meter using chopstick electrodes. TEER was measured from days 1 to 3 to ensure that the monolayer was confluent, and this was confirmed by light microscopy. The resistance of an insert lacking cells was subtracted from all measurements to correct for the resistance of the Transwell. On day 3, the apical medium was replaced with fresh medium containing the NPs (2mg/mL) and TEER was measured immediately and again after 1, 2, 3, 4 and 5 days.

5.3.3.11 Cell uptake study

CFBE41o- cells ($1x10^6$ cells) were seeded in FluoroDish FD35-100 (Tissue culture dish with cover glass bottom, Dish: 0.35mm, glass: 0.23 mm) EMEM with 10% FBS, 1% 20 mM glutamine and 1% penicillin/ streptomycin and incubated at 37 °C, 5% CO_2 for 24 hour. After 24 hour, the EMEM was replaced and cells were washed three times with PBS. Then cells were treated 6-coumarin NPs and incubated for 24 h at 37◦C. After 24 hour incubation, cells were washed three times with PBS. The nuclei were finally labeled with a Hoechst dye and cell membrane were labeled with FM® 4-64 membrane stain for 10 min at room temperature and observed under confocal microscope (Carl Zeiss, Confocol LSM 510 META, ×63, NA 1.4, oil immersion).

The uptake amount of 6-coumarinloaded NPs were further quantified for more exact comparison. Briefly, CFBE41o- cells were seeded into 96 well plates (Falcon 3072) at density $4×10^4$ cells/well in EMEM containing 10 % FBS and 1% antibiotic and incubated at 37°C, 5% CO_2 for 24 h. After 24 h, the cells were treated with 6-coumarin NPs (100µg/mL) and incubated for 24 h at 37◦C. After 24 h the incubation was terminated by the addition of ice-cold PBS (100 µL), and then PBS was removed. This process was repeated twice to remove NPs that were not taken up by the cells. Then cell membrane was lysed with 50 µL of 0.5% triton X-100 solution in 0.2 N NaOH, and 20 µl of the cell lysate from each well was used to determine the total cell protein

content using the Pierce® BCA protein assay kit (Thermo Scientific BioRad Protein Assay) with bovine serum albumin as protein standard. (The amount of protein in the supernatant was determined, after a suitable dilution). The remaining cell lysates were used for the analysis of 6-coumarin. 6-coumarin from the NPs was extracted with 150 µL of chloroform: methanol (1:1) at 37 °C for 4 h with shaking. The concentration of coumarin-6 was determined using a microplate reader (Synergy™ MxMonochromator-Based Multi-Mode Microplate Reader; BioTek Instruments, Winooski, VT, USA) at excitation and emission wavelengths of 430 and 485 nm, respectively. The uptake of NPs was calculated from the standard curve and expressed as the amount of NPs (µg) taken up per mg cell protein.

5.3.3.12 DNAse protection assay

To test whether NPs can protect encapsulated plasmid DNA from nucleases digestion, 2 µg pDNA and NPs containing 10 µg pDNA were suspended in 1 mL of TE (10 mM Tris–HCl, 1 mM EDTA, pH 7.5) containing 1 U of DNAse I per microgram of DNA. The DNAse I stock solution prepared by dissolving the purified enzyme (2000 units ~ 0.5 mg of enzyme) in equal ratio of 10 mM Tris-HCl (pH 7.5) containing 50 mM Sodium Chloride and 1 mM Magnesium Chloride and Glycerol in the concentration of 1 mg/ml. The stock was stored at -20 ^{o}C in aliquots until used. The working solution was prepared in the strength of 1 µg/µl by diluting with the dilution buffer of 10 mM Tris HCl (pH 7.5) containing 50 mM sodium chloride and 1 mM magnesium chloride. The suspension was incubated for 4 h at 37 ^{o}C in a water bath. The reaction was stopped by addition of 20 µL of 0.5 M EDTA solution. The NPs were separated by centrifugation at 13000 rpm for 15 min. Then, NPs were dissolved in 500 µL of chloroform and diluted in 125 µL TE buffer. The extracted DNA was collected by centrifugation (13000 rpm, 15 min) and analyzed by agarose gel electrophoresis.

5.3.3.13 Mucus penetration study

The penetration of fluorescent NPs through artificial mucus was evaluated by the method suggested by Yang et al with some modification (43). Briefly, 50 mL of artificial mucus was prepared adding 500 mg of DNA, 250 µL of sterile egg yolk emulsion, 250 mg of mucin, 0.295 mg DTPA, 250 mg NaCl, 110 mg KCl, 1 mL of RPMI to 50 mL of water. The adjust pH to 7 pH using a sterile NaOH solution. 1 mL of 10% (w/v) gelatin solution was placed in each well of a 24-well plate, hardened at room temperature and stored at 4 °C until use. 1 mL of artificial mucus was placed on the hardened gelatin gel. Then, 500 µL of a water dispersion of 6-coumarin loaded

NPs (1mg/mL) were placed on the artificial mucus layer and maintained at closed humid chamber, emulating the humid environment of the airways (44). After 8, 12, 24 h, the NP-containing artificial mucus was withdrawn, gelatin plates washed three times with water and subsequently melted at 60 °C. The 6-Coumarin amount in gelatin was evaluated using a microplate reader (Synergy™ MxMonochromator-Based Multi-Mode Microplate Reader; BioTek Instruments, Winooski, VT, USA) at excitation and emission wavelengths of 430 and 485 nm, respectively. Results are reported as percentage of 6-coumarin penetrated through artificial mucus (amount of 6-coumarin in gelatin plates/total amount of 6-coumarin in NPs × 100) ± SD.

5.3.3.14 Stability study

To determine in vitro stability, the NPs were suspended in saline (0.9% sodium chloride solution), 10% fetal bovine serum and simulated lung fluid (prepared as described by Moss et al. and incubated at 37 ^{o}C for 48 h. Particle size was measured every 1, 2, 3, 6, 12, 24, 48 h. DLS was used to measure particle size at each interval.

5.3.3.15 Statistical analysis

The experiments were performed in triplicate, unless otherwise stated. All data were expressed as mean ± standard deviation. The statistical significance of the results was determined using a Student's t-test where $P<0.05$ as minimum level of significance.

5.4 Results and discussion

5.4.1 Development of Netilmicin sulfate loaded NPs

5.4.1.1 Development of PLGA NPs

Results of the preliminary study suggested that five factors greatly influence the entrapment efficiency and particle size of NPs. These independent process parameters were varied according to the coded value mentioned in Table 1 to obtain the optimized formulation by use of the double emulsification method.

5.4.1.1.1 Optimization of the NS-loaded PLGA NPs formulation

2^{5-1} FFD was developed to analyze the effects of the five independent variables on the response variables; i.e. the EE and particle size (Table 5.2). These responses are discussed below.

5.4.1.1.2 Encapsulation efficiency (EE)

While developing NPs formulations, the high solubility caused the antibiotic to diffuse easily into aqueous phase during preparation of the NPs, resulting in low entrapment. Therefore, the main aim was to maximize the EE (Y1) of the NS in the NPs. The developed formulations

showed EE ranging from 41.55% to 93.23% (Table 5.2). Based on the process parameters, a statistical model was obtained with three most significant effects and one significant interaction describing 0.99 of the variation (Table 5.3 & 5.4). The most significant process parameters affecting the EE of NS into NPs were the DS: NS charge ratio (X4, β 9.08), the PLGA concentration (X2, β 8.94), and the Vw1/V0 ratio (X5, β 2.88). The positive sign of the X2, X4 and X5 independent variables indicates they had positive correlations with the EE; i.e. an increase in value of these parameters caused an increase in the EE. The level of significance of the charge ratio and PLGA concentration suggests their direct interaction with drug, which affected EE of NS. Indeed, EE varied with changes in the DS to NS charge ratio, demonstrating the important role of electrostatic interaction between DS and NS in the preparation of the NPs. Some recent studies (45-47) have shown that complexation of ionic polymers and drugs results in increased EE. The electrostatic interactions have been validated between the water-soluble cationic drugs and counter-ionic polymers (46, 48, 49).The positive charges on the ionic NS molecule are neutralized by the negative charges of DS. The DS is a clinically applicable polymer showing high charge density due to high substitution of the sulfate group (45). The NS-DS complexes formed under these conditions were insoluble in the aqueous phase and their hydrophobicity enhances the incorporation of NS in NPs. Another important factor for the entrapment of NS in NPs is the polymer concentration. It was observed that EE increased with increasing polymer concentration (50-52). Increase in the polymer concentration results in increased viscosity of the organic phase, resulting in reduced diffusion of the drug towards the aqueous solution through polymer drops. Also, high polymer concentration results in faster precipitation of the polymer on the surface of the dispersed phase (50, 51).

Tables 5.3: Results of the fractional factorial design

Term	**% EE (Y1)**			**Particle size (nm) (Y2)**		
	Estimate	**t Ratio**	**Prob>|t|**	**Estimate**	**t Ratio**	**Prob>|t|**
Intercept	63.90	109.61	<.0001*	133.22	974.37	<.0001*
X1	1.44	2.34	0.1443	1.03	7.17	0.0189*
X2	8.94	14.47	0.0047*	4.62	31.86	0.0010*
X3	1.61	2.62	0.1204	-1.24	-8.61	0.0132*
X4	9.08	14.69	0.0046*	0.97	6.74	0.0213*
X5	2.88	4.67	0.0429*	-0.66	-4.58	0.0445*

X1×X2	-1.72	-2.79	0.1082	0.29	2.03	0.1795
X1×X3	-0.72	-1.17	0.3625	-0.32	-2.24	0.1548
X1×X4	1.53	2.48	0.1317	0.08	0.58	0.6195
X1×X5	-1.39	-2.25	0.1536	1.53	10.61	0.0088*
X2×X3	-1.52	-2.47	0.1322	-0.0025	-0.06	0.9604
X2×X4	2.28	3.69	0.0663	-0.27	-1.93	0.1939
X2×X5	-0.88	-1.44	0.2872	0.52	3.64	0.0678
X3×X4	3.58	5.80	0.0285 *	-1.24	-8.61	0.0132*
X3×X5	2.14	3.46	0.0742	0.79	5.49	0.0316*
X4×X5	2.32	3.77	0.0638	1.44	9.97	0.0099*
R^2 value		0.9964			0.9987	
F value		37.41			103.37	
Significance		0.0263			0.0096	

Table 5.4: Analysis of variance table obtained by statistical evaluation of the results of % EE

Source	**Sum of Squares**	**df**	**Mean Square**	**F Value**	**p-value Prob> F**
Model	3434.35	15	228.95	37.41	0.0263
X1-Vw1/V0	33.46	1	33.46	5.46	0.1443
X2-CPLGA	1280.92	1	1280.92	209.32	0.0047
X3-CPluoronic F68	41.86	1	41.86	6.84	0.1204
X4-DS:Drug Charge ratio	1321.32	1	1321.32	215.92	0.0046
X5-tsonication	133.51	1	133.51	21.81	0.0429
X1×X2- Vw1/V0*CPLGA	47.54	1	47.54	7.76	0.1082
X1×X3 -Vw1/V0*CPluoronic F68	8.38	1	8.38	1.36	0.3625
X1×X4-Vw1/V0*DS:Drug Charge ratio	37.51	1	37.51	6.13	0.1317
X1×X5-Vw1/V0*tsonication	30.91	1	30.91	5.05	0.1536
X2×X3-CPLGA*CPluoronic F68	37.33	1	37.33	6.10	0.1322
X2×X4-CPLGA*DS:Drug Charge ratio	83.17	1	83.17	13.59	0.0663
X2×X5-CPLGA*tsonication	12.63	1	12.63	2.06	0.2872
X3×X4-CPluoronic F68*DS:Drug Charge ratio	205.63	1	205.63	33.60	0.0285

X3×X5-CPluoronic F68*tsonication	73.35	1	73.35	11.98	0.0742
X4×X5-DS:Drug Charge ratio*tsonication	86.76	1	86.76	14.17	0.0638
Residual	12.23	2	6.11		
Lack of Fit	11.24	1	11.24	11.31	0.1840
Pure Error	0.9940	1	0.9940		
Cor Total	3446.59	17			

Table 5.5: Analysis of variance table obtained by statistical evaluation of the results of particle size (nm)

Source	**Sum of Squares**	**df**	**Mean Square**	**F Value**	**p-value Prob> F**
Model	521.51	15	34.76	103.31	0.0096
X1-Vw1/V0	17.28	1	17.28	51.36	0.0189
X2-CPLGA	341.60	1	341.60	1015.11	0.0010
X3-CPluoronic F68	24.92	1	24.92	74.06	0.0132
X4-DS:Drug Charge ratio	15.30	1	15.30	45.48	0.0213
X5-tsonication	7.06	1	7.06	20.98	0.0445
X1×X2- Vw1/V0*CPLGA	1.38	1	1.38	4.12	0.1795
X1×X3 -Vw1/V0*CPluoronic F68	1.68	1	1.68	5.00	0.1548
X1×X4-Vw1/V0*DS:Drug Charge ratio	0.11	1	0.11	0.33	0.6195
X1×X5-Vw1/V0*tsonication	37.94	1	37.91	112.66	0.0088
X2×X3-CPLGA*CPluoronic F68	0.001	1	0.001	0.003	0.9604
X2×X4-CPLGA*DS:Drug Charge ratio	1.24	1	1.24	3.71	0.1939
X2×X5-CPLGA*tsonication	4.46	1	4.46	13.26	0.0678
X3×X4-CPluoronic F68*DS:Drug Charge ratio	24.92	1	24.95	4.06	0.0132
X3×X5-CPluoronic F68*tsonication	10.16	1	10.16	30.12	0.0316
X4×X5-DS:Drug Charge ratio*tsonication	33.43	1	33.43	99.36	0.0099
Residual	0.67	2	0.33		
Lack of Fit	0.35	1	0.35	1.10	0.4844
Pure Error	0.32	1	0.32		
Cor Total	522.18	17			

The volume ratio of the inner water phase to the oil phase in the primary emulsion also showed marked effects on the encapsulation of the NS in NPs. We observed that a lower volume ratio enhances encapsulation. The efficiency was increased significantly when the volume ratio was increased from 0.3 to 0.7. Increasing the inner water phase volume should reduce the NS concentration gradient between the inner and outer water phase and, consequently limiting the diffusion of NS from the inner to the outer water phase to promote its encapsulation in the PLGA core. However, increasing volume ratio of the inner water phase to oil phase needs to be done with care as it may also lead to formation of a less stable primary emulsion due to coalescence of water droplets and increased particle size. The obtained results are in agreement with the previous reported studies (39, 53).

Sonication time plays important role in determining the particle size of the primary emulsion droplets. A smaller difference in droplet size between primary and secondary emulsion results in the formation of a thin oil layer around the water droplet allowing easy pass for drug from inner aqueous phase can through oil phase resulting in lower EE (54). Increasing sonication time results in larger size difference between primary and secondary emulsions, which enhances encapsulation of the drug.

The ratio between the inner water phase and the organic phase was varied by changing the volume of the inner water phase, and this also impacted the EE of NS in NPs. Surfactant concentration did not exert a significant direct effect on EE, however an interaction is evident between the surfactant concentration (X3) and the DS: NS ratio (X4), indicating that a high NS: DS ratio is required to obtain high EE (Figure 5.3). The described two-factor interaction between the surfactant concentration and the NS: DS ratio shows that there is a positive effect of including surfactant in the formulation at high NS: DS ratio. Surfactant plays a role in stabilizing colloidal solutions (55). These results indicate that the emulsion is unstable at high NS: DS ratio and thus require a high surfactant concentration for stability, which in turn enhances the EE.

5.4.1.1.3 Particle Size

Particle size is responsible for the biopharmaceutical properties of the NPs formulation. The size can also play key role in particle endocytosis and macrophage escape (56). Based on the literature we defined 150 nm as the maximum acceptable diameter for NPs to have NPs with above-mentioned characteristics.

The size of formed NPs varied between 121.43 nm and 140.83 nm (Table 5.2). However the particle size depended on several process parameters, namely PLGA concentration (X2, β 4.62), ratio of volume of inner aqueous phase to the organic phase (Vw_1/Vo) (X1, β 1.03), and DS: NS charge ratio (X4, β 0.978). Other parameters had little impact on the particle size and were part of the significant interaction term; therefore, all of them were included in the statistical model to describe the particle size of NPs (Table 5.3 & 5.5). The variation accounted for by the statistical model was 0.9987. The positive sign of variables X1, X2 and X4 indicated their positive correlations with particle size while the negative sign of variables X3, X5 indicated their negative correlation with the particle size. A large interaction was observed between the ratio of the inner water phase to the organic phase and sonication time (X1 & X5), concentration of the surfactant and sonication time (X3 & X5), drug charge ratio and sonication time (X2 & X5), and PLGA concentration and DS: Drug charge ratio (X2 & X4). These provided a positive synergistic effect between the respective two factors. The interaction between the ratio of the PLGA concentration and sonication time (X2 & X5) may indicate that a longer sonication time is required to obtain a stable emulsion with small particle size when PLGA is added at high concentration (Figure 5.3). The ratio of the inner water phase to the organic phase was varied by changing the volume of the inner water phase. Low ratio results in the formation of the unstable emulsion thus longer sonication time is required to form stable emulsion, which reduces particle size (Figure 5.3). Also it was observed that high surfactant concentration is necessary to form a stable emulsion at high DS:NS ratio. Further synergistic effect was observed at high surfactant concentration and long sonication time, results in lower particle size (Figure 5.3).

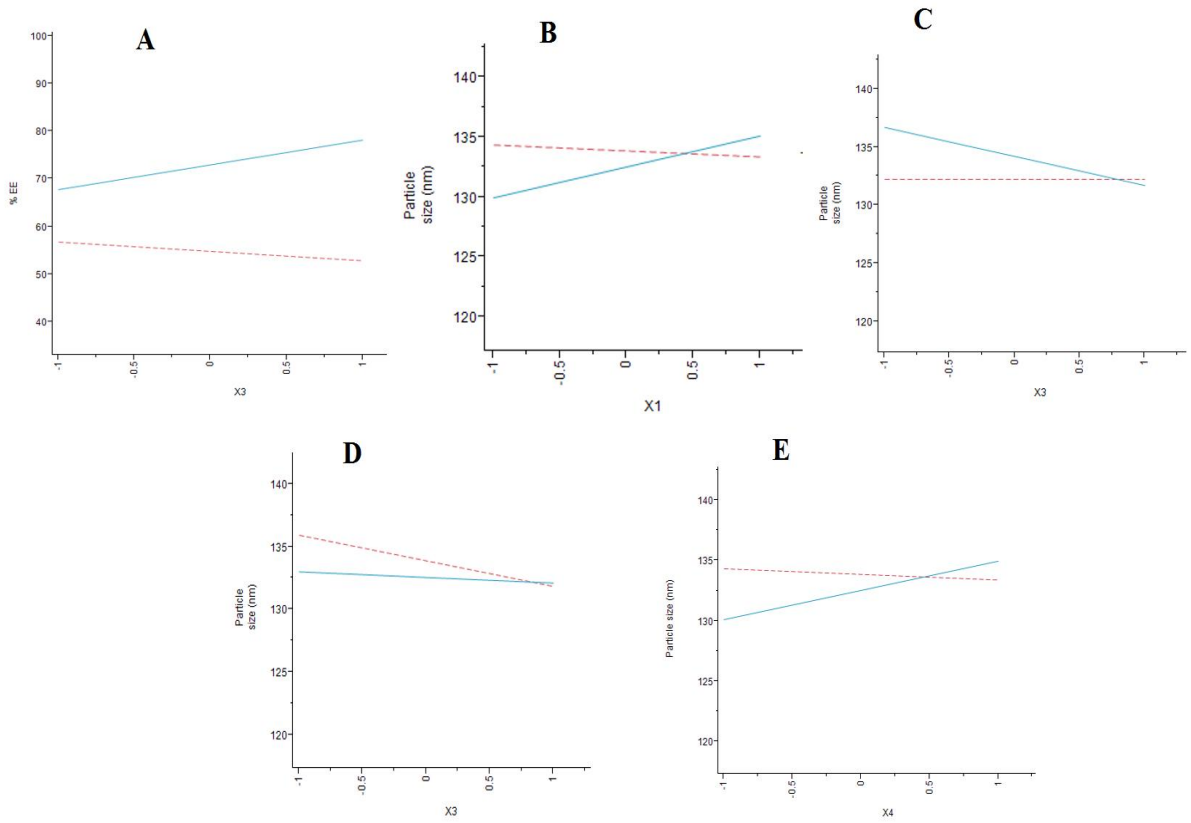

Figure 5.3: Interaction plots showing significant two-way interaction terms for the dependent variables. Solid lines display factor at high level, whereas dashed lines are the low level of the factors. A: interaction term X3X4–Puronic F 68 concentration/ DS:NS ratio. B: X1X5– Volume ratio/sonication time. C: X3X4 – Pluronic F 68 concentration/ DS:NS ratio. D: X3X5– Pluronic F 68 concentration/Sonication time. E: X4X5– NS:DS ratio/sonication time. A: Encapsulation efficiency. B-E: particle size

5.4.1.1.4 Response Surface plot

Three-dimensional response surface plots generated by the JMP 10 software are presented in Figure 5.4 and 5.5, for PLGA NPs. Figure 5.4 depicts effect of different factors on % EE of NS in PLGA NPs. It was observed that EE increases with increase in DS to NS ratio, PLGA concentration, sonication time. While, Figure 5.5 depict effects of different factors on PS of PLGA NPs. It was observed that PS size was increases with increase in PLGA concentration, ratio of volume of inner aqueous phase to the organic phase, DS: NS charge ratio and with decrease in surfactant concentration & sonication time

5.4.1.1.5 Counter plot

Figure 5.6 shows the contour plots for % EE values which were also found to be non-linear and having curved segment indicating non-linear relationship between variables. It was determined from the contour that higher % EE could be obtained at higher level of all variables. Figure 5.7 shows the contour plot for PS of PLGA NPs values which were also found to be non-linear with curved segment signifying non-linear relationship between variables. It was observed that PS increases at higher level of PLGA concentration, ratio of volume of inner aqueous phase to the organic phase, DS: NS charge ratio and at lower level of surfactant concentration & sonication time.

The zeta potential of all the particles was negative and in the range of -20.3 mV to -24.5 mV. High negative values of the zeta potential create an electrostatic repulsion between particles, which helps to prevent aggregation and thus stabilizes the NPs dispersion (57). Zeta potential values in the range -15 to -30 mV is common for stabilized NPs (58).

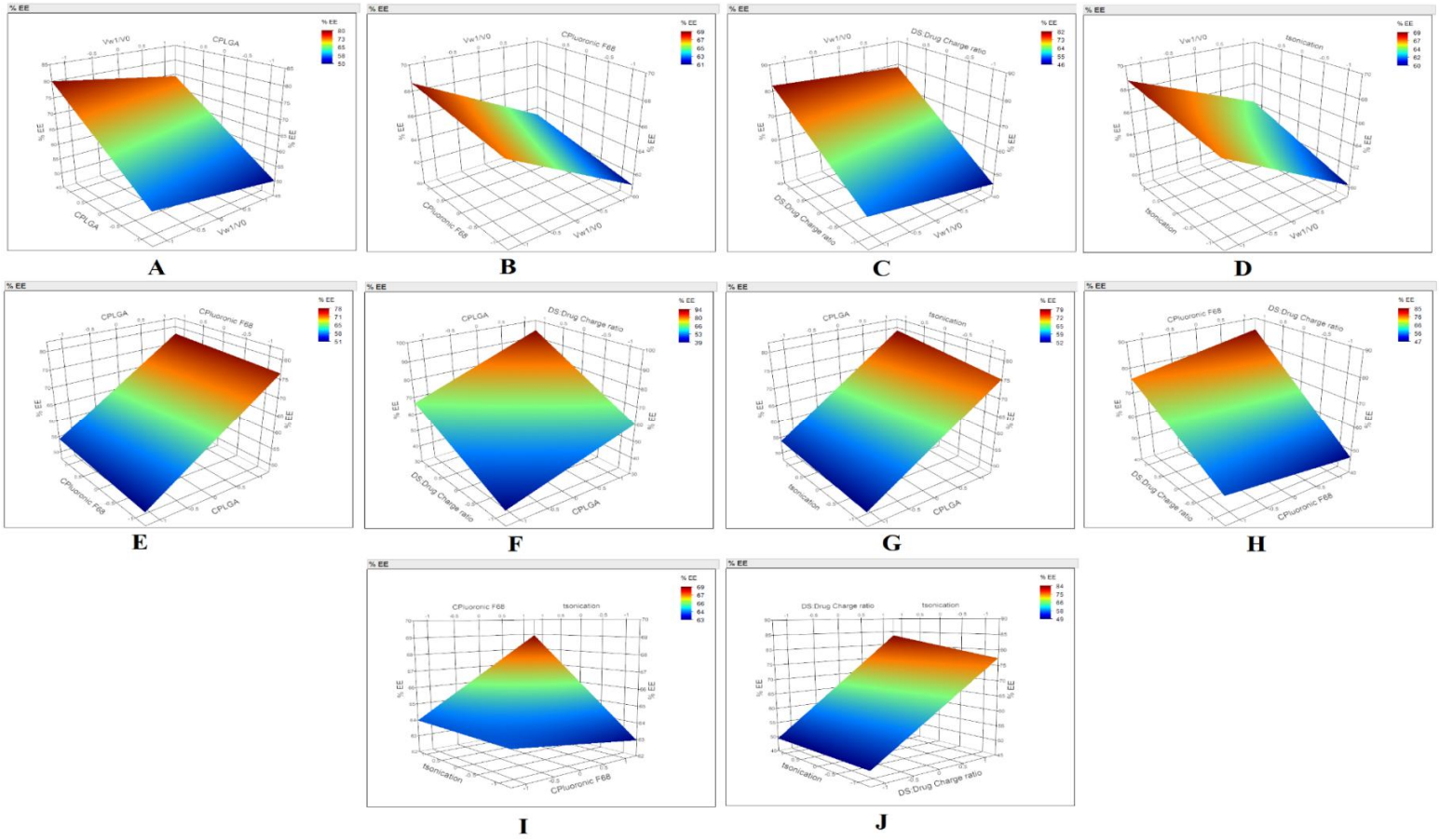

Figure 5.4: Surface plot for PLGA NPs; A) effect of PLGA concentration & Volume ratio on EE; B) effect of Pluronic F 68 concentration & Volume ratio on EE; C) effect of DS:NS ratio & Volume ratio on EE; D) effect of Sonication time & Volume ratio on EE; E) effect of Pluronic F 68 concentration & PLGA concentration on EE; F) effect of DS:NS ratio & PLGA concentration on EE; G) effect of sonication time & PLGA concentration on EE; H) effect of DS:NS ratio & Pluronic F 68 concentration on EE; I) effect of sonication time & Pluronic F 68 concentration on EE; J) effect of DS:NS ratio & sonication time on EE

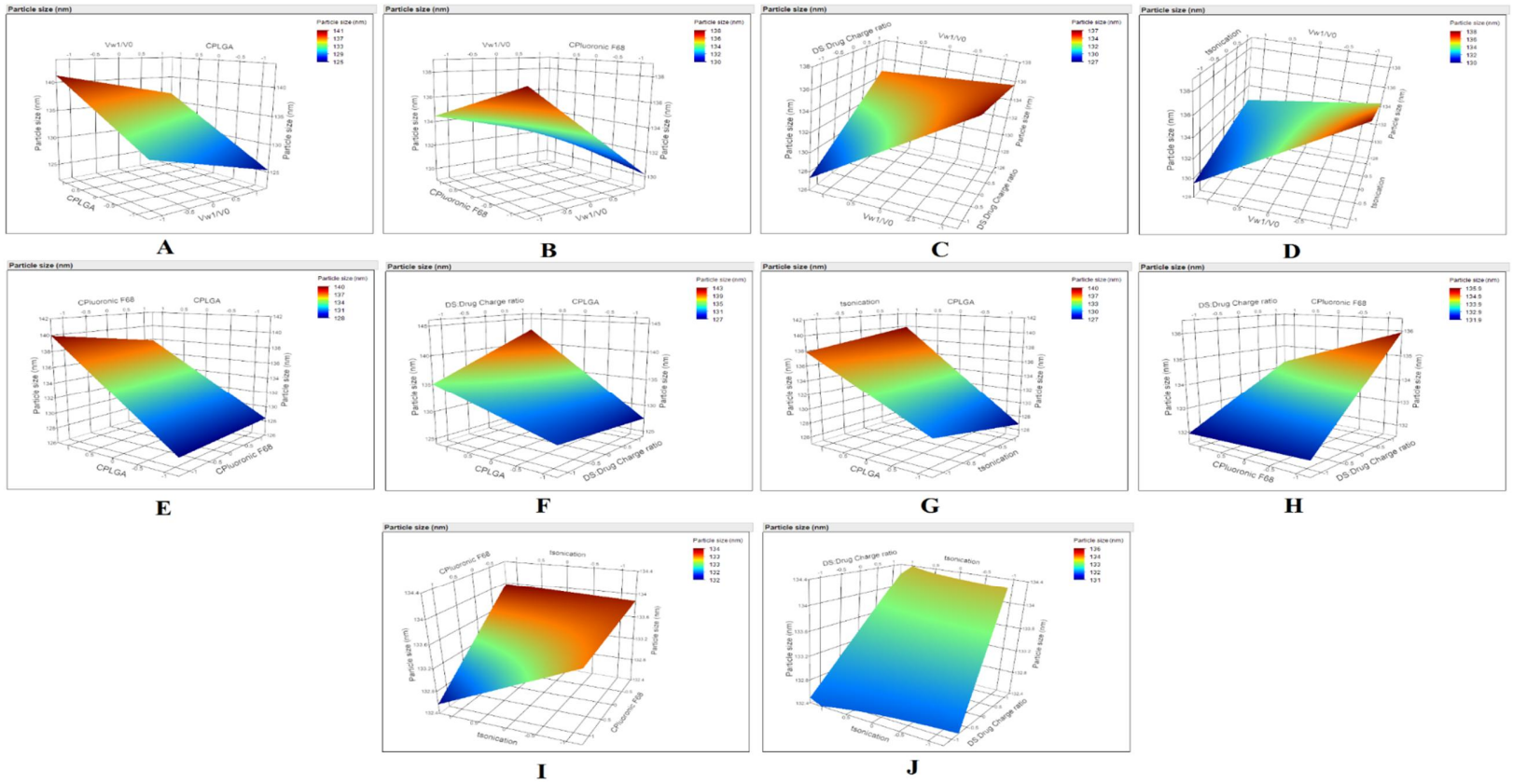

Figure 5.5: Surface plot for PLGA NPs; A) effect of PLGA concentration & Volume ratio on PS; B) effect of Pluronic F 68 concentration & Volume ratio on PS; C) effect of DS:NS ratio & Volume ratio on PS; D) effect of Sonication time & Volume ratio on PS; E) effect of Pluronic F 68 concentration & PLGA concentration on PS; F) effect of DS:NS ratio & PLGA concentration on PS; G) effect of sonication time & PLGA concentration on PS; H) effect of DS:NS ratio & Pluronic F 68 concentration on PS; I) effect of sonication time & Pluronic F 68 concentration on PS; J) effect of DS:NS ratio & sonication time on PS

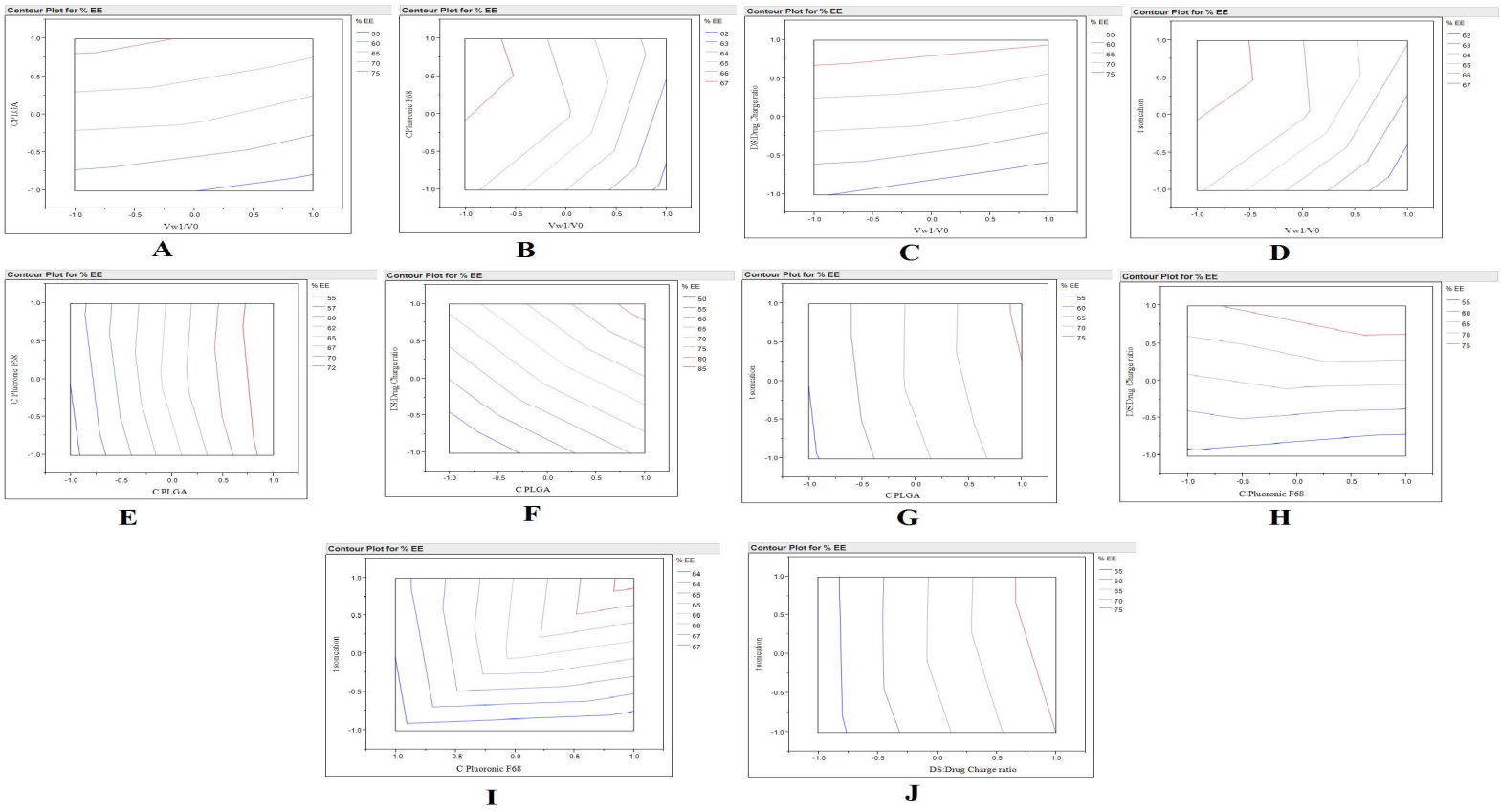

Figure 5.6: Counter plot for PLGA NPs; A) effect of PLGA concentration & Volume ratio on EE; B) effect of Pluronic F 68 concentration & Volume ratio on EE; C) effect of DS:NS ratio & Volume ratio on EE; D) effect of Sonication time & Volume ratio on EE; E) effect of Pluronic F 68 concentration & PLGA concentration on EE; F) effect of DS:NS ratio & PLGA concentration on EE; G) effect of sonication time & PLGA concentration on EE; H) effect of DS:NS ratio & Pluronic F 68 concentration on EE; I) effect of sonication time & Pluronic F 68 concentration on EE; J) effect of DS:NS ratio & sonication time on EE

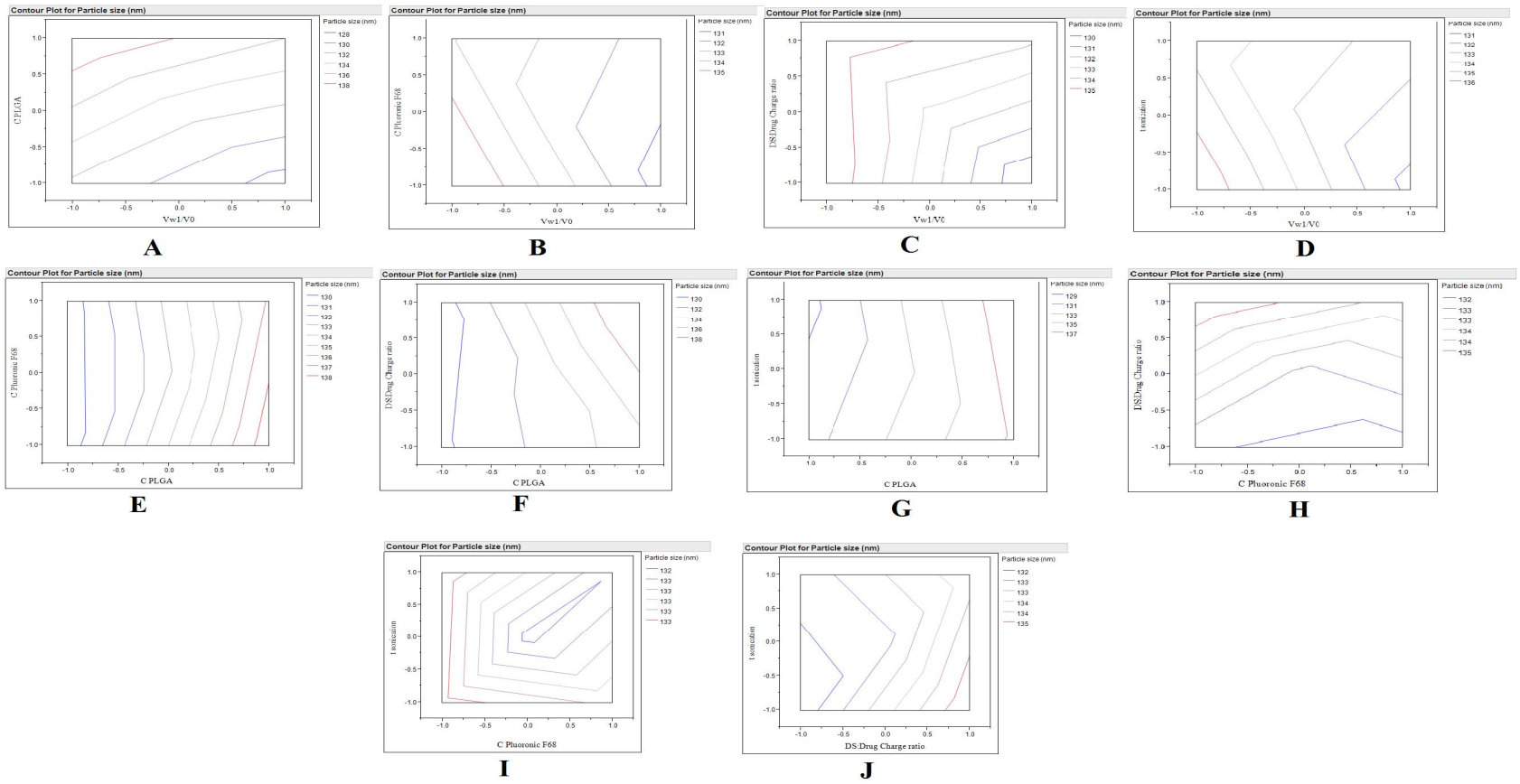

Figure 5.7: Counter plot for PLGA NPs; A) effect of PLGA concentration & Volume ratio on PS; B) effect of Pluronic F 68 concentration & Volume ratio on PS; C) effect of DS:NS ratio & Volume ratio on PS; D) effect of Sonication time & Volume ratio on PS; E) effect of Pluronic F 68 concentration & PLGA concentration on PS; F) effect of DS:NS ratio & PLGA concentration on PS; G) effect of sonication time & PLGA concentration on PS; H) effect of DS:NS ratio & Pluronic F 68 concentration on PS; I) effect of sonication time & Pluronic F 68 concentration on PS; J) effect of DS:NS ratio & sonication time on PS

Based on the aforementioned experiments, the optimized parameters were identified and are listed in Table 5.6. Optimized NPs showed EE of 93.23±2.7%, size 140.83±2.4 nm, with a polydispersity index (PDI) of 0.130±0.018 (Figure 5.8 A) and zeta potential -23.45±3.06 mV (Figure 5.8 B). The TEM image of NPs reveals that NPs are spherical in shape and uniform in size (Figure 5.8 C).

Table 5.6: Optimal parameters for NS-loaded PLGA NPs

Parameters	**Optimized level**	**Parameters**	**Optimized level**
V_{w1}	0.35 ml	EE[a]	93.23 ± 2.7%,
C_{PLGA}	15 mg	Particle size[a]	140.83 ± 2.4 nm
Ethyl acetate	0.5 ml	Polydispersivity index[a]	0.130 ± 0.018
$C_{Pluoronic\ F68}$ (1.5%)	2 + 5 ml	Zeta Potential[a]	-23.45 ± 3.06 mV.
DS:NS Charge ratio	2.5		

[a]Values represent mean ± SD (n = 3).

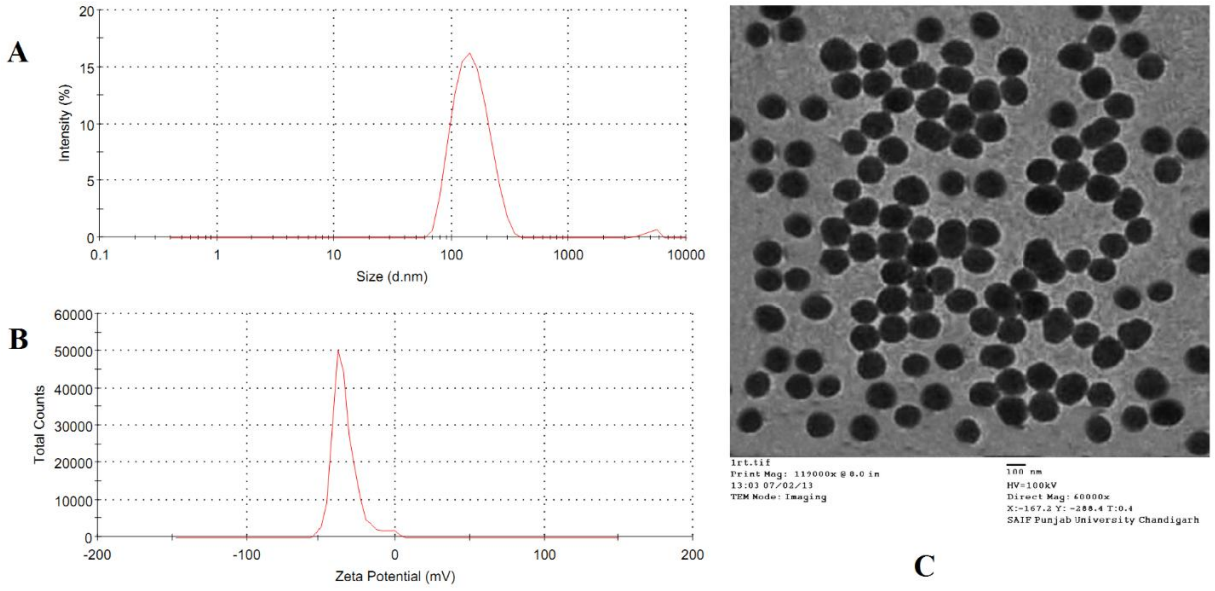

Figure 5.8: A) The DLS results show that size of NSDS PLGA NPs is 140.83± 2.4 nm (PDI = 0.130 ± 0.018); **B)** zeta potential (-23.45±3.06 mV) of NS-loaded NPs; C) TEM micrographs of NSDS PLGA NPs. DLS & TEM based characterization of NPs confirms that size distribution and colloidal stability of mono-dispersed particles.

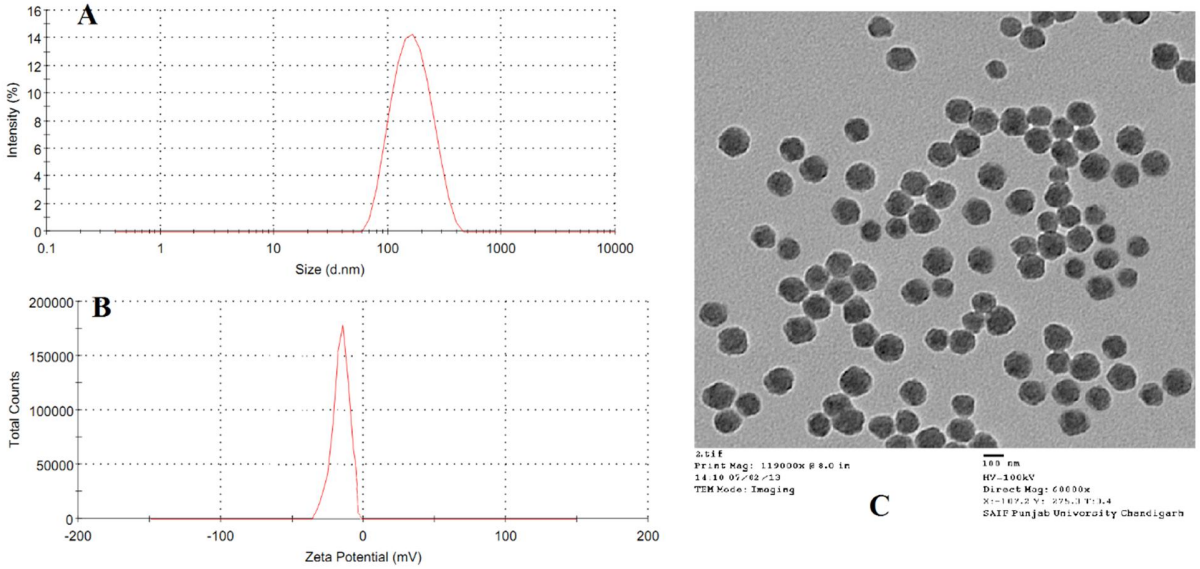

Figure 5.9: A) The DLS results show that size of PEG NSDS PLGA NPs is 150.13±3.20 nm (PDI = 0.295±0.07); **B)** zeta potential (-12.53±1.78 mV); C) TEM micrographs of PEG NSDS PLGA NPs. DLS & TEM based characterization of NPs confirms that size distribution and colloidal stability of mono-dispersed particles.

Finally optimized formulation was surface modified using DSPE-PEG at a 3 % w/w lipid to-polymer ratio. Characteristics of prepared PEGylated NS-loaded NPs are summarized in Table 5.7 in terms of size, PI, zeta potential and encapsulation efficiency. The PEGylated NPs were successfully prepared with essentially spherical morphology and mean particle diameter of ~ 150 nm (Figure 5.9). PEGylation doesn't affect EE of NS in PLGA NPs. Blank and non PEGylated PLGA NPs had similar particle sizes indicating that the encapsulation of NS did not change the particle size. Zeta potential was significantly increased as compared with blank PLGA NPs. The high negative surface charges on the NS-PLGA NPs were due to presence of the anionic charge on the DS chains, which further supported the role of electrostatic interaction with NS. However slight reduction in zeta potential was observed in case of PEGylated NPs, it might be due the presence of the PEG moiety on the surface of the NPs. Similar findings were found in the reported references (46, 48, 49). Further PEGylation was confirmed by FTIR spectroscopy as explained in later section.

Table 5.7: Summary of drug encapsulation efficiency, particle diameter and Zeta potential of PEGylated NS loaded PLGA NPs (mean ± SD, n = 3).

Formulation	DS:NS charge Ratio	Particle size (nm)	PDI	Zeta potential (mV)	EE %
Blank	--	138.76±3.80	0.388±0.05	-3.72±0.41	--
NS-DS-PLGA NPs	2.5	140.83±2.40	0.310±0.10	-23.45±3.06	93.23±2.70
PEG-NS-DS-PLGA NPs	2.5	150.13±3.20	0.295±0.07	-12.53±1.78	95.70±1.50

Further optimized formula was used to prepare fluorescently-labelled NPs (Rhodamine B-loaded NPs) for *in-vitro*/*in-vivo* deposition studies. They were prepared in a same way by replacing NS with Rhodamine B. Particles were characterized in terms of size, PI, zeta potential and encapsulation efficiency (Table 5.8). Total amount of rhodamine B entrapped in PLGA NPs was determined after dissolving NPs in Chloroform: Methanol (1:1). The amount of rhodamine B in resulting solution was then determined by using a Spectrofluorometer (RF-5301PC, Shimadzu) at excitation and emission wavelengths of 560 and 595 nm. The obtained particles were uniform in size with similar characteristics as that of drug loaded NPs (Table 5.8).

Table 5.8: Summary of drug encapsulation efficiency, particle diameter and Zeta potential of rhodamine loaded PLGA NPs (mean ± SD, n = 3).

Formulation	Particle size (nm)	PDI	Zeta potential (mV)	EE %
Rho-PLGA NPs	143.18±3.3	0.230±0.31	-24.88±1.35	85.47±4.41
PEG-Rho-PLGA NPs	149.51±4.2	0.187±0.10	-13.91±2.298	83.53±3.35

5.4.1.2 Differential scanning calorimetry (DSC)

DSC analysis is useful for demonstrating possible interactions between different compounds in a mixture. The DSC analysis was performed on NS, PLGA, blank NPs and NS-loaded NPs (Figure 5.10 a). PLGA shows the endothermic peak at 44^{o}C. DSC curves of the blank NPs show an endothermic peak at 50^{o}C owing to the PLGA. The DSC curve of the NS showed an endothermic peak at 187.74°C and drug melting was followed by thermal decomposition.

However, endothermic peak of NS was absent in the DSC curve of NS-loaded NPs, indicating that NS was present in an amorphous phase in the NPs.

5.4.1.3 FTIR Spectroscopy

FTIR spectra of all the samples are shown in (Figure 5.10 b). The NS FTIR spectrum showed peaks of C-O and C-N stretching band at 1010.91 cm^{-1}& 1125.94 cm^{-1}, aliphatic C-H stretching band at 3017.34 cm^{-1} & C-H bending band at 619.51 cm^{-1}, -NH stretching and -OH stretching bands at 3100 to 3391.36 cm^{-1}. N-H bending band observed at 1609.83, 1506, 1284.13 cm^{-1}. In the PLGA FTIR spectrum, peaks at 3506.64 cm^{-1} for –OH stretching and 3000.18– 2955.77 cm^{-1} for C-H stretching bands were observed as the typical band of PLGA. The ester C=O stretching band of PLGA was observed at 1757.01 cm^{-1}. All the typical bands of PLGA and NS were also present in the FTIR spectrum of their physical mixture. However, the FTIR spectrum of NS loaded NPs had only the characteristic peaks of the polymer. The absence of characteristic drug peaks in the NPs sample indicates that non encapsulated drug was not present, which is in agreement with previous studies involving PLGA particulate systems (59).

In Figure 5.11 DSPE PEG 2000 FTIR spectrum showed peaks of C=O at 1738.59 cm^{-1}, aliphatic CH_2 band at 2919.29 cm^{-1}, CH_3 band at1352.79 cm^{-1}, O-CH_2band at 1101.19 cm^{-1} and C=C band at 1642.67 cm^{-1}.All these characteristic peaks are also observed in PEGylated NPs which confirms the PEGylation of NPs.

5.4.1.4 In-vitro release study

Conceiving NPs for lung delivery, NS release studies were performed in experimental conditions able to simulate the properties of the delivery site. On this matter, lung fluid should be taken into consideration (60). To reproduce such a complex system in vitro, simulated lung fluids (SLF) were used for NS release studies as an alternative to classical physiological buffer at pH 7.4.The release profiles of NS from the NS loaded PLGA NPs in phosphate buffer (pH 7.4) and simultaneous lung fluid at 37°C is shown in Figure 5.12 (A & B).

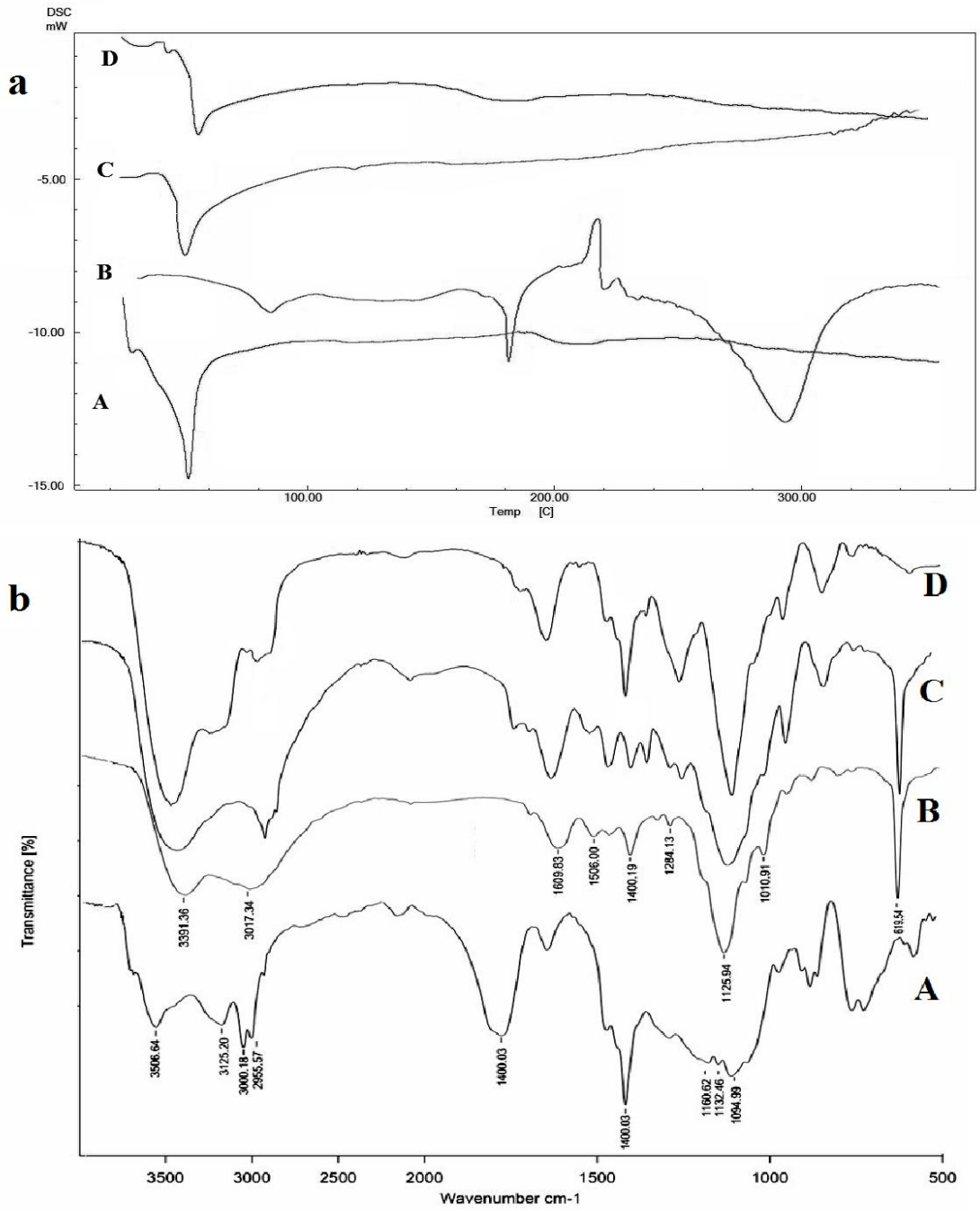

Figure 5.10: a) Differential scanning calorimetry curves of (A) PLGA, (B) NS, (C) blank NPs, (D) NS-loaded NPs; **b)** Overlay of FTIR spectra of A) PLGA, B) NS, C) Physical mixture, D) NS loaded NPs. The absence of characteristic drug peaks in the NPs sample indicates that nonencapsulated drug on NPs surface was not present

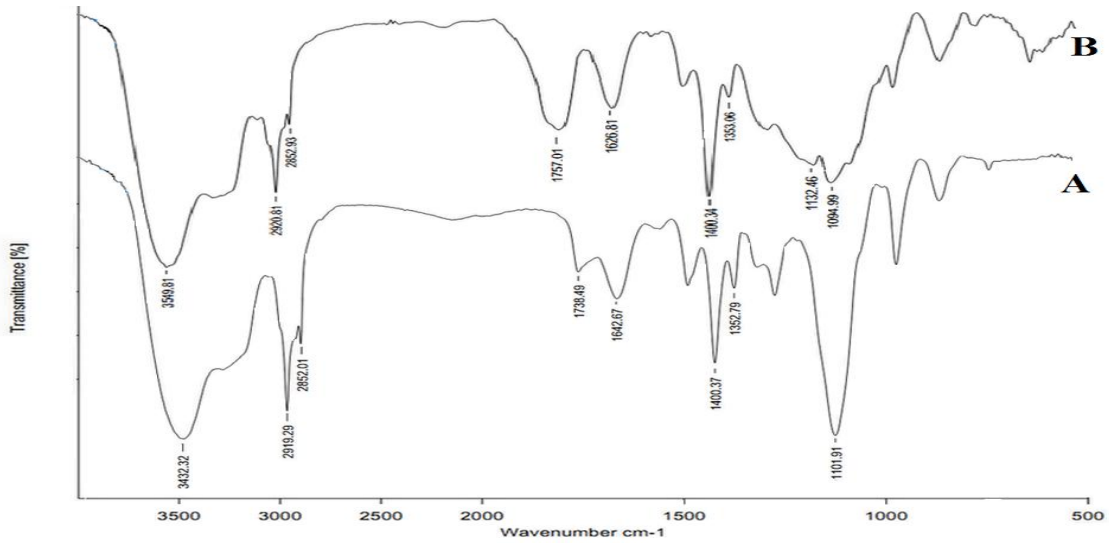

Figure 5.11: Overlay of FTIR spectra of A) DSPE PEG 2000 B) PEG NSDS PLGA NPs. The characteristic DSPE PEG 2000 peaks in the NPs sample confirms the PEGylation of NPs.

In both media, bi-phasic release behavior was observed, characterized by initial burst release followed by sustained release of NS from NPs. Lower burst release was observed due to the uniform distribution of the NS in NPs rather than just on the surface of the NPs (46). About 25% of drug content was released within the first 24h, followed by sustained drug release. Though polar structure of DS contained ether bonds and –OH groups, the strong electrostatic interaction between NS and DS made the complex neutral and hydrophobic enough to be stored in the PLGA for prolonged time, thus sustaining the drug release from NPs. In addition, the lipophilic nature and solid matrix of NPs as well as immobility of the polymer chains results into slower water penetration and drug diffusion. This can be explained by assuming that when the release medium penetrates into the tiny pores of NPs the counter ions from the release medium compete with NS to release it from the NS–DS complex through ion exchange, the dissociated NS diffuses out through the pores. As the ion exchange and drug release progresses, more flexible and hydrophilic polymer chains would be produced. Eventually the dissociated DS molecules are dissolved and diffuse out, leaving the solid matrix more porous and accessible for aqueous medium to diffuse in, which accounts for the later acceleration of release (46).Thus, results indicate the role of DS in release behavior of the NS from NPs. However significant difference was observed in release behavior of NS DS PLGA and PEG NS DS PLGA NPs ($p= 0.00001$; $p < 0.05$ & $p=0.00001$; $p< 0.05$ for PBS pH 7.4 & SLF respectively). Being a hydrophilic molecule

DSPE-PEG enable a greater influx of water into the NP matrix, promoting greater degradation of PLGA and improved NS release from NPs.

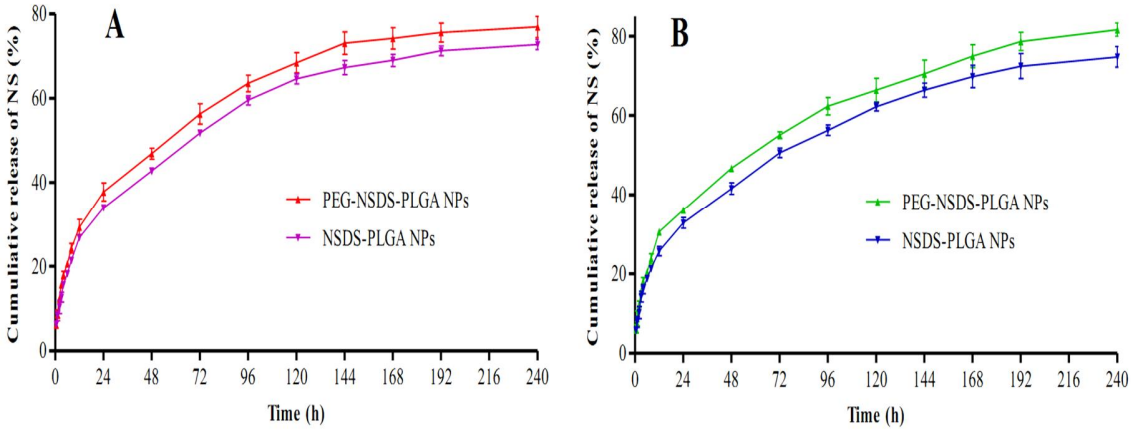

Figure 5.12: A) Cumulative percent drug released in PBS pH 7.4; **B)** Cumulative percent drug released in SLF.

Interestingly, no significant difference in NS release rate was observed in simulated lung fluids as compared to results achieved in buffer at pH 7.4, suggesting that ion concentration in SLF does not affect NS release properties. Projecting these results in humans, the fact that the developed NP release NS according to a biphasic kinetics and a prolonged release helps to maintain NS level above MIC to treat bacterial infection effectively.

To evaluate the mechanism of drug release from NPs, the release data were analyzed by using the Korsmeyer–Peppas equation: $Q_t/Q_\infty = k \times t^n$

Where, Q_t/Q_∞ is the fraction of released drug, t is the release time, k is a constant characteristic of the drug–polymer system, and n is release exponent that characterizes the mechanism of drug release (61). When log Q_t/Q_∞ vs. log t was plotted, it gave straight lines and the exponents n, k were calculated from the slope and the intercept of the regression lines, respectively. The calculated diffusional exponent (n) and kinetic constant (k) for the PEG NSDS PLGA NPs formulations were found to be 0.4351& 0.9933in PBS pH 7.4; 0.4302& 0.9917in SLF respectively. While that for diffusional exponent (n) and kinetic constant (k) for the NSDS PLGA NPs formulations were found to be 0.4333& 0.9958 in PBS pH 7.4; 0.4291 & 0.9938 in SLF respectively. As the n value is <0.5, one can conclude that the release of NS from NPs was by Fickian diffusion (62)

5.4.1.5 Antibacterial efficiency

Bacteria were exposed to different concentrations of blank NPs for 24 h and optical density was measured at 600 nm (OD 600). In addition, microbial growth was ascertained by growing bacteria on agar plates after suitable dilution. For both control and blank NPs, bacterial growth and CFU counts were found to remain closely similar (Figure 5.13), which indicates that the blank NPs do not possess any intrinsic antibacterial activity and antibacterial activity of the NS loaded NPs was exclusively due to the NS. Moreover, increasing the concentration of the blank NPs did not affect the growth of bacteria. This was further evaluated by growing bacterial cells on agar plates. As the presence of the NPs did not have any effect on bacterial growth, bacterial susceptibility testing was compared using only the NS solution collected from the *in-vitro* release study without the presence of NPs during the assay.

The antibacterial activity of NS-loaded NPs was determined as MIC on *P. aeruginosa*. A MIC value was found approximately equal to 18 μg/mL. In the same experimental conditions, the MIC of control free NS was 2.4 μg/mL (Figure 5.14A), while the complete eradication of the bacteria was observed at 44 μg/mL and 10 μg/mL for NS loaded NPs and native NS, respectively. The higher MIC value for NS-loaded NPs was attributed to the progressive release of the drug from the NPs; i.e. the amount of drug released by the particles after 12 h was ~ 25 %, which should result in a concentration of available drug similar to the MIC observed for the NS alone. Therefore, it could be estimated that the MIC and MBC value for the native NS and NS released from NPs were similar. In case of PEG NSDS NPs MIC & MBC values were found 14 μg/mL & 36 μg/mL respectively.

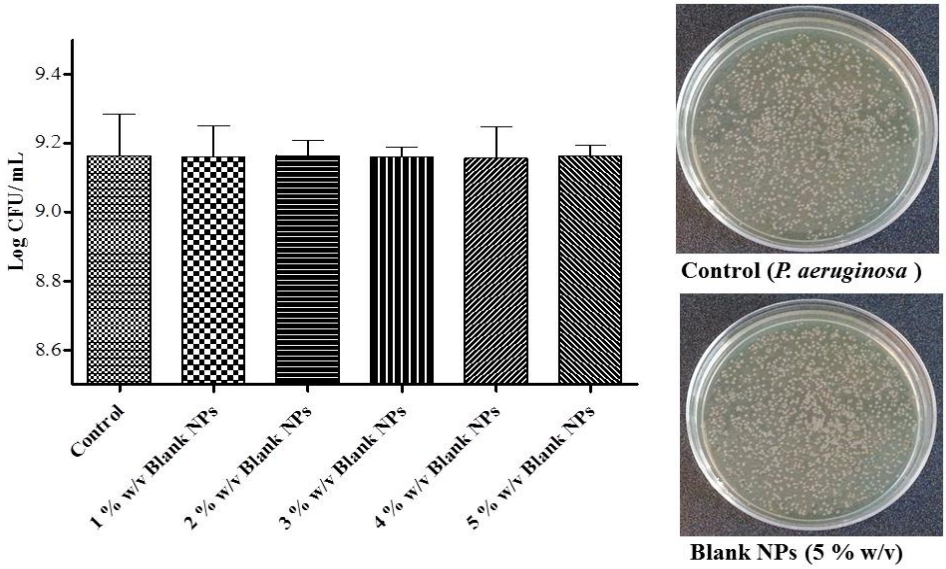

Figure 5.13: CFU count from blank NPs susceptibility testing. We observed that CFU count for both control and the blank NPs, were closely similar, which demonstrate that the blank NPs do not possess any antibacterial activity. The antibacterial effect is mainly due to the NS encapsulated in the NPs.

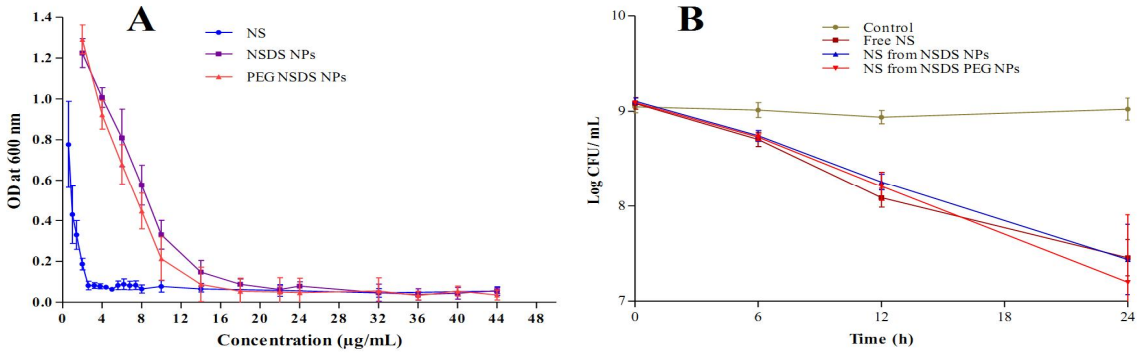

Figure 5.14: A) In vitro antibacterial activity of free NS and NS-encapsulated PLGA NPs against *P. aeruginosa*. (OD = absorbance at 600 nm of UV-spectrophotometer measurement). The higher MIC value for NS-loaded NPs was attributed to the sustained release of the drug from the NPs, however the amount of drug released by the particles after 24 hour was similar to the MIC observed for the NS alone; **B)** Effect of the encapsulation on the antibacterial activity of NS. We observed that there is no significant difference ($p > 0.05$) ($p=0.138$; $p > 0.05$ & $p=0.385$; $p > 0.05$ for NSDS PLGA & PEG-NSDS PLGA NPs respectively) in the bacterial eradication rates of the encapsulated NS and native NS, which confirm that encapsulation of NS in NPs doesn't affect it's antibacterial activity.

Further effect of the encapsulation of NS in NPs on the antibacterial efficiency of NS was evaluated by comparing the native NS and NS released form the NPs. Bacterial cells were exposed to the same antibiotic concentration (2.4 µg/mL) and OD_{600} was measured after 6, 12 and 24 h. The results (Figure 5.14B) indicate no difference between the bacterial eradication rates of encapsulated NS and native NS after 6, 12 and 24 h antibiotic exposures ($p=0.138$; $p > 0.05$ & $p=0.385$; $p> 0.05$ for NSDS PLGA & PEG-NSDS PLGA NPs respectively). Hence, the results confirm that NS can be efficiently encapsulated into the polymeric NPs without compromising its antibacterial activity

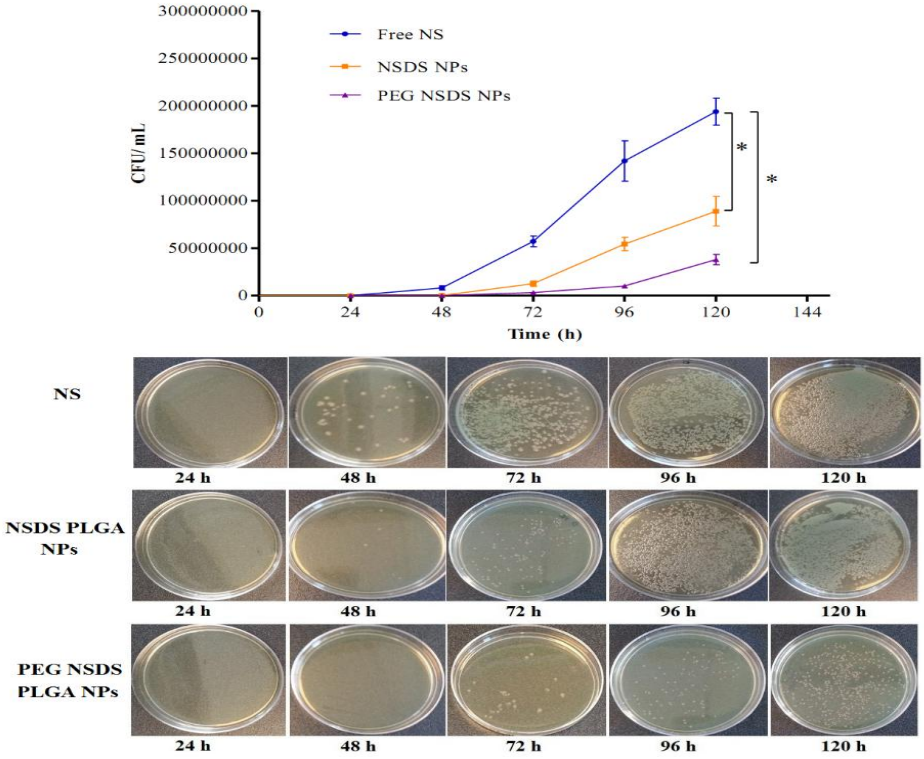

Figure 5.15: Fate of NS antibacterial activity *in-vivo.* NPs show the better performance than free NS due to the protection of the NS by NPs when incubated with bronchial cells. NS was released slowly from NPs over the period of time and retains its antibacterial activity against *P. aeruginosa*. *Significant difference; $P < 0.05$.

To mimic the *in-vivo* condition, CFBE41o- cells were incubated with free NS or NS-loaded NPs, and antimicrobial activity was tested every 24 h for 5 days. It was observed that NPs were more

effective in eradicating the bacterial growth as compare to free NS. The cations present in the airway surface fluid (63) antagonized the activity of the NS when incubated with bronchial cells and decreased its antibacterial efficiency (27). However improved efficacy was observed with NPs due to the protection of the NS by NPs during incubation with the bronchial cells. NS was released slowly from NPs over days and retained its antibacterial activity against *P. aeruginosa*. Encapsulation in NPs significantly reduced ($p < 0.05$) ($p=0.039$ $p <0.05$ & $p=0.046$; $p< 0.05$ for NSDS PLGA & PEG-NSDS PLGA NPs respectively) the decline in the antibacterial activity of NS (Figure 5.15), and could provide better activity against bacteria *in-vivo*. Further, it was observed that PEGylated NPs were found more effective than non-PEGylated NPs. Reduced negative charge of PEGylated NPs could promote the NPs penetration in bacterial cells. Also faster release of drug from PEGylated NPs as compare to non-PEGylated NPs could enhance it's antibacterial activity.

5.4.1.6 Mucus Penetration

To assess how the composition of the formulation affected NP diffusion through lung lining fluids, the amount of Rhodamine permeated through an artificial mucus layer after 8, 12, and 24 h of release from fluorescent NPs was assessed. As can be seen in Figure 5.16 a higher percent of Rhodamine was found in gelatin when PEG-modified NPs were deposited on the mucus layer as compared to non PEGylated NPs. Mucus is mainly comprised of mucin. Mucin fibers form a network with a mesh spacing size of 30-100 nm which can physically entrap any foreign particulates that exceed this low spacing cut-off (64). The mucus barrier poses a serious obstacle that prevents the penetration of therapeutics across epithelial lining.

Studies shows that particulates as small as 30-60nm can diffuse across mucus matrices (65), however particles above 100 nm in size exhibit retarded diffusivity in mucus. The surface chemistry of the NPs plays a crucial role since mucus could bind various surfaces that come in contact with it by either lipophilic or hydrophilic interactions (66). Consequently, NPs with cationic termini are more likely to adhere to the mucus layer retarding its diffusion. Negatively charged NPs however can also be problematic as they can be electrostatically repelled by the anionic barrier which could explain the retarded diffusion of some negatively charged NPs (67). Uncharged or neutral NPs on the other hand could be highly hydrophobic, which causes considerable hydrophobic interactions and retardation in the mucus in the same fashion as with different bacteria (68).

Quantitative data were supported by visual inspection of the well plates as shown in Figure 5.16, indicating that Rhodamine loaded PEG-NPs diffused faster through mucus. This could be explained by surface charge present on the NPs. Non PEGylated NPs can be electrostatically repelled by the anionic barrier of mucin due to strong negative surface charge which retard their diffusion through the mucus. While PEGylation of NPs enhance their interaction with mucin through formation of hydrogen bonding thus promote their diffusion through mucus (69).

Taken together, these results suggest the great potential of the PEGylated NPs to act in vivo as a drug reservoir which slowly releases the active agent to the target to have a prolonged therapeutic effect.

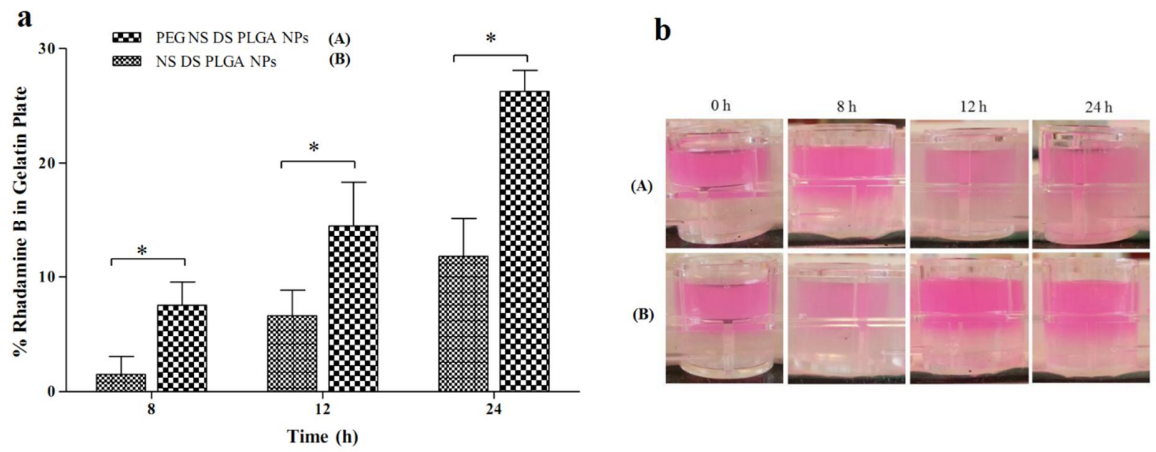

Figure 5.16: a) Percent amount of Rhodamine permeated in the gelatin layer after 8. 12, 24 h. Data are mean ± SD (n = 3); b) visual inspection of NP penetration through an artificial mucus layer (representative image at 8, 12, 24 h). A: PEG NSDS PLGA NPs; B: NSDS PLGA NPs. *Significant difference; $P < 0.05$

5.4.1.7 Safety studies

5.4.1.7.1 Cell viability

Results of the MTT assay are reported in Figure 5.17A. The percentage of cell viability was compared to control cells (100%) obtained at the same time under the same experimental conditions. Positive control SDS treatments showed cell viability of only 10.74±1.92% after 24h of incubation when compared with control cells (100±6.04%). However, test samples containing NS-loaded NPs and blank NPs formulations both demonstrated cell viability of ~80% even after 24h at concentrations as high as 5mg/mL compared to control. Results showed that NPs exhibit

cell toxicity in a dose-dependent fashion. Further incorporation of DSPE-PEG in formulation helps in improving cell viability (Figure 5.17 A) due to reduction in surface charge, suggesting their safe use in these formulations

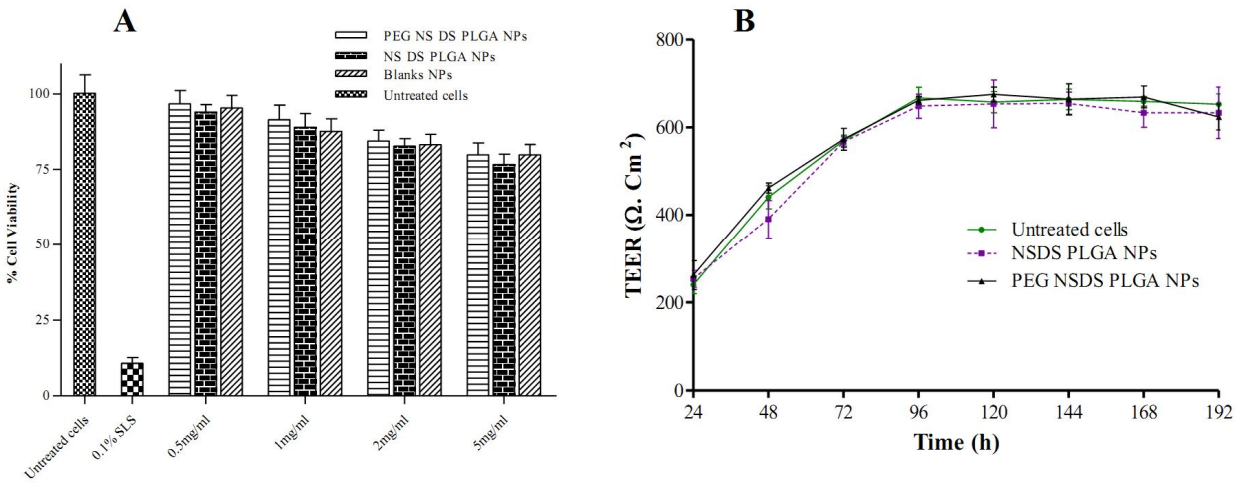

Figure 5.17: A) Effects of NP formulations on viability of CFBE 41 o- cells after 24 h incubation.Test samples contained 0.5 mg/mL, 1 mg/mL, 2 mg/mL and 5 mg/mL of formulation. Datarepresent mean ± SD, n =6; 6 (* results are significantly different from other treatment groups, $p < 0.05$) **B)** TEER analysis of CFBE 41 o- cells layers exposed to NPs over time. We observed that there was significant difference in TEER when using the NSDS PLGA NPs as compared to the control ($p=0.03$; $p<0.05$ for NSDS PLGA NPs and control & $p=0.22$; $p>0.05$ PEG-NSDS PLGA NPs and control). The results of MTT & TEER study suggest the safe use of developed NPs system.

5.4.1.7.2 TEER Analysis

Transepithelial electrical resistance (TEER) measurements were performed on CFBE41o- cells to determine the effect of NS-loaded NPs on cells under liquid/liquid culture conditions. The presence of an intact cell monolayer was confirmed by steady TEER values (450−500 Ωcm^2) after 3 days of culturing and the monolayer was visible by light microscopy. After exposure to the NPs, TEER was measured at a defined time interval for 5 days. TEER depends on tight junctions between cells, which can be disrupted by noxious stimuli (70) and therefore provides a convenient measure of barrier function (71). NPs at a concentration of 2mg/mL, which was shown to yield at least 85 % cell viability, was used to evaluate the resistance of the epithelial

layer. The PEGylated NPs doesn't show any significant difference in the TEER value when compared to the control ($p=0.22$; $p > 0.05$). While in case of the non-PEGylated NPs the decrease in TEER value observed. This could be attributed to the charge on the particles. (Figure 5.17B). Although Fiegal et al. reported change in the barrier properties of lung epithelial cells during exposure to PLGA NPs (72), this was not observed with PEGylated PLGA NPs mentioned in the present work. Taken together, these results suggest that the safety of NPs *in vitro* and need *in vivo* evaluation for further confirmation.

5.4.1.8 Cell uptake study

Rhodamine loaded NPs used to assess cellular association and uptake of NPs (Figure 5.18). Both PEGylated and non-PEGylated NPs showed cell uptake, as revealed by fluorescence microscopy. PEGylated NPs shows significantly higher cell uptake than non-PEGylated NPs. This observation was further confirmed by the quantitative fluorescence spectrophotometric analysis (Figure 5.18 C). The uptake of PEGylated NPs in the cells was significantly higher than non-PEGylated NPs ($P=0.02$; $P <0.05$).The results shows that PEGylated NPs has lower zeta potential as compare to non PEGylated NPs, which seems to provide better cell uptake. A. Ibricevic et al reported that entry of PEGylated particles followed clathrin-independent endocytosis pathway, while non-PEGylated particles follow clathrin-dependent route for endocytosis (73). Thus, PEGylation promote the uptake of the NPs. PEG could serve a variety of functions such as to reduce aggregation and aid in diffusion of the particles, and shield the high surface charge of NPs. Suh et al (74) also reported that the PEGylation increases average NPs diffusivities by 100% compared to nonPEGylated particles in live cells. They hypothesized that PEGylation of therapeutic colloids improve their cytoplasmic transport (once the particles have escaped endosomal vesicles) by minimizing attractive forces to cytoskeletal elements, such as microtubules or actin filaments, or to other intracellular organelles. Saduzuka et al. (75) also studied the cellular uptake of PEGylated liposomes and reported significantly higher cellular uptake due to PEGylation.

These findings will opens new door to treat intracellular bacterial infections in CF. To treat intracellular bacterial infections, it is important that, drug must penetrate across the mucus layer and deliver the drug pay load to the underlying epithelium. This phenomenon is important to treat intracellular infections in CF (76, 77).

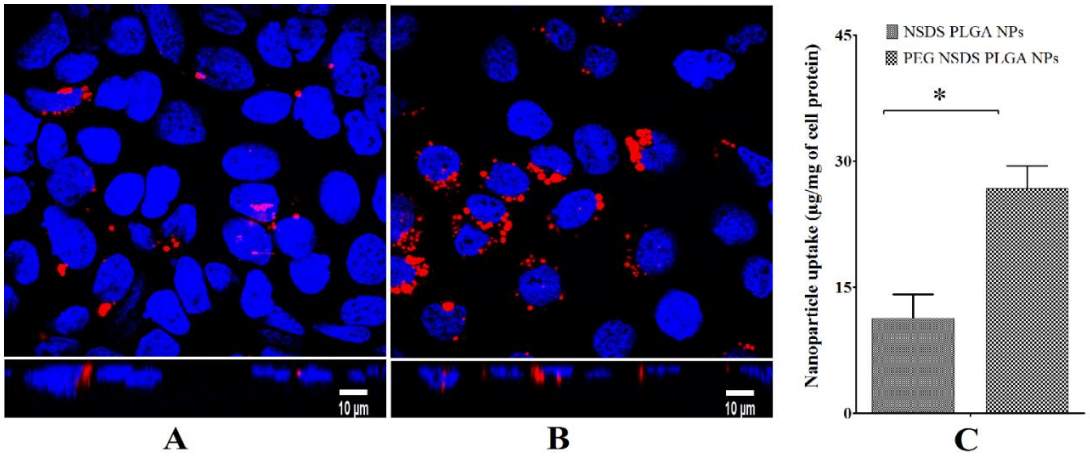

Figure 5.18: Confocal microscopy of CFBE cells (63X) after 24 hours of incubation with NPs: A)PEG NSDS PLGA NPs; B) NSDS PLGA NPs; C) The NPs uptake in CFBE cells (n = 9). Top images represent slices from the middle of a z-stack of a CFBE cells. Bottom images are projections in the z-axis created from a z-stack of the same CFBE cells displayed in the top image*Significant difference; P=0.02; P < 0.05. Cells were treated with Rhodamine loaded NPs (red), fixed and nucleus stained with Hoechst dye. A more efficient NP uptake is apparent for PEGylated NPs as compared to non-PEGylated NPs.

5.4.1.9 Stability study

The stability of NPs was assessed by suspension in 0.9% saline simulated lung fluid & 10% fetal bovine serum by evaluating particle size measurements at fixed time intervals. The NSDS PLGA NPs showed increased particle size over the period of time (Figure 5.19).The enhanced particle size is due to the flocculation effect induced by cations present in the solutions. However serum proteins (particularly albumin) bind with NPs which also responsible for enhanced particles size when incubated with serum. The resulted aggregates limits their cell uptake (78). Addition of PEG in NPs preparation gives a significant advantage in shielding the NPs from adsorption of proteins (79). DLS sizing measurements demonstrate that the PEG NSDS PLGA NPs remain stable over 48 h with no significant change in size (Figure 5.19). This result suggests that the DSPE–PEG 2000–COOH density on the NPs does not drop below the range of full electrostatic and steric stabilizations over the time period. This result suggests that the current formulation has sufficient stability derived from steric repulsion due to the hydrodynamic diameter of the PEG chain and electrostatic repulsion from the negatively charged carboxylic-end group, as well as

adequate coverage of the polymeric core (80-82). Based on this study, NSDS PLGA NPs are less favorable, compared to PEGylated NPs, for pulmonary administration as their instability in media may lead to reduced therapeutic efficacy due to faster clearance from the lung.

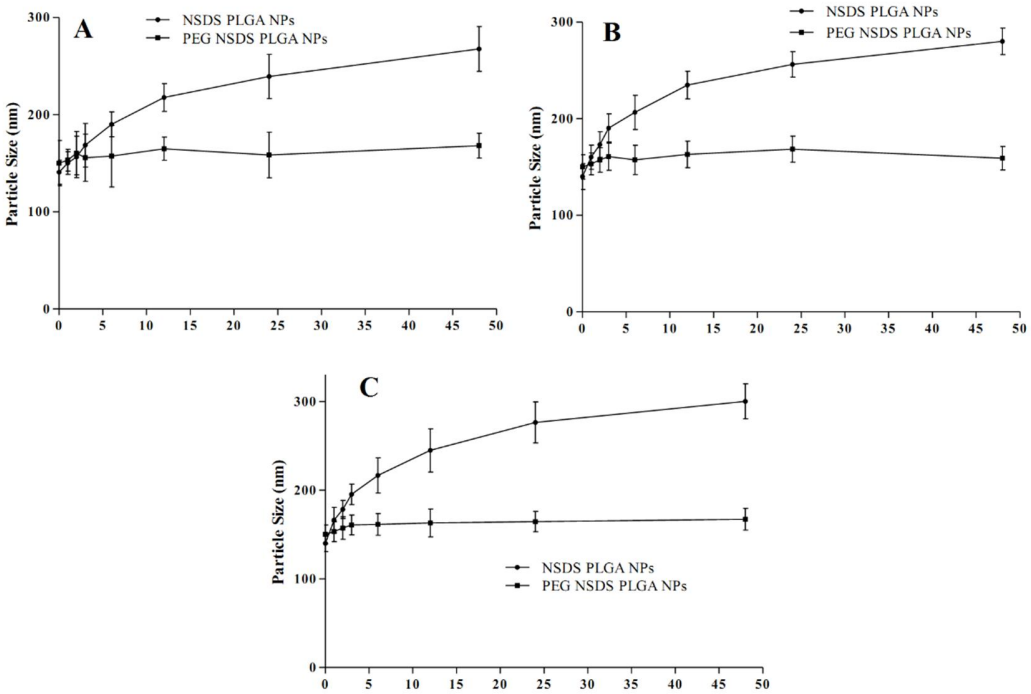

Figure 5.19: Stability of NPs was tested by measuring particle size in (A) saline solution; (B) simulated lung fluid at 37 °C; (C) 10% fetal bovine serum. The PEGylated NPs remained stable for up to 2 days while non PEGylaed NPs tended to show aggregation, indicating comparatively less stability. Data are shown as mean ± SD (n = 3)

From the all results obtained it is observed that PEGylated NPs system is most promising drug delivery system hence, it will be used for further studies.

5.4.2 Development of pDNA loaded NPs

Lack of efficiency and/or safety of viral and liposomal vectors for the treatment of genetic disorders, such as CF, has prompted investigation into novel polymer-based systems for disease treatment. PLGA represents an FDA-approved, biocompatible material that has been extensively studied for gene delivery purposes but has also lacked efficiency as a gene delivery vehicle on its own (21,83,84). This lack of efficient expression is probably due to the negative charge on PLGA at physiologic pH, which leads to low DNA encapsulation and limited association with the negatively charged plasma membrane of cells. Gene delivery efficiency is highly affected by the physicochemical properties of NPs which in turn depends on the method of preparation of NPs. Prior to systematic comparison between two different PLGA-based NPs systems, we have evaluated various formulations for determination of the optimal PLGA-based NPs.

5.4.2.1 Preparation and characterization of pDNA-loaded, PEI-modified PLGA NPs

In this study, we used modified water/oil/water (w/o/w) emulsion method for preparation of PLGA-PEI NPs. According to several literatures, PEI dissolved in organic solvent likely partitions the water/organic interface during the process of NP formation due to its hydrophilicity (85). Various solvents were tried for initial screening and based on initial evaluations chloroform was selected as an organic solvents for preparation of NPs. D.N. Nguyen et al. (85) reported that bulk of the PEI was distributed within the surface of the poly(ortho ester)(POE) microsphere matrix due to diffusion, and only little amount of PEI was found in the core which also increased zeta-potential. POE has two monomeric units, glycolic acid and lactic acid in their backbone and has been synthesized by the incorporation of residues of glycolic and lactic acid by pH-sensitive orthoester linkage into the polymer backbone. It is noteworthy that POE microspheres have similar hydrophobic features as that of PLGA. Sonication process was used for preparation of NPs may affect the pDNA integrity which results in loss of pDNA activity. Thus, before processing for the NPs preparation effect of process parameters mainly sonication amplitude and sonication time were evaluated of pDNA integrity. Initial trials were taken to decide the sonication amplitude and sonication time for primary and secondary emulsification.

During preparation of NPs particles were sonicated using probe sonicator at 10, 20, 30 amplitude for 20 sec to generate primary and secondary emulsion. The effect of sonication on pDNA integrity was evaluated by extracting pDNA at various stage using chloroform and diluted with TE buffer. The extracted plasmid was then analyzed by using agarose gel electrophoresis (0.8 %)

(Figure 5.20). The results of gel electrophoresis showed intact nature of the pDNA extracted from both 1° and 2° emulsion when compared to untreated pDNA, indicates that the used amplitude for emulsification process doesn't disrupt pDNA. The amplitude 20 was used for further process.

Further primary and secondary emulsions were sonicated at amplitude 20 for 20, 30, 40 seconds to know the effect of sonication time on pDNA integrity and evaluated by agarose gel electrophoresis (0.8 %) (Figure 5.21). The results of gel electrophoresis showed intact nature of the pDNA extracted from both 1° and 2° emulsion at various time points when compared to untreated pDNA, indicate that the used sonication time for emulsification process doesn't have strong impact on integrity of DNA. The sonication time 30 sec was used for further process.

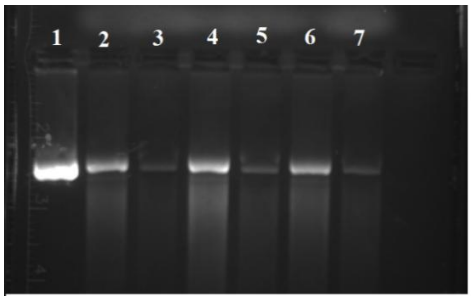

Figure 5.20: Agarose gel electrophoresis of pDNA extracted at various stage during process optimization.Lane 1: Control non-treated Plasmid; Lane 2: Amplitude 10, 1^0 Emulsion; Lane 3: Amplitude 10, 2^0 Emulsion; Lane 4: Amplitude20, 1^0 Emulsion; Lane 5: Amplitude20, 2^0 Emulsion; Lane 6: Amplitude30, 1^0 Emulsion; Lane 7: Amplitude30, 2^0 Emulsion.

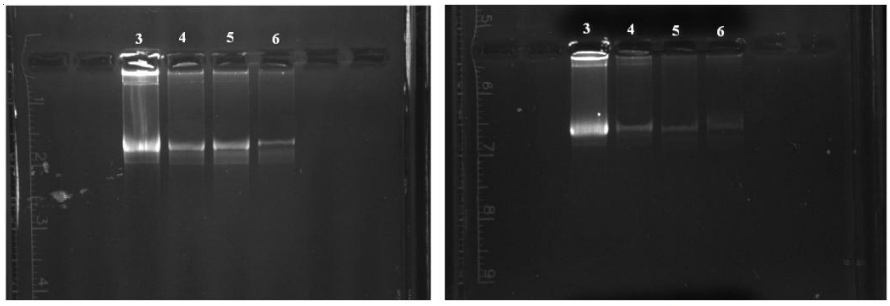

A **B**

Figure 5.21: Agarose gel electrophoresis of pDNA extracted at various stage during process optimization. **A**: Primary emulsion: Lane 3: Control non-treated Plasmid, Lane 4: Sonication time 20 sec, Lane 5: Sonication time 30 sec, Lane 6: Sonication time 40 sec; **B**: Secondary emulsion: Lane 3: Control non-treated Plasmid, Lane 4: Sonication time 20 sec, Lane 5: Sonication time 30 sec, Lane 6: Sonication time 40 sec.

The PEI-modified PLGA NPs were prepared by inclusion of PEI in the organic phase at different PEI to PLGA weight ratios. The composition, size, PDI and zeta-potential of the resulting formulations are listed in Table 5.9. The size of the NPs was affected by inclusion of PEI into the PLGA matrix, and a significant concentration-dependent decrease in size was observed at increased PEI concentrations ranging from 246.8 ± 7.59 nm for the unmodified NPs to 166.2 ± 2.55 nm at 12.5% (w/w) PEI. The PDIs were below 0.216 for all compositions, suggesting relatively mono-disperse suspensions (Table 5.9). The incorporation of increasing amounts of the cationic polymer PEI into the PLGA matrix resulted in a significant reduction of the particle size and PDI. The decreased particle size along with the introduction of PEI into the PLGA matrix occur as a result of the reduced interfacial tension between the particle surface and the aqueous medium. In addition, the reduced particle size could be a result of a condensation of the PLGA polymer upon interaction with the cationic polymer PEI (86).

The zeta-potential was also significantly affected by the inclusion of PEI and a PEI-ratio dependent increase in the zeta-potential was observed ranging from - 06.53±1.00 mV for unmodified PLGA NPs to + 34.00±2.44 for particles containing 12.5% (w/w) PEI. This negative charge for unmodified PLGA NPs is due to uncapped end carboxyl groups of PLGA present on the surface of the particles(87). However, such negatively charged particles are unable to encapsulate negatively charged pDNA. To render the PLGA NPs with a positive zeta potential, in the present study, we dissolved PEI in the organic phase along with PLGA. The results of Table 5.9 show that indeed positively charged PLGA NPs were obtained. The zeta-potential of the PLGA NPs was increased from negative to positive at increasing content of PEI, suggesting that PEI molecules are present on the surface of the NPs, which is further confirmed by FTIR study. Figure 5.22 A & B shows the results of particle size and zeta potential of NPs containing 10 % PEI (particle size: 180.3± 2.06 nm (PDI = 0.097 ± 0.004); zeta potential: + 27.66 ± 2.05 mV).The TEM image (Figure 5.22C) of NPs further reveals that NPs are spherical in shape and uniform in size

The pDNA encapsulation efficiency was also positively affected by the addition of PEI (Table 5.9). The results showed a significantly increased pDNA encapsulation efficiency as PEI increase. ~100 % pDNA loading was obtained at 10 % PEI. pDNA is negatively charged and highly hydrophilic in nature make it difficult to entrap into negatively charged highly hydrophobic polymer. Addition of the positively charged PEI molecule in the system results in

the formation of hydrophobic complex between positively charged PEI with negatively charged pDNA. This hydrophobic cationic complex get easily entrapped in PLGA core thus enhances pDNA loading (86).

Table 5.9: Physicochemical characterization of pDNA loaded PEI-PLGA NPs.

Formulation (% PEI)	Particle size (nm ± SD)	PDI ± SD	Zeta Potential (mV ± SD)	Encapsulation efficiency % ± SD
PLGA alone	246.8 ± 7.59	0.216 ± 0.016	- 06.53 ± 1.00	10.46 ± 3.83
2.5	230.56 ± 6.50	0.170 ± 0.024	+ 07.63 ± 1.53	30.20 ± 5.47
5	208.2 ± 6.52	0.123 ± 0.020	+ 12.46 ± 2.12	57.66 ± 5.43
7.5	192.7 ± 5.51	0.186 ± 0.028	+ 20.93 ± 2.69	81.00 ± 4.54
10	180.3 ± 2.06	0.097 ± 0.004	+ 27.66 ± 2.05	98.66 ± 1.24
12.5	166.2 ± 2.55	0.092 ± 0.005	+ 34.00 ±2.44	99.16 ± 0.84

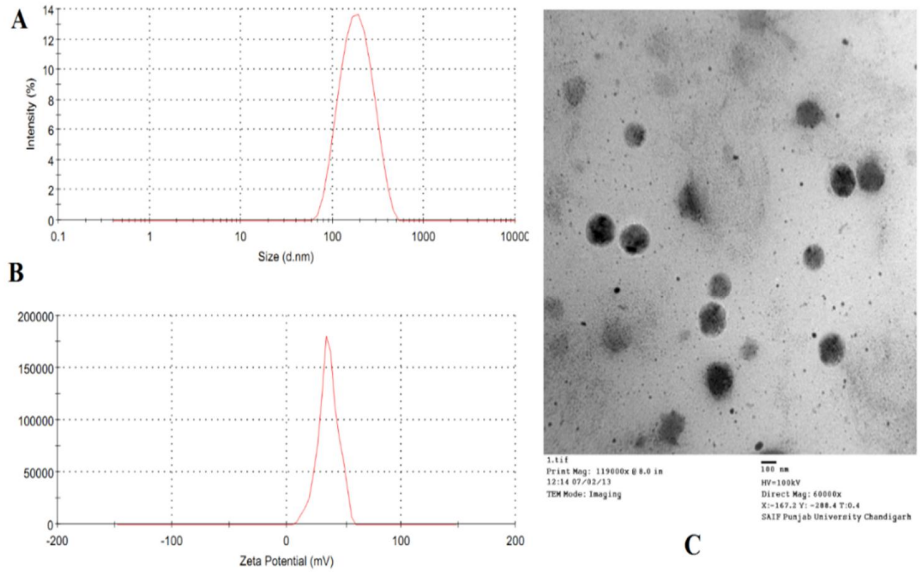

Figure 5.22: **A)** The DLS results show that size of NPs is 180.3 ± 2.06 nm (PDI = 0.097 ± 0.004); **B)** zeta potential (+ 27.66 ± 2.05 mV) of PEI-PLGA NPs (10%w/w PEI); **C)** TEM micrographs of PEI-PLGA NPs (10%w/w PEI). DLS based characterization of size and zeta potential of NPs confirms that size distribution and colloidal stability of mono-dispersed particles. TEM based size and surface characterization of NPs confirms size distribution and colloidal stability of mono-dispersed particles

5.4.2.2 FTIR studies

FTIR study was used to confirm the presence of PEI on NPs surface. When PEI added to organic solution containing PLGA, process involves the electrostatic interactions of PEI with the negatively charged surface of PLGA NPs, but possibly PEI also had reacted with PLGA by aminolysis (88). This reaction results in the formation of amide bonds connecting PEI and PLGA which was further confirmed by FTIR spectroscopy. The FTIR spectrum of the PEI, PLGA, PLGA/PEI NPs are shown in Figure 5.23. The FTIR spectrum of PEI shows peaks at 2955.80 and 2847.49 cm^{-1} that can be attributed to asymmetric and symmetric vibrations of the CH2 group, respectively, and the peak at 1457.07 cm^{-1} corresponds to in-plane bending of CH2. The peaks for the bending vibration of the NH group and the stretching vibration of the C-N groups of PEI can be seen at 1589.12 cm^{-1} and1124.30 cm^{-1}, respectively (89). Peak at 1635.92 cm^{-1} evident of NH2-vibration of PEI (90). In the PLGA FTIR spectrum, peaks at 3506.64 cm^{-1} for –OH stretching and 3000.18 – 2955.77 cm^{-1} for C-H stretching bands were observed as the typical band of PLGA. The ester C=O stretching band of PLGA was observed at 1757.01 cm^{-1}.On the other hand, the spectrum of the PEI PLGA NPs showed a peak at 1752.82 cm^{-1} indication the PLGA ester C= O stretching peak. Apart from a NH2-vibration of PEI at 1636.26 cm^{-1}, a weak but evident absorbance at 1623.12 cm^{-1} of amide bonds (90) is also detected in PEI PLGA NPs.

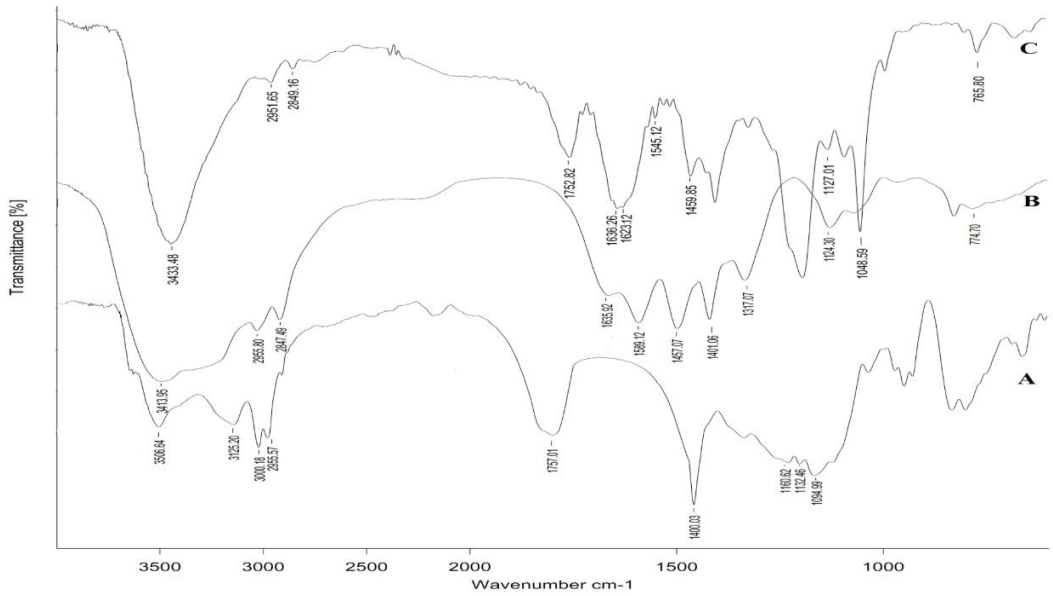

Figure 5.23: Overlay of FTIR spectra of A) PLGA, B) PEI, C) PEI PLGA (10%) NPs. Presence of characteristic PEI peaks in the NPs sample indicates that the presence of PEI on NPs surface.

5.4.2.3 In-vitro release study

The timing of NP degradation and DNA release appears to have a significant modulating effect on the gene expression (91).We hypothesized that incorporation of PEI into the PLGA matrix would influence the release kinetics of pDNA as well as transfection efficiency. Therefore the comparison between two systems could provide a complete understanding of their physicochemical properties and it will also give rational view for excipient selection for formulation development. The in-vitro release of pDNA from both of the two formulations was studied at pH 7.4 and pH 5.0. DNA quantity was calculated from a standard curve of known concentrations as discussed in chapter 4. Here we compared the kinetics of pH-triggered release of pDNA from PLGA NPs containing different weight of PEI. To simulate acidic condition in the endolysosome of cells following intracellular uptake, NPs were incubated in PBS pH 7.4 for 24 h and then the half of NPs were transferred to a solution having pH 5.0 to mimic endolysosomal condition. At predetermined time points, pDNA release was measured by QuantiFluor™ dsDNA System (Promega). It was observed that the incorporated pDNA were released rapidly from NPs within 48 h, followed by very slow release until day 10 (Figure 5.24). Initial higher burst of pDNA release was observed for the unmodified PLGA NPs systems than that observed for PLGA-PEI NPs. It was observed that increasing concentration of PEI in NPs system significantly reduces burst release. This difference might be due to the strong electrostatic interactions between PEI and pDNA. Also being a hydrophilic molecule located at the NPs surface, PEI may facilitate degradation of the NPs by increasing hydration and thus accelerate PLGA hydrolysis (92). However, the cationic nature of PEI may retard pDNA release due to the electrostatic attractions between them thus sustain the PEI release. Further PEI content could be judiciously utilized in controlling the sustained release of pDNA.

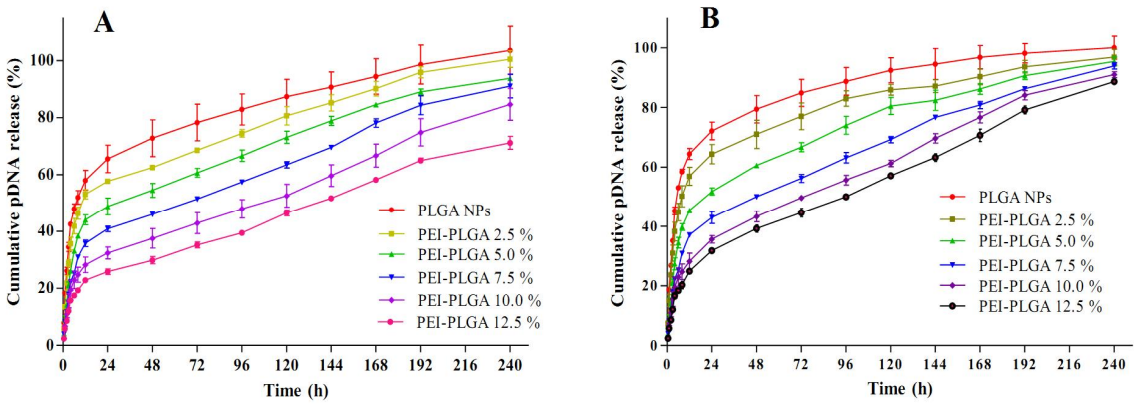

Figure 5.24: Cumulative release of pDNA from NPs A: PBS pH 7.4; B: Sodium acetate buffer (pH 5.0) at 37 ^{o}C

In both the cases, at the initial phases no significant change in release rate was detected even though the samples were incubated at pH 5.0. But, the release rates were abruptly accelerated around day after 24 h only at pH 5.0 for all formulations. This result could be attributed to the pH dependent degradation nature of PLGA. PLGA is degraded through cleavage of the ester linkage which leads to the generation of lactic acid (LA) and glycolic acid (GA), and finally to CO_2 and H_2O (93). They have observed that after one day PLGA microparticles (MW = 25,000) started to change their spherical geometry and showed a decrease in MW as well. The results showed the fragmentation of microparticles at pH 5.0, however, at pH 7.4, the surface erosion was noticed (93). These results indicates that the release of the pDNA from PLGA-PEI or PLGA-NPs is depends on the on the degradation kinetics of PLGA matrix after initial burst of the pDNA that located at the NPs surface.

The structural integrity of the plasmid released from NPs at various time point was observed using 0.8% agarose gel in comparison with control DNA (Figure 5.25). It can be observed that the DNA released specifically from PLGA-PEI (10%) was predominantly supercoiled in form, intact and comparable with the native DNA in both media. These results indicate that NPs could protect the loaded plasmid DNA from degradation in the release duration.

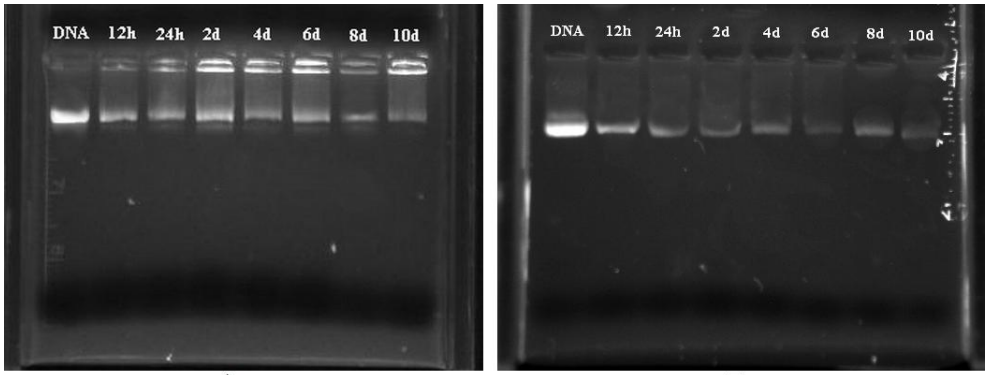

Figure 5.25: Structural integrity of pDNA released from NPs (PLGA-PEI 10 %) A: PBS pH 7.4; B: Sodium acetate buffer (pH 5.0).

5.4.2.4 In vitro bioactivity

Particle formulations were evaluated for their ability to transfect cells in culture. CFBE41o − cells were chosen as a relevant target cell line for therapy. Transfection efficacy for all particle preparations was determined by quantifying the expression of luciferase encoded on the plasmid on 2, 4 and 10 days after transfection. The blending of PEI with the PLGA matrix resulted in increased transfection. Other research groups also have shown increased transfections with surface modified PLGA nano- and microparticles with cationic polymers (94-96). It was observed that increased PEI concentration increases luciferase transfection (Figure 5.26). This could be attributed to the increase positive charge on particles which promote cell uptake and thus luciferase expression. These results are in agreements till PLGA PEI NPs 10%. At 12.5% PEI luciferase expression was reduced as compared to 10 % PEI. These results could be explained by considering PEI-induced cytotoxicity as well as intracellular localization. Surface adsorbed PEI chain promote cellular uptake which results in large amount of cell death and induced decrease in transfection efficiency of PLGA-PEI NPs 12.5 %. High coating concentrations of PEI showed high membrane toxicity in cells (97).

Naked pDNA transfected cells were used as negative control and the Lipofectamine plus (Invitrogen) transfected cells were used as a positive control. In case of naked DNA, luciferase expression were observed negligible as compare to the NPs and lipofectamine plus. This could be attributed to the low transfection efficiency due to the negative charge of pDNA. Though pDNA gets internalized into cells pDNA could be degraded in endosome before reaching to the

nuclei. After 48 h lipofectamine plus shows highest luciferase expression than NPs. But following 48 h luciferase expression was reduced as compared to NPs. While in case of NPs luciferase expression was observed consistent even till 144 h. This could be attributed to the sustained release of DNA from NPs. In case of PLGA NPs, the majority of DNA may have been released prior to internalization into the cells in transfection medium due to initial burst release. However negative charge on the PLGA NPs also reduces its internalization in cell could also be attributed to the reduced luciferase expression. With increase in PEI %, positive charge on the NPs surface increase, which results in much more favorable electrostatic interactions with the cell membrane, facilitating internalization into the cells. Cationic charge on the surface of microparticles has demonstrated increased uptake of particles in both monocytes and dendritic cells (98). Additionally, being a hydrophilic molecule mounted at the NPs surface, PEI may accelerate NPs degradation by inducing hydration. Following hydration, NPs release PEI/pDNA complex only without any release of free pDNA (99), and as a result it may promote transport of PEI/pDNA complexes towards the nuclei (100). On the other hand, in case of PLGA-NPs, pDNA located at the surface of NPs was released very rapidly due to absence of any electrostatic interactions.

We observed that, out of all formulations PLGA-PEI NPs 10 % showed better transfection efficiency, thus we chose it for further evaluations.

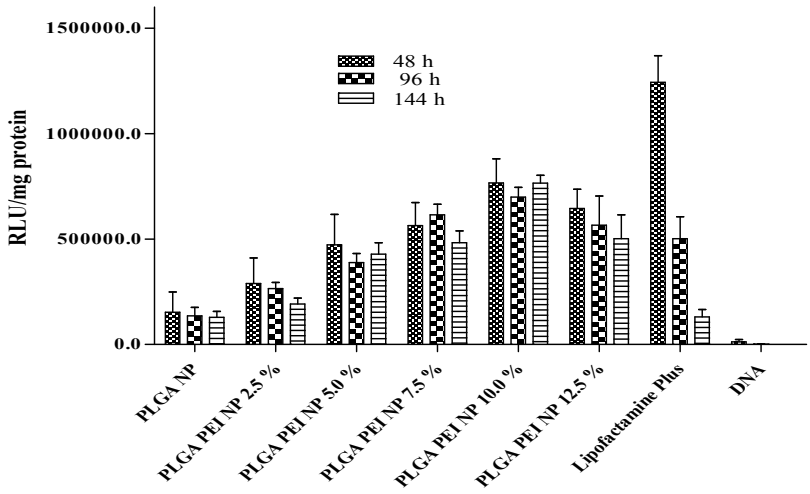

Figure 5.26: Transfection of CFBE cells treated with PEI-PLGA NPs encapsulating pCDNA-3 LUC-WT plasmid along with large T antigen and normalized to total protein content. Particle formulations contained PLGA and 0%, 2.5%, 5%, 7.5%, 10% and 12.5% PEI. Transfection

efficiencies were compared to Lipofectamine plus (prepared according to the manufacturer's instructions) as a positive control and pDNA as a negative control.

5.4.2.5 Safety studies

5.4.2.5.1 Cell viability

Particle toxicity was evaluated by using the MTT assay after exposure to controlled doses of particles (Figure 5.27). There was a substantial increase in particle toxicity which increases in dose and PEI content. NP-10 and NP-12.5 formulations produced considerable cell toxicity especially at high doses. These cytotoxic effects are likely due to the high positive surface charge imparted by the PEI, which is apparent from the increased zeta potential with increasing PEI content. Though PEI is considered to be the most effective cationic polymer for gene delivery, it is also associated with dose-dependent toxicity, especially at high molecular weight which further results in reduced transfection efficiency (101). Thus, we aimed to reduce the toxicity of the formulations and thus to improve the transfection efficiency.

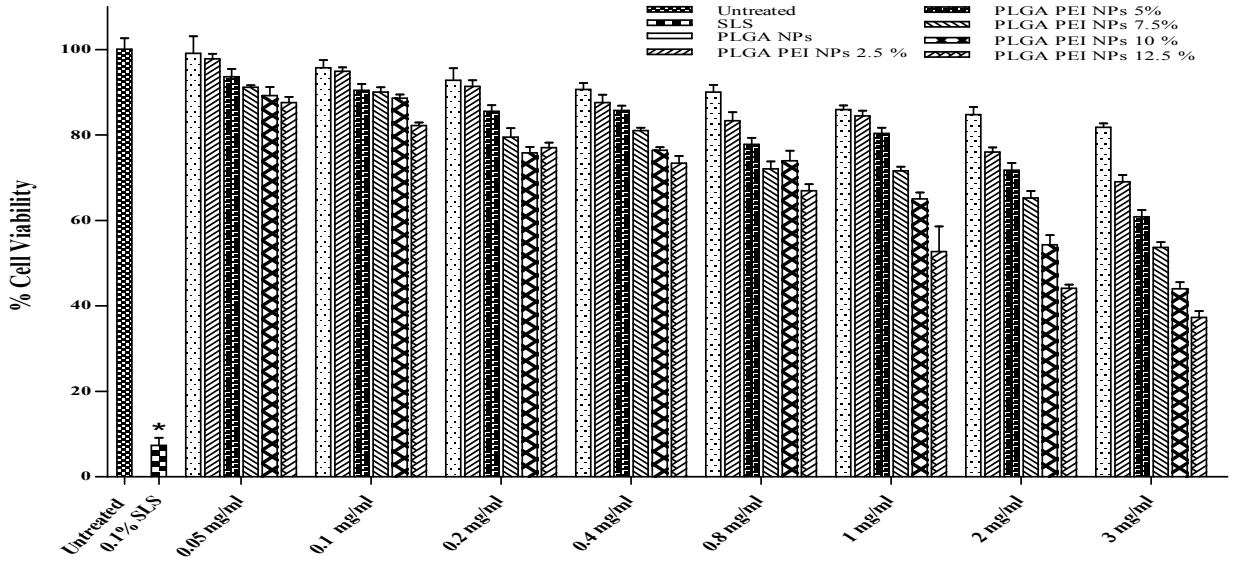

Figure 5.27: A) Effects of NP formulations on viability of CFBE 41 o- cells after 24 h incubation. Test samples contained 0.05 mg/mL, 0.1 mg/mL, 02 mg/mL, 0.4 mg/mL, 0.8 mg/mL, 1 mg/mL, 2 mg/mL and 3 mg/mL of formulation. Data represent mean ± SD, n =6; (* results are significantly different from other treatment groups, $p < 0.05$)

5.4.2.6 PEGylated PEI-PLGA NPs

It was reported that PEG covalently linked to DSPE - a lipid that tethers PEG to the NP surface through interaction with the hydrophobic polymer matrix can be used to coat the surface of

PLGA NPs with PEG and PEG-ligand conjugates (24). Here, we used that approach to add PEG to PEI-PLGA NPs. We chose to add this surface modification to PLGA-PEI NPs 10 % particles because they showed the most promise as a transfection vehicle in CFBE41o– cells (Figure 5.26). DSPE-PEG is amphiphilic molecule was designed to hydrophobically associate with sthe polymer matrix via the acyl chains in DSPE, and present a PEG moiety on the particle surface(24).

5.4.2.6.1 Characterization of PEGylated PEI-PLGA NPs

PLGA-PEI NPs 10 % formulation was surface modified using DSPE-PEG at 3 % w/w lipid to-polymer content. Characteristics of prepared PEGylated PLGA-PEI NPs are summarized in Table 5.10 in terms of size, PI, zeta potential and EE. The PEGylated NPs were successfully prepared with essentially spherical morphology and mean particle diameter of ~ 190 nm (Figure 5.28). PEGylation doesn't affect EE of pDNA in NPs (Table 5.10).

Table 5.10: Physicochemical characterization of PEGylated pDNA loaded PEI-PLGA NPs. Results denote mean ± SD

Formulation	Particle size (nm ± SD)	PDI ± SD	Zeta Potential (mV ± SD)	Encapsulation efficiency % ± SD
PLGA NPs	240.1±5.20	0.223±0.012	- 07.46 ± 1.46	12.73 ± 2.37
PEI-PLGA NPs 10 %	178.9±4.33	0.090±0.008	+ 28.33 ± 2.86	99.00 ± 0.81
PEG- PEI-PLGA NPs 10 %	189.5±4.22	0.059±0.041	+ 16.66 ±2.49	99.90 ± 0.14

Surface modification with PEG significantly reduces zeta potential as compared with PLGA-PEI NPs (Table 5.10). This could be due to the shielding effect imparted by PEG. Further presence of PEG on NPs surface further confirmed by FTIR spectroscopy (Figure 5.29). In Figure 5.29 DSPE PEG 2000 FTIR spectrum showed peaks of C=O at 1738.59 cm^{-1}, aliphatic CH_2 band at 2919.29 cm^{-1}, CH_3 band at1352.79 cm^{-1}, O-CH_2 band at 1101.19 cm^{-1} and C=C band at 1642.67 cm^{-1}. All these characteristic peaks were also observed in PEGylated NPs which confirms the PEGylation of NPs.

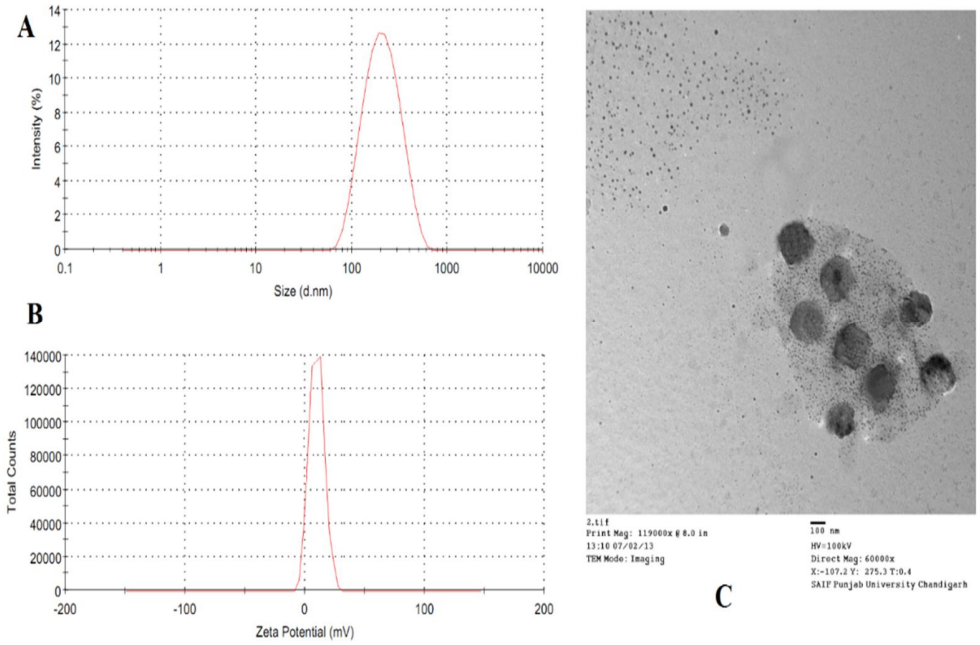

Figure 5.28: **A)** The DLS results show that size of NPs is 189.5 ± 4.22 nm (PDI = 0.059 ± 0.041); **B)** zeta potential + 13.66 ±1.69 mV of PEGylated PEI-PLGA NPs (10%w/w PEI); **C)** TEM micrographs of PEGylated PEI-PLGA NPs (10%w/w PEI). DLS based characterization of size and zeta potential of NPs confirms that size distribution and colloidal stability of mono-dispersed particles. TEM based size and surface characterization of NPs confirms size distribution and colloidal stability of mono-dispersed particles

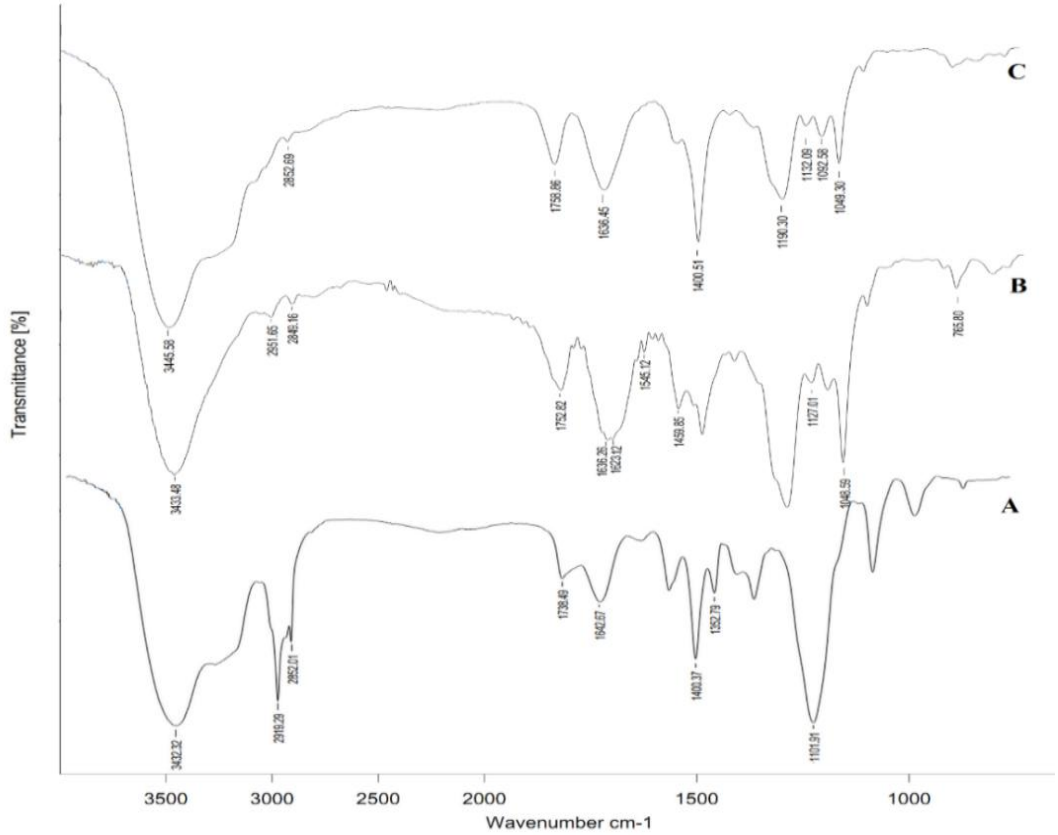

Figure 5.29: FTIR spectra of A) DSPE PEG 2000 B) PEI PLGA NPs, C) PEGylated PEI PLGA NPs. The characteristic DSPE PEG 2000 peaks in the NPs confirms the PEGylation of NPs.

Further this formulations were used to prepare fluorescently-labelled NPs (6-coumarin loaded NPs) for *in-vitro*/*in-vivo* studies. Particles were characterized in terms of size, PI, zeta potential and encapsulation efficiency (Table 5.8). Total amount of 6-coumarin entrapped in NPs was determined after dissolving NPs in Chloroform: Methanol (1:1). The amount of 6-coumarin in resulting solution was then determined by using a Spectrofluorometer (RF-5301PC, Shimadzu) at excitation and emission wavelengths of 430 and 485 nm. The obtained particles were uniform in size with similar characteristics as that of pDNA loaded NPs (Table 5.8).

Table 5.11: Summary of drug encapsulation efficiency, particle diameter and Zeta potential of 6-coumarin loaded PLGA NPs (mean ± SD, n = 3).

Formulation	Particle size (nm ± SD)	PDI ± SD	Zeta Potential (mV ± SD)	EE % ± SD
C-6 PLGA NPs	248.4±4.80	0.230±0.014	- 08.06±1.51	97.66±1.24
C-6 PEI-PLGA NPs 10 %	181.6±4.05	0.091±0.030	+ 29.66±3.09	96.33±3.09
C-6 PEG- PEI-PLGA NPs 10 %	193.8±5.20	0.062±0.043	+ 17.33±2.49	95.23±3.99

5.4.2.6.2 In-vitro release study

Further effect of PEGylation on the in-vitro release of pDNA from NPs was studied at pH 7.4 and pH 5.0 (Figure 5.30). DNA quantity was calculated from a standard curve of known concentrations as discussed in chapter 4. There was a significant difference in release from non-PEGylated and PEGylated NPs in both media ($p= 0.00001$; $p < 0.05$ & $p=0.012$; $p< 0.05$ for PBS pH 7.4 & Sodium acetate buffer pH 5.0 respectively). However it was observed that the incorporation of PEG enable a greater influx of water into the NPs matrix, accelerate PLGA hydrolysis and thus promoting greater degradation of PLGA and improved DNA release from NPs.

To evaluate the mechanism of pDNA release from NPs, the release data were analyzed by using the Korsmeyer–Peppas equation: $Q_t/Q_\infty = k \times t^n$

Where, Q_t/Q_∞ is the fraction of released drug, t is the release time, k is a constant characteristic of the drug–polymer system, and n is release exponent that characterizes the mechanism of drug release (61). The calculated diffusional exponent (n) and kinetic constant (k) for the PEI-PLGA NPs 10 % formulations were found to be 0.4448 & 0.9899 in PBS pH 7.4; 0.4729 & 0.9914 in Sodium acetate buffer (pH 5.0) respectively. While that for diffusional exponent (n) and kinetic constant (k) for the PEG PEI-PLGA NPs 10 % formulations were found to be 0.4462 & 0.9918 in PBS pH 7.4; 0.4890 & 0.9909 in Sodium acetate buffer (pH 5.0) respectively. As the n value is < 0.5, one can conclude that the release of pDNA from NPs was by Fickian diffusion (62). Further structural integrity of the plasmid released from NPs at various time point was observed using 0.8% agarose gel in comparison with control DNA (Figure 5.31). It can be observed that the DNA released from PEG PEI-PLGA NPs (10%) was predominantly supercoiled (S.C.) in

form, intact and comparable with the native DNA in both media. These results indicate that NPs could protect the loaded plasmid DNA from degradation in the release duration

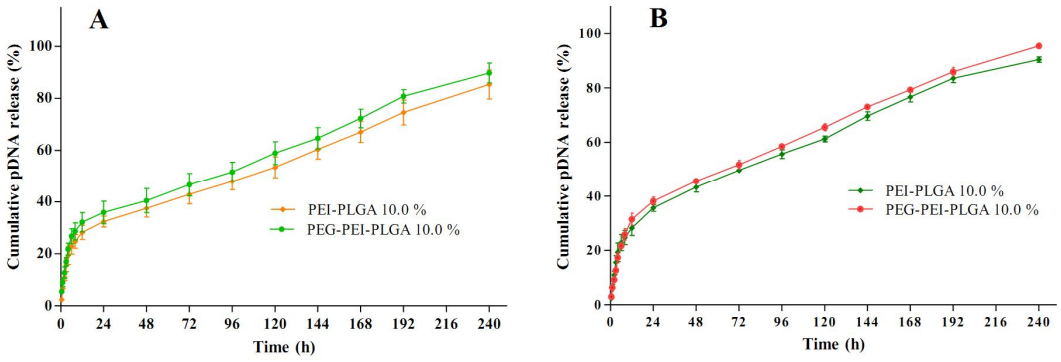

Figure 5.30: Cumulative release of pDNA from NPs A: PBS pH 7.4; B: Sodium acetate buffer (pH 5.0) at 37 °C

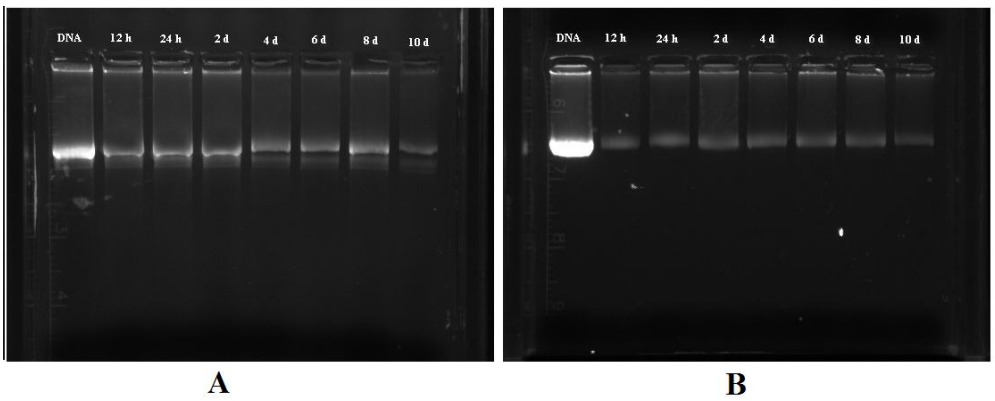

Figure 5.31: Structural integrity of pDNA released from NPs (PEG-PEI-PLGA 10 %) A: PBS pH 7.4; B: Sodium acetate buffer (pH 5.0).

5.4.2.6.3 In-vitro bioactivity

5.4.2.6.3.1 Luciferase Expression

PEGylated particle formulations were evaluated for their ability to transfect cells in culture. CFBE41o − cells were chosen as a relevant target cell line for therapy. Transfection efficacy for all particle preparations was determined by quantifying the expression of luciferase encoded on the plasmid on 2, 4 and 10 days after transfection. It was observed that PEGylation of NPs showed improved luciferase activity (Figure 5.32). These results could be explained by considering reduced cytotoxicity (Figure 5.34) as compare to the non-PEGylated NPs as well as improved cellular uptake of NPs (Figure 5.35). It has been reported that entry of PEGylated

particles followed clathrin-independent endocytosis pathway (73). Thus, apart from electrostatic interactions with negatively charged cell membrane due to presence of PEI PEGylated particles also followed clathrin-independent endocytosis pathway which help in improved cellular uptake of particles. Additionally, being a hydrophilic molecule (both PEI and PEG) mounted at the NPs surface, they accelerate NPs degradation of PLGA NPS by inducing hydration. Following hydration, NPs releases PEI/pDNA complex (99), and promote intact transport of PEI/pDNA complexes towards the nuclei (100). PEI is one of a few polycations that has a high transfection potential due to its intrinsic endosomolytic activity caused by high buffer capacity. The efficient gene transduction ability of PEI proceeds via the proton sponge effect, implying that the primary amines buffer the protons being pumped into the lysosomal compartment by the v-ATPase (proton pump). This results in heightened pump activity, leading to the accumulation of a Cl^- ion and a water molecule for each proton that is retained; ultimately, this leads to osmotic rupture of the endosome and delivering the particles to the cytosol (102, 103). PEG could serve a variety of functions such as to reduce aggregation and aid in diffusion of the particles. Also it was reported that PEGylation of therapeutic colloids improve their cytoplasmic transport (once the particles have escaped endosomal vesicles) by minimizing attractive forces to cytoskeletal elements, such as microtubules or actin filaments, or to other intracellular organelles (74) thus helpful to deliver pDNA to nucleus.

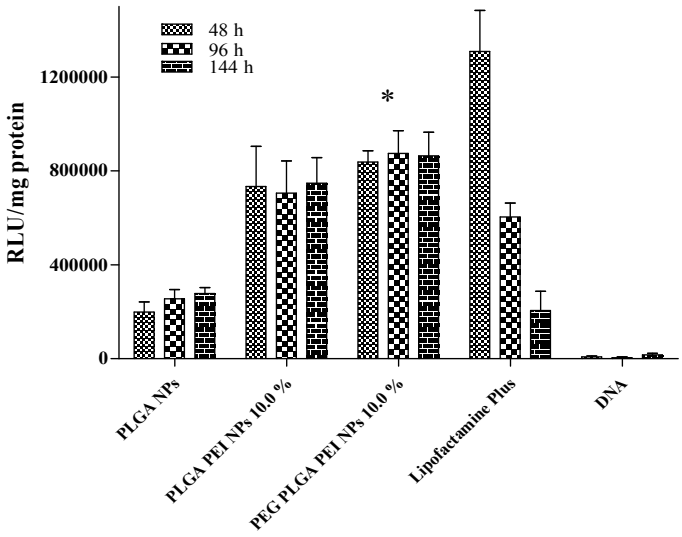

Figure 5.32: Transfection of CFBE cells treated with NPs encapsulating pCDNA-3 LUC-WT plasmid along with large T antigen and normalized to total protein content. Particle formulations

contained PLGA NPs, PEI-PLGA 10 % and PEG-PEI-PLGA 10 %. Transfection efficiencies were compared to Lipofectamine plus (prepared according to the manufacturer's instructions) as a positive control and pDNA as a negative control.

5.4.2.6.3.2 Western blot analysis

Results of luciferase expression were further confirmed with western blot analysis. Fluorescence spectroscopy and western blotting assays were performed to estimate efficiency of the NPs to transfer pDNA into CFBE 41o- cells, which transiently express CFTR after transfection. After 144 h expression of GFP (Figure 5.33) was observed under confocal microscope (Carl Zeiss, Confocol LSM 510 META, 20×) and then cells were used for western blot analysis. WT-CFBE cells were used as positive control. The western blot analysis showed that the monoclonal antibody directed against the C-terminal of the CFTR protein detected two bands: one band around 170 kDa corresponded to the fully processed and fully glycosylated form of CFTR; another band at about 150 kDa referred to the immature, core-glycosylated form of CFTR that is retained in the endoplasmic reticulum (ER) or in an intermediate ER-associated compartment (104, 105). While sodium potassium ATPase was used as internal control. The most intense signals were reported with a PEG PEI-PLGA NPs (10%) followed by PEI-PLGA NPs (10%), PLGA NPs, Lipofectamine plus. Absence of any CFTR band in cells treated with DNA (Figure 5.31 F2; Lane 1) only indicated the need of the delivery vector. The Western blot observations shows similar results when correlated with the GFP expression. Highest GFP expression was obtained with PEG PEI-PLGA NPs (10%) (Figure 5.33 D).

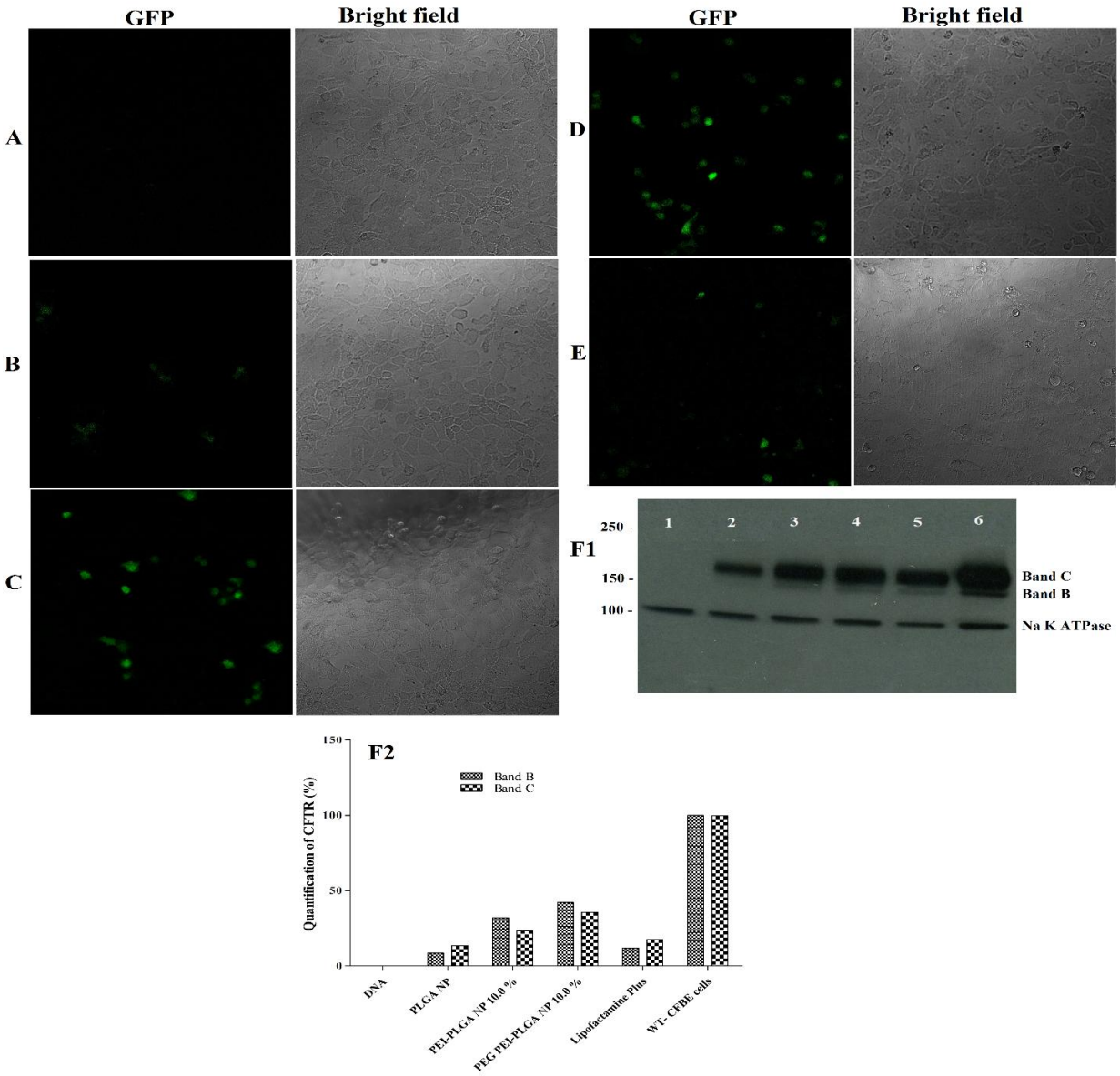

Figure 5.33: Fluorescence image of GFP expressing cells 144 h after cells were treated with NPs that had been loaded with pIRES2-EGFP-CFTR cDNA. A) cells treated with DNA alone; B) cells treated with PLGA NPs; C) cells treated with PEI-PLGA NPs (10%); D) cells treated with PEG-PEI-PLGA NPs (10%); E) cells treated with Lipofectamine plus; F1) CFTR expression 144 h after transfection of CFBE 41o- cells with different NPs. Lane 1: cells treated with DNA; Lane 2: cells treated with PLGA NPs; Lane 3: cells treated with PEI-PLGA NPs (10%); Lane 4: cells treated with PEG-PEI-PLGA NPs (10%); Lane 5: cells treated with Lipofectamine plus; Lane 6: WT- CFBE cells (positive control), band C corresponds to mature, complex-glycosylated CFTR,

whereas band B corresponds to core-glycosylated CFTR. Na-K ATPase alpha subunit serves as an internal control; F2): Quantification of immunoblots by densitometry by monitoring the relative amounts of bands C and B normalized to the background and the WT- CFBE cells control. The optical density of all the bands and background were measured, and then the two bands for WT-CFBE cells were designated 100% and the background as 0%. The percentage for each band is then calculated separately.

5.4.2.6.4 Cell viability & TEER analysis

It was observed that PEGylation significantly reduces toxicity of the particles. The reduced surface charge further reduces the toxicity of the particles significantly (Figure 5.34 A). PEG shield the particle surface, reduces surface charge thus improve the cell tolerance. Further it was confirmed from TEER analysis on cells under liquid/liquid culture conditions (Figure 5.34 B). The presence of an intact cell monolayer was confirmed by steady TEER values (450−500 Ωcm^2) after 3 days of culturing and the monolayer was visible by light microscopy. After exposure to the NPs, TEER was measured at a defined time interval for 5 days. TEER depends on tight junctions between cells, which can be disrupted by noxious stimuli (70) and therefore provides a convenient measure of barrier function (71). Incubation of monolayers with PEI-PLGA NPs at a concentration of 1 mg/mL, which was shown to yield at least ~70% cell viability, did alter the resistance of the epithelial layer. This was confirmed by the progressive decrease in TEER value over the period of time with significant difference between PEG-PEI PLGA NPs and control cells ($p=0.011$; $p < 0.05$ & $p=0.027$; $p< 0.05$ for cells &PEG-PEI PLGA NPs respectively) (Figure 5.34 B). While there was no significant difference in TEER value of cells and PEG-PEI PLGA. Taken together, these results suggest that the PEGylated NPs do not interfere with the integrity of the airway epithelial cells *in vitro* and may not have toxicity effect when used *in vivo* to treat lung disorders.

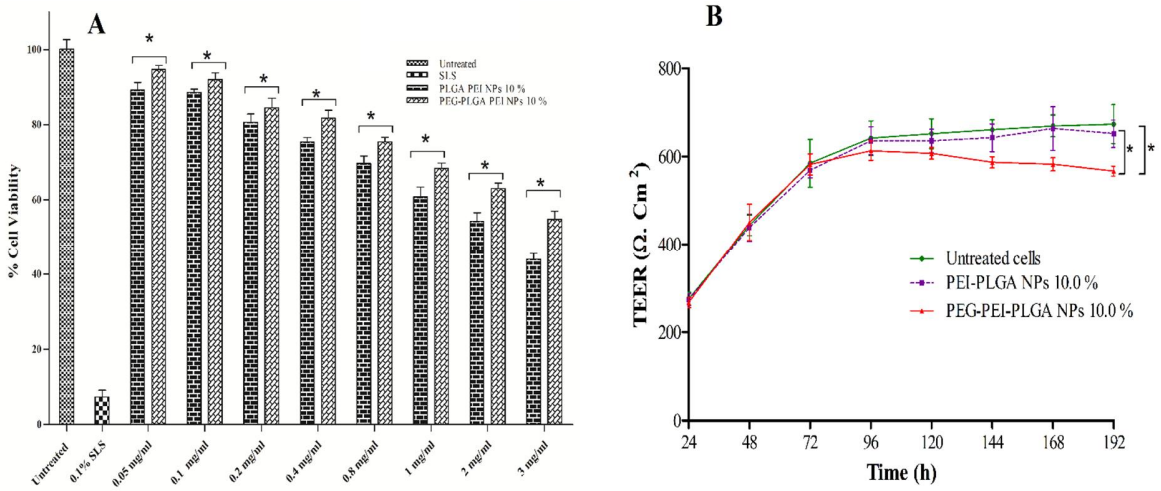

Figure 5.34: A) Effects of PEI-PLGA NPs 10% & PEG-PEI-PLGA NPs 10% formulations on viability of CFBE 41o- cells after 24 h incubation Test samples contained 0.05 mg/mL, 0.1 mg/mL, 02 mg/mL, 0.4 mg/mL, 0.8 mg/mL, 1 mg/mL, 2 mg/mL and 3 mg/mL of formulation. Data represent mean ± SD, n =6; (* results are significantly different from other treatment groups, $p < 0.05$) **B)** TEER analysis of CFBE 41o- cells layers exposed to NPs over time. We observed that there is a significant difference in TEER when using the PEI-PLGA NPs ($p=0.011$; $p < 0.05$ & $p=0.027$; $p< 0.05$ against untreated cells and PEG-PEI-PLGA NPs respectively). The results of MTT & TEER study suggest the safe use of developed PEGylated NPs system.

5.4.2.6.5 Cell uptake study

6-coumarin loaded NPs used to assess cellular association and uptake of NPs (Figure 5.35). Both PEGylated and non-PEGylated NPs showed cell uptake, as revealed by fluorescence microscopy. PEI-PLGA NPs shows significantly higher cell uptake than PLGA NPs. This observation was further confirmed by the quantitative fluorescence spectrophotometric analysis (Figure 5.35 D). The uptake of PEI-PLGA NPs in the cells was significantly higher than PLGA NPs ($P= 0.001$; $P <0.05$). The presence of PEI on NPs surface imparts a positive charge to the NPs, which helps in the electrostatic interaction with the negatively charged cell membrane thus promote their uptake. Further PEGylation of these particles again improved their uptake ($P<0.05$; $P=0.003$ against PEI-PLGA NPs & PEG PEI-PLGA NPs; $P=0.001$ against PLGA NPs & PEG PEI-PLGA NPs). Though presence of PEI shows enhanced uptake but their cell uptake is limited as serum proteins (particularly albumin) bind with PEI prior to cell uptake which abrogate the uptake of NPs (78).Addition of PEG in NPs preparation gives a significant advantage in shielding the NPs

from adsorption of proteins (79). This promote the uptake of the PEGylated NPs. PEG could also serve a variety of functions such as to reduced aggregation and aid in diffusion of the particles. This promotes interactions with the cell membrane and thus improve cell uptake. These findings are in concert with results of previous studies. Suh et al (74) also reported that the PEGylation increases average NPs diffusivities by 100% compared to nonPEGylated particles. They hypothesized that PEGylation of therapeutic colloids improve their cytoplasmic transport (once the particles have escaped endosomal vesicles) by minimizing attractive forces to cytoskeletal elements, such as microtubules or actin filaments, or to other intracellular organelles.

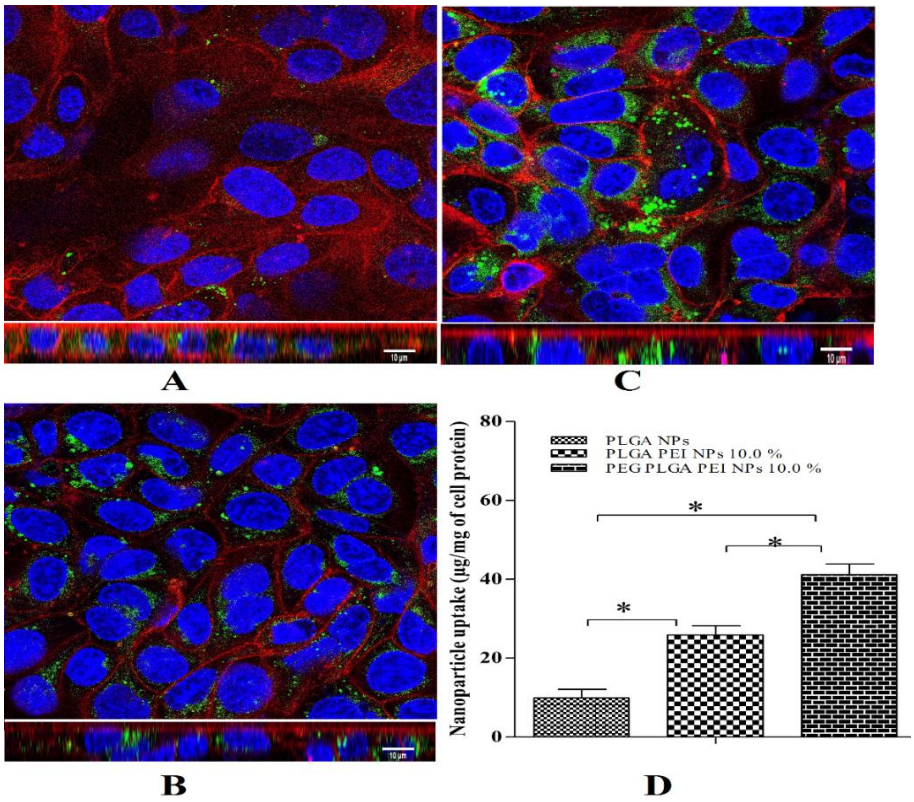

Figure 5.35: Confocal microscopy of CFBE cells (63X) after 24 hours of incubation with 6-coumarin loaded NPs: A) PLGA NPs; B) PEI PLGA NPs (10%); C) PEG PEI PLGA NPs (10%); Cells were treated with 6-coumarin loaded NPs (green), fixed and nucleus stained with Hoechst dye & cell membrane with FM® 4-64 membrane stain. Top images represent slices from the middle of a z-stack of a CFBE cells. Bottom images are projections in the z-axis created from a z-stack of the same CFBE cells displayed in the top image; D) The NPs uptake in CFBE cells (n = 9). *Significant difference; $P < 0.05$. A more efficient NP uptake is apparent for PEGylated NPs as compared to non-PEGylated NPs.

5.4.2.6.6 DNAse protection assay

Efficiency of NPs to protect encapsulated pDNA against nuclease digestion was evaluated by exposing them to DNAse I followed by agarose gel electrophoresis (Figure 5.36). It was observed that naked plasmid DNA (lane 3) was completely digested within 5 min of incubation, while DNA encapsulated in NPs (lane 4-6) remained intact up to 4 h when incubated with DNAse I (Figure 5.36).When compared with controlled pDNA, pDNA extracted from NPs doesn't showed any degradation while naked DNA was completely degraded, which shows the efficiency of the encapsulation process against the degradation effect of the enzyme. Thus Hydrophobic PLGA matrix can be served as an effective protection layer to encapsulated pDNA when administered in-vivo from protein and enzyme.

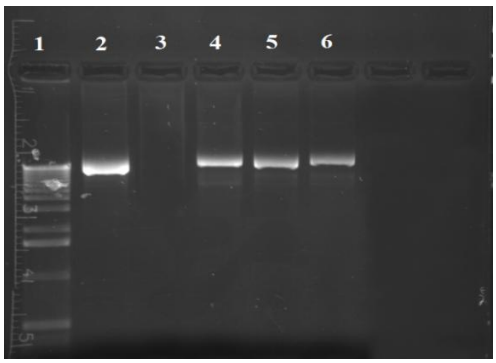

Figure 5.36: Agarose gel electrophoresis of plasmid DNA extracted from particles after treatment with DNase I. Lane 1: marker DNA; Lane 2: control non-treated pDNA; lane 3: naked pDNA after incubation with DNase I; Lane 4: pDNA encapsulated in PLGA NPs; Lane 5: pDNA encapsulated in PEI-PLGA NPs; Lane 4: pDNA encapsulated in PEG PEI-PLGA NPs; after incubation with DNase I for 4 h.

5.4.2.6.7 Mucus penetration study

To assess how the composition of the formulation affected NP diffusion through lung lining fluids, the amount of 6-Coumarin permeated through an artificial mucus layer after 8, 12, and 24 h of release from fluorescent NPs was assessed. As can be seen in Figure 5.37 a higher percent of 6-Coumarin was found in gelatin when PEG-modified NPs were deposited on the mucus layer as compared to non PEGylated NPs. Mucus is mainly comprised of mucin. Mucin fibers form a network with a mesh spacing size of 30-100 nm which can physically entrap any foreign

particulates that exceed this low spacing cut-off (64). The mucus barrier poses a serious obstacle that prevents the penetration of therapeutics across epithelial lining.

Studies shows that particulates as small as 30-60nm can diffuse across mucus matrices (65), however particles above 100 nm in size exhibit retarded diffusivity in mucus (106). Diffusivity of these particles can be improved by increasing the residence time of the NPs in the tightly packed layer of mucus (107). The surface chemistry of the NPs plays a crucial role since mucus could bind various surfaces that come in contact with it by either lipophilic or hydrophilic interactions (66). Consequently, NPs with cationic termini are more likely to adhere to the mucus layer retarding its diffusion (108). Negatively charged NPs however can also be problematic as they can be electrostatically repelled by the anionic barrier which could explain the retarded diffusion of some negatively charged NPs (67). Uncharged or neutral NPs on the other hand could be highly hydrophobic, which causes considerable hydrophobic interactions and retardation in the mucus in the same fashion as with different bacteria (68).

Quantitative data were supported by visual inspection of the well plates is shown in Figure 5.37, indicating that 6-Coumarin loaded PEGylated NPs diffused faster through mucus. This could be explained by surface charge present on the NPs. Non PEGylated NPs can electrostatically interact with the anionic barrier of mucin due to presence of positive surface charge which retard their diffusion through the mucus. While PEGylation of NPs reduces their electrostatic interaction with mucin but promote formation of hydrogen bonding with mucin thus promote their diffusion through mucus (69, 109).

Taken together, these results suggest the great potential of the PEGylated NPs to act in vivo as a drug reservoir which slowly releases the active agent to the target to have a prolonged therapeutic effect. Further-more, according to therapeutic requirements, NP composition can also be considered a useful means by which pDNA release rate, activity and NP interactions with mucus can be tuned.

Nonetheless, NPs will be released in vivo in the lung mucus, which will prevent them from reaching the target and affect NP therapeutic potential. Thus, the assessment of mucoadhesive properties of the NPs is also fundamental to the development of clinically -relevant gene delivery systems for treatment of cystic fibrosis.

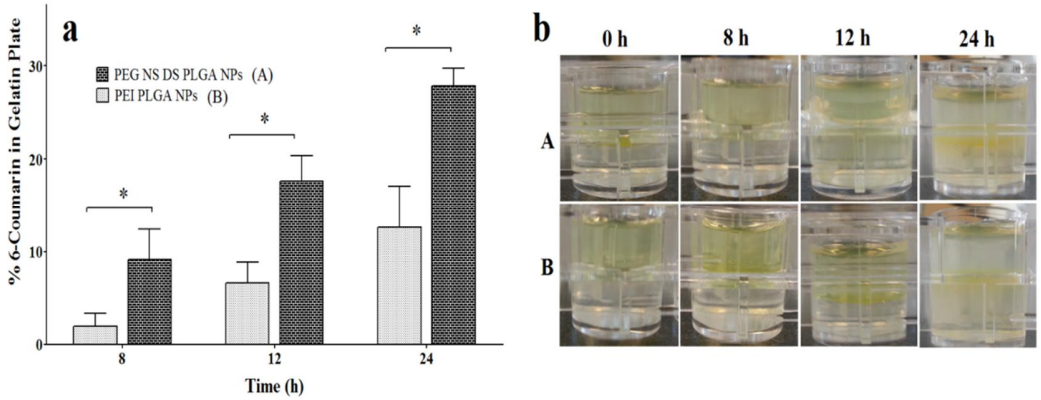

Figure 5.37: a) Percent amount of 6-coumarin permeated in the gelatin layer after 0, 8, 12, 24 h. Data are mean ± SD (n = 3); b) visual inspection of NP penetration through an artificial mucus layer (representative image at 8, 12, 24 h). A: PEG PEI PLGA NPs; B: PEI PLGA NPs *Significant difference; $P < 0.05$

5.4.2.9 Stability study

The stability of NPs was assessed by suspension in 0.9 % saline simulated lung fluid & 10% fetal bovine serum by evaluating particle size measurements at fixed time intervals. The PEI PLGA NPs showed increased particle size over the period of time (Figure 5.38). The enhanced particle size is due to the flocculation effect induced by ions present in the solutions. However serum proteins (particularly albumin) bind with surface PEI of NPs which is also responsible for enhanced particles size when incubated with serum. The resulted aggregates limits their cell uptake (78). Addition of PEG in NPs preparation gives a significant advantage in shielding the NPs from adsorption of proteins (79). DLS sizing measurements demonstrate that the PEG PEI PLGA NPs remain stable over 48 h with no significant change in size (Figure 5.38). This result suggests that the DSPE–PEG 2000–COOH density on the NPs does not drop below the range of full electrostatic and steric stabilizations over the time period. It could be that the DSPE–PEG covalent bond in PEGylated lipid molecules is very stable and the PEG group is not hydrolyzed off, or that the lipid monolayer does not peel off over 48 h. Thus, the NPs prepared in this study should remain stable in vitro for relatively long periods. This result suggests that the current formulation has sufficient stability derived from steric repulsion due to the PEG chain (80-82). Based on this study, PEI PLGA NPs are less favorable for pulmonary administration as their instability in media may lead to reduced therapeutic efficacy due to faster clearance from the lung.

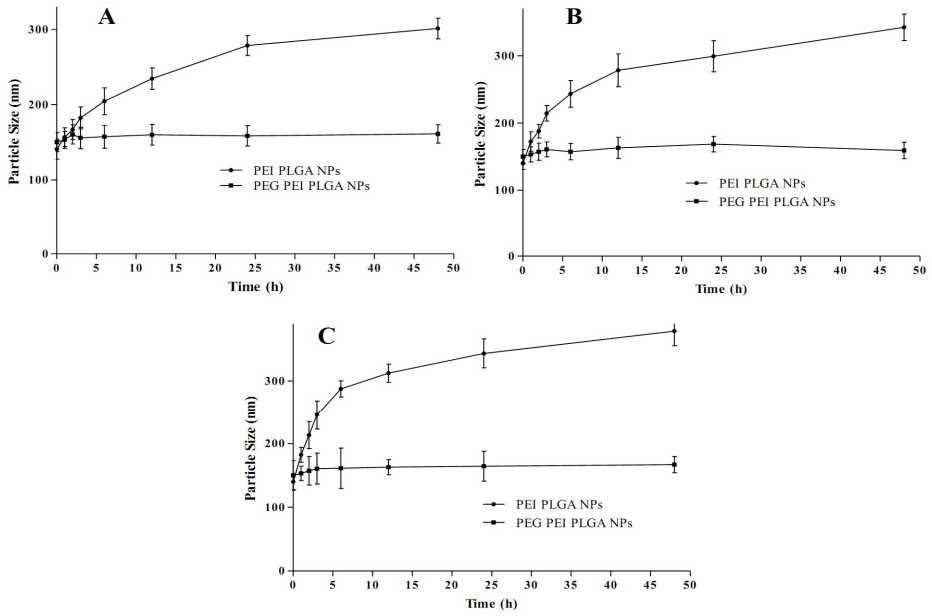

Figure 5.38: Stability of NPs was tested by measuring particle size in (A) saline solution; (B) simulated lung fluid at 37 ^{o}C; (C) 10% fetal bovine serum. The PEGylated NPs remained stable for up to 2 days while non PEGylated NPs tended to show aggregation, indicating comparatively less stability. Data are shown as mean ± SD (n = 3)

From the all results obtained, it is observed that PEGylated NPs system in most promising delivery system hence, it will be used for further studies.

5.5 Conclusion

PLGA nanoparticles were successfully developed and optimized for maximum entrapment efficiency as it was one of the major challenges for development of NPs of highly hydrophilic therapeutics like netilmicin sulfate (NS) and pDNA. In case of NS loaded NPs, EE was improved due to formation of drug- dextran sulfate complex and it subsequently lead to sustained drug release with improved antibacterial activity. Further incorporation of PEG results in improved cell viability as well as better penetration of the NPs through mucus. Also improved cell uptake will be benefitted to treat intracellular bacterial infections in CF. In case of pDNA loaded NPs, interaction between PEI and PLGA helped to encapsulate pDNA for its sustained delivery. Sustained release of pDNA was might be due to electrostatic interaction between PEI and pDNA. Blending of PEI with the PLGA matrix also resulted into increased transfection efficiency of pDNA. Moreover,

incorporation of PEG to PEI-PLGA NPs emerged as the most promising vector for transfection in CFBE41o– cells. However it was observed that the incorporation of PEG enable a greater influx of water into the NPs matrix, accelerate PLGA hydrolysis and thus promoting greater degradation of PLGA and improved DNA release from NPs. Qualitative and quantitative studies showed that uptake of PEI-PLGA NPs was significantly higher than that of PLGA NPs. pDNA extracted from NPs did not show any degradation while naked DNA was completely degraded against DNAse enzyme which proved the importance of delivery vehicle. It was observed that PEGylated formulations were stable in pulmonary fluids and can be used effectively for pulmonary administration.

5.6 References

1. Jenkins RG, McAnulty RJ, Hart SL, Laurent GJ. Pulmonary gene therapy. Realistic hope for the future, or false dawn in the promised land? Monaldi archives for chest disease, Universita di Napoli, Secondo ateneo. 2003;59(1):17-24.
2. Griesenbach U, Alton EW. Progress in gene and cell therapy for cystic fibrosis lung disease. Current pharmaceutical design. 2012;18(5):642-62.
3. Factor P. Gene therapy for asthma. Molecular therapy. 2003;7(2):148-52.
4. Moon C, Oh Y, Roth JA. Current status of gene therapy for lung cancer and head and neck cancer. Clinical cancer research. 2003;9(14):5055-67.
5. Pouton CW, Seymour LW. Key issues in non-viral gene delivery. Advanced drug delivery reviews. 2001;46(1-3):187-203.
6. De Smedt SC, Demeester J, Hennink WE. Cationic polymer based gene delivery systems. Pharmaceutical research. 2000;17(2):113-26.
7. Kumari A, Yadav SK, Yadav SC. Biodegradable polymeric nanoparticles based drug delivery systems. Colloids and surfaces B, Biointerfaces. 2010;75(1):1-18.
8. Mundargi RC, Babu VR, Rangaswamy V, Patel P, Aminabhavi TM. Nano/micro technologies for delivering macromolecular therapeutics using poly(D,L-lactide-co-glycolide) and its derivatives. Journal of controlled release. 2008;125(3):193-209.
9. Okada H. One- and three-month release injectable microspheres of the LH-RH superagonist leuprorelin acetate. Advanced drug delivery reviews. 1997;28(1):43-70.

10. Qaddoumi MG, Ueda H, Yang J, Davda J, Labhasetwar V, Lee VH. The characteristics and mechanisms of uptake of PLGA nanoparticles in rabbit conjunctival epithelial cell layers. Pharmaceutical research. 2004;21(4):641-8.
11. Cartiera MS, Johnson KM, Rajendran V, Caplan MJ, Saltzman WM. The uptake and intracellular fate of PLGA nanoparticles in epithelial cells.Biomaterials.2009;30(14):2790-8.
12. Danhier F, Ansorena E, Silva JM, Coco R, Le Breton A, Preat V. PLGA-based nanoparticles: an overview of biomedical applications. Journal of controlled release. 2012;161(2):505-22.
13. Barichello JM, Morishita M, Takayama K, Nagai T. Encapsulation of hydrophilic and lipophilic drugs in PLGA nanoparticles by the nanoprecipitation method. Drug development and industrial pharmacy. 1999;25(4):471-6.
14. Saxena V, Sadoqi M, Shao J. Indocyanine green-loaded biodegradable nanoparticles: preparation, physicochemical characterization and in vitro release. International journal of pharmaceutics. 2004;278(2):293-301.
15. Tewes F, Munnier E, Antoon B, Ngaboni Okassa L, Cohen-Jonathan S, Marchais H, et al. Comparative study of doxorubicin-loaded poly(lactide-co-glycolide) nanoparticles prepared by single and double emulsion methods. European journal of pharmaceutics and biopharmaceutics. 2007;66(3):488-92.
16. Lecaroz MC, Blanco-Prieto MJ, Campanero MA, Salman H, Gamazo C. Poly(D,L-lactide-coglycolide) particles containing gentamicin: pharmacokinetics and pharmacodynamics in Brucella melitensis-infected mice. Antimicrobial agents and chemotherapy. 2007;51(4):1185-90.
17. Gao H, Jones M-C, Chen J, Liang Y, Prud'homme RE, Leroux J-C. Hydrophilic Nanoreservoirs Embedded into Polymeric Micro/Nanoparticles: An Approach To Compatibilize Polar Molecules with Hydrophobic Matrixes. Chemistry of Materials. 2008;20(13):4191-3.
18. Yu C, Hu Y, Duan J, Yuan W, Wang C, Xu H, et al. Novel aptamer-nanoparticle bioconjugates enhances delivery of anticancer drug to MUC1-positive cancer cells in vitro. PloS one. 2011;6(9):e24077.
19. Cu Y, Booth CJ, Saltzman WM. In vivo distribution of surface-modified PLGA nanoparticles following intravaginal delivery. Journal of controlled release. 2011;156(2):258-64.

20. Nie H, Khew ST, Lee LY, Poh KL, Tong YW, Wang CH. Lysine-based peptide-functionalized PLGA foams for controlled DNA delivery. Journal of controlled release. 2009;138(1):64-70.
21. Bertram JP, Jay SM, Hynes SR, Robinson R, Criscione JM, Lavik EB. Functionalized poly(lactic-co-glycolic acid) enhances drug delivery and provides chemical moieties for surface engineering while preserving biocompatibility.Acta biomaterialia.2009;5(8):2860-71.
22. Fahmy TM, Samstein RM, Harness CC, Mark Saltzman W. Surface modification of biodegradable polyesters with fatty acid conjugates for improved drug targeting. Biomaterials. 2005;26(28):5727-36.
23. Cu Y, LeMoellic C, Caplan MJ, Saltzman WM. Ligand-modified gene carriers increased uptake in target cells but reduced DNA release and transfection efficiency. Nanomedicine : nanotechnology, biology, and medicine. 2010;6(2):334-43.
24. Cheng CJ, Saltzman WM. Enhanced siRNA delivery into cells by exploiting the synergy between targeting ligands and cell-penetrating peptides.Biomaterials.2011;32(26):6194-203.
25. Prayle A, Smyth AR. Aminoglycoside use in cystic fibrosis: therapeutic strategies and toxicity. Current opinion in pulmonary medicine. 2010;16(6):604-10.
26. Karlowsky JA, Zhanel GG, Davidson RJ, Hoban DJ. Postantibiotic effect in Pseudomonas aeruginosa following single and multiple aminoglycoside exposures in vitro. The Journal of antimicrobial chemotherapy. 1994;33(5):937-47.
27. Kuhn RJ. Formulation of aerosolized therapeutics. Chest. 2001;120(3 Suppl):94S-8S.
28. Honeybourne D. Antibiotic penetration into lung tissues. Thorax. 1994 49(2):104-6.
29. Ratjen F, Brockhaus F, Angyalosi G. Aminoglycoside therapy against Pseudomonas aeruginosa in cystic fibrosis: a review. Journal of cystic fibrosis. 2009;8(6):361-9.
30. Forge A, Schacht J. Aminoglycoside antibiotics. Audiology & neuro-otology.2000;5(1):3-22.
31. Montier T, Delepine P, Pichon C, Ferec C, Porteous DJ, Midoux P. Non-viral vectors in cystic fibrosis gene therapy: progress and challenges. Trends in biotechnology. 2004;22(11):586-92.

32. Sanders NN, De Smedt SC, Van Rompaey E, Simoens P, De Baets F, Demeester J. Cystic fibrosis sputum: a barrier to the transport of nanospheres. American journal of respiratory and critical care medicine. 2000;162(5):1905-11.
33. Suk JS, Lai SK, Wang YY, Ensign LM, Zeitlin PL, Boyle MP, et al. The penetration of fresh undiluted sputum expectorated by cystic fibrosis patients by non-adhesive polymer nanoparticles. Biomaterials. 2009;30(13):2591-7.
34. Cohen H, Levy RJ, Gao J, Fishbein I, Kousaev V, Sosnowski S, et al. Sustained delivery and expression of DNA encapsulated in polymeric nanoparticles. Gene therapy. 2000;7(22):1896-905.
35. Luten J, van Nostrum CF, De Smedt SC, Hennink WE. Biodegradable polymers as non-viral carriers for plasmid DNA delivery. Journal of controlled release. 2008;126(2):97-110.
36. Gao P, Nie X, Zou M, Shi Y, Cheng G. Recent advances in materials for extended-release antibiotic delivery system. The Journal of antibiotics. 2011;64(9):625-34.
37. Abdelghany SM, Quinn DJ, Ingram RJ, Gilmore BF, Donnelly RF, Taggart CC, et al. Gentamicin-loaded nanoparticles show improved antimicrobial effects towards Pseudomonas aeruginosa infection. International journal of nanomedicine. 2012;7:4053-63.
38. Asadi A. Streptomycin-loaded PLGA-alginate nanoparticles: preparation, characterization, and assessment. Appl Nanosci. 2013:1-6.
39. Bilati U, Allemann E, Doelker E. Poly(D,L-lactide-co-glycolide) protein-loaded nanoparticles prepared by the double emulsion method--processing and formulation issues for enhanced entrapment efficiency. Journal of microencapsulation. 2005;22(2):205-14.
40. Diaz-Lopez R, Tsapis N, Santin M, Bridal SL, Nicolas V, Jaillard D, et al. The performance of PEGylated nanocapsules of perfluorooctyl bromide as an ultrasound contrast agent. Biomaterials. 2010;31(7):1723-31.
41. Moss OR. Simulants of lung interstitial fluid. Health Phys 1979;36:447– 8.
42. Wikler MA. Methods for dilution antimicrobial susceptibility tests for bacteria that grow aerobically - Approved Standard. 8th ed: Clinical and Laboratory Standards Institute (CLSI); 2008.
43. Yang Y, Tsifansky MD, Shin S, Lin Q, Yeo Y. Mannitol-guided delivery of Ciprofloxacin in artificial cystic fibrosis mucus model. Biotechnology and bioengineering. 2011;108(6):1441-9.

44. Marini J. Physiological Basis of Ventilatory Support. 1 ed: Informa Healthcare; 1998.
45. Lu E, Franzblau S, Onyuksel H, Popescu C. Preparation of aminoglycoside-loaded chitosan nanoparticles using dextran sulphate as a counterion. Journal of microencapsulation. 2009;26(4):346-54.
46. Li Y, Wong HL, Shuhendler AJ, Rauth AM, Wu XY. Molecular interactions, internal structure and drug release kinetics of rationally developed polymer-lipid hybrid nanoparticles. Journal of controlled release : official journal of the Controlled Release Society. 2008;128(1):60-70.
47. Wong HL, Bendayan R, Rauth AM, Wu XY. Simultaneous delivery of doxorubicin and GG918 (Elacridar) by new polymer-lipid hybrid nanoparticles (PLN) for enhanced treatment of multidrug-resistant breast cancer. Journal of controlled release. 2006;116(3):275-84.
48. Wang Y, Wang R, Lu X, Lu W, Zhang C, Liang W. Pegylated phospholipids-based self-assembly with water-soluble drugs. Pharmaceutical research. 2010;27(2):361-70.
49. Li Y, Taulier N, Rauth AM, Wu XY. Screening of lipid carriers and characterization of drug-polymer-lipid interactions for the rational design of polymer-lipid hybrid nanoparticles (PLN). Pharmaceutical research. 2006;23(8):1877-87.
50. Song X, Zhao Y, Hou S, Xu F, Zhao R, He J, et al. Dual agents loaded PLGA nanoparticles: systematic study of particle size and drug entrapment efficiency. European journal of pharmaceutics and biopharmaceutics. 2008;69(2):445-53.
51. Song X, Zhao Y, Wu W, Bi Y, Cai Z, Chen Q, et al. PLGA nanoparticles simultaneously loaded with vincristine sulfate and verapamil hydrochloride: systematic study of particle size and drug entrapment efficiency. International journal of pharmaceutics. 2008;350(1-2):320-9.
52. Lalani J, Rathi M, Lalan M, Misra A. Protein functionalized tramadol-loaded PLGA nanoparticles: preparation, optimization, stability and pharmacodynamic studies. Drug development and industrial pharmacy. 2013;39(6):854-64.
53. Jeffery H, Davis SS, O'Hagan DT. The preparation and characterization of poly(lactide-co-glycolide) microparticles. II. The entrapment of a model protein using a (water-in-oil)-in-water emulsion solvent evaporation technique. Pharmaceutical research. 1993;10(3):362-8.

54. Ito F, Fujimori H, Makino K. Factors affecting the loading efficiency of water-soluble drugs in PLGA microspheres. Colloids and surfaces B, Biointerfaces. 2008;61(1):25-9.
55. Blanco D, Alonso MJ. Protein encapsulation and release from poly(lactide-co-glycolide) microspheres: effect of the protein and polymer properties and of the co-encapsulation of surfactants. European journal of pharmaceutics and biopharmaceutics. 1998;45(3):285-94.
56. Calvo P, Alonso MJ, Vila-Jato JL, Robinson JR. Improved ocular bioavailability of indomethacin by novel ocular drug carriers. The Journal of pharmacy and pharmacology. 1996;48(11):1147-52.
57. Feng S, Huang G. Effects of emulsifiers on the controlled release of paclitaxel (Taxol) from nanospheres of biodegradable polymers. Journal of controlled release. 2001;71(1):53-69.
58. Musumeci T, Ventura CA, Giannone I, Ruozi B, Montenegro L, Pignatello R, et al. PLA/PLGA nanoparticles for sustained release of docetaxel. International journal of pharmaceutics. 2006;325(1-2):172-9.
59. Gupta H, Aqil M, Khar RK, Ali A, Bhatnagar A, Mittal G. Sparfloxacin-loaded PLGA nanoparticles for sustained ocular drug delivery. Nanomedicine : nanotechnology, biology, and medicine. 2010;6(2):324-33.
60. Ng AW, Bidani A, Heming TA. Innate host defense of the lung: effects of lung-lining fluid pH. Lung. 2004;182(5):297-317.
61. Costa P, Sousa Lobo JM. Modeling and comparison of dissolution profiles. European journal of pharmaceutical sciences. 2001;13(2):123-33.
62. Peppas NA. Analysis of Fickian and non-Fickian drug release from polymers. Pharmaceutica acta Helvetiae. 1985;60(4):110-1.
63. Knowles MR, Robinson JM, Wood RE, Pue CA, Mentz WM, Wager GC, et al. Ion composition of airway surface liquid of patients with cystic fibrosis as compared with normal and disease-control subjects. The Journal of clinical investigation. 1997;100(10):2588-95.
64. Knowles MR, Boucher RC. Mucus clearance as a primary innate defense mechanism for mammalian airways. J Clin Invest. 2002;109(5):571-7.
65. Saltzman WM, Radomsky ML, Whaley KJ, Cone RA. Antibody diffusion in human cervical mucus. Biophysical journal. 1994;66(2 Pt 1):508-15.

66. Brayshaw DJ, Berry M, McMaster TJ. Optimisation of sample preparation methods for air imaging of ocular mucins by AFM. Ultramicroscopy. 2003;97(1-4):289-96.
67. Kas HS. Chitosan: properties, preparations and application to microparticulate systems. Journal of microencapsulation. 1997;14(6):689-711.
68. Mantle M, Basaraba L, Peacock SC, Gall DG. Binding of Yersinia enterocolitica to rabbit intestinal brush border membranes, mucus, and mucin. Infection and immunity. 1989;57(11):3292-9.
69. Efremova NV, Huang Y, Peppas NA, Leckband DE. Direct Measurement of Interactions between Tethered Poly(ethylene glycol) Chains and Adsorbed Mucin Layers. Langmuir. 2002;18(3):836-45.
70. Kapus A, Szaszi K. Coupling between apical and paracellular transport processes. Biochemistry and cell biology. 2006;84(6):870-80.
71. Florea BI, Cassara ML, Junginger HE, Borchard G. Drug transport and metabolism characteristics of the human airway epithelial cell line Calu-3. Journal of controlled release. 2003;87(1-3):131-8.
72. Fiegel J, Ehrhardt C, Schaefer UF, Lehr CM, Hanes J. Large porous particle impingement on lung epithelial cell monolayers--toward improved particle characterization in the lung. Pharmaceutical research. 2003;20(5):788-96.
73. Ibricevic A, Guntsen SP, Zhang K, Shrestha R, Liu Y, Sun JY, et al. PEGylation of cationic, shell-crosslinked-knedel-like nanoparticles modulates inflammation and enhances cellular uptake in the lung. Nanomedicine : nanotechnology, biology, and medicine. 2013;9(7):912-22.
74. Suh J, Choy KL, Lai SK, Suk JS, Tang BC, Prabhu S, et al. PEGylation of nanoparticles improves their cytoplasmic transport. International journal of nanomedicine. 2007;2(4):735-41.
75. Sadzuka Y, Kishi K, Hirota S, Sonobe T. Effect of polyethyleneglycol (PEG) chain on cell uptake of PEG-modified liposomes. Journal of liposome research. 2003;13(2):157-72.
76. Griesenbach U, Alton EW. Gene transfer to the lung: lessons learned from more than 2 decades of CF gene therapy. Advanced drug delivery reviews. 2009;61(2):128-39.

77. Darling KE, Dewar A, Evans TJ. Role of the cystic fibrosis transmembrane conductance regulator in internalization of Pseudomonas aeruginosa by polarized respiratory epithelial cells. Cellular microbiology. 2004;6(6):521-33.
78. Forrest ML, Meister GE, Koerber JT, Pack DW. Partial acetylation of polyethylenimine enhances in vitro gene delivery. Pharmaceutical research. 2004;21(2):365-71.
79. Giri J, Diallo MS, Simpson AJ, Liu Y, Goddard WA, Kumar R, et al. Interactions of poly(amidoamine) dendrimers with human serum albumin: binding constants and mechanisms. ACS nano. 2011;5(5):3456-68.
80. Riley T, Govender T, Stolnik S, Xiong CD, Garnett MC, Illum L, et al. Colloidal stability and drug incorporation aspects of micellar-like PLA–PEG nanoparticles. Colloids and Surfaces B: Biointerfaces. 1999;16(1–4):147-59.
81. Chan JM, Zhang L, Yuet KP, Liao G, Rhee JW, Langer R, et al. PLGA-lecithin-PEG core-shell nanoparticles for controlled drug delivery. Biomaterials. 2009;30(8):1627-34.
82. Avgoustakis K, Beletsi A, Panagi Z, Klepetsanis P, Livaniou E, Evangelatos G, et al. Effect of copolymer composition on the physicochemical characteristics, in vitro stability, and biodistribution of PLGA-mPEG nanoparticles. International journal of pharmaceutics. 2003;259(1-2):115-27.
83. Rytting E, Nguyen J, Wang X, Kissel T. Biodegradable polymeric nanocarriers for pulmonary drug delivery. Expert opinion on drug delivery. 2008;5(6):629-39.
84. Tse MT, Blatchford C, Oya Alpar H. Evaluation of different buffers on plasmid DNA encapsulation into PLGA microparticles. International journal of pharmaceutics. 2009;370(1-2):33-40.
85. Nguyen DN, Raghavan SS, Tashima LM, Lin EC, Fredette SJ, Langer RS, et al. Enhancement of poly(orthoester) microspheres for DNA vaccine delivery by blending with poly(ethylenimine). Biomaterials. 2008;29(18):2783-93.
86. Kim IS, Lee SK, Park YM, Lee YB, Shin SC, Lee KC, et al. Physicochemical characterization of poly(L-lactic acid) and poly(D,L-lactide-co-glycolide) nanoparticles with polyethylenimine as gene delivery carrier. International journal of pharmaceutics. 2005;298(1):255-62.
87. Stolnik S, Garnett MC, Davies MC, Illum L, Bousta M, Vert M, et al. The colloidal properties of surfactant-free biodegradable nanospheres from poly(β-malic acid-co-benzyl

malate)s and poly(lactic acid-co-glycolide). Colloids and Surfaces A: Physicochemical and Engineering Aspects. 1995;97(3):235-45.

88. Croll TI, O'Connor AJ, Stevens GW, Cooper-White JJ. Controllable Surface Modification of Poly(lactic-co-glycolic acid) (PLGA) by Hydrolysis or Aminolysis I: Physical, Chemical, and Theoretical Aspects. Biomacromolecules. 2004;5(2):463-73.
89. Choosakoonkriang S, Lobo BA, Koe GS, Koe JG, Middaugh CR. Biophysical characterization of PEI/DNA complexes. Journal of pharmaceutical sciences. 2003;92(8):1710-22.
90. Chakravarthi SS, Robinson DH. Enhanced cellular association of paclitaxel delivered in chitosan-PLGA particles. International journal of pharmaceutics. 2011;409(1-2):111-20.
91. Wang C, Ge Q, Ting D, Nguyen D, Shen HR, Chen J, et al. Molecularly engineered poly(ortho ester) microspheres for enhanced delivery of DNA vaccines. Nature materials. 2004;3(3):190-6.
92. Yin Y, Chen D, Qiao M, Wei X, Hu H. Lectin-conjugated PLGA nanoparticles loaded with thymopentin: ex vivo bioadhesion and in vivo biodistribution. Journal of controlled release. 2007;123(1):27-38.
93. Zolnik BS, Burgess DJ. Effect of acidic pH on PLGA microsphere degradation and release. Journal of controlled release : official journal of the Controlled Release Society. 2007;122(3):338-44.
94. Oster CG, Kim N, Grode L, Barbu-Tudoran L, Schaper AK, Kaufmann SH, et al. Cationic microparticles consisting of poly(lactide-co-glycolide) and polyethylenimine as carriers systems for parental DNA vaccination. Journal of controlled release. 2005;104(2):359-77.
95. Boussif O, Lezoualc'h F, Zanta MA, Mergny MD, Scherman D, Demeneix B, et al. A versatile vector for gene and oligonucleotide transfer into cells in culture and in vivo: polyethylenimine. Proceedings of the National Academy of Sciences of the United States of America. 1995;92(16):7297-301.
96. Kasturi SP, Sachaphibulkij K, Roy K. Covalent conjugation of polyethyleneimine on biodegradable microparticles for delivery of plasmid DNA vaccines. Biomaterials. 2005;26(32):6375-85.
97. Hunter AC, Moghimi SM. Cationic carriers of genetic material and cell death: a mitochondrial tale. Biochimica et biophysica acta. 2010;1797(6-7):1203-9.

98. Wischke C, Borchert HH, Zimmermann J, Siebenbrodt I, Lorenzen DR. Stable cationic microparticles for enhanced model antigen delivery to dendritic cells. Journal of controlled release : official journal of the Controlled Release Society. 2006;114(3):359-68.
99. Messai I, Munier S, Ataman-Önal Y, Verrier B, Delair T. Elaboration of poly(ethyleneimine) coated poly(d,l-lactic acid) particles. Effect of ionic strength on the surface properties and DNA binding capabilities. Colloids and Surfaces B: Biointerfaces. 2003;32(4):293-305.
100. Drake DM, Pack DW. Biochemical investigation of active intracellular transport of polymeric gene-delivery vectors. Journal of pharmaceutical sciences. 2008;97(4):1399-413.
101. Kunath K, von Harpe A, Fischer D, Petersen H, Bickel U, Voigt K, et al. Low-molecular-weight polyethylenimine as a non-viral vector for DNA delivery: comparison of physicochemical properties, transfection efficiency and in vivo distribution with high-molecular-weight polyethylenimine. Journal of controlled release. 2003;89(1):113-25.
102. Kircheis R, Wightman L, Wagner E. Design and gene delivery activity of modified polyethylenimines. Advanced drug delivery reviews. 2001;53(3):341-58.
103. Xia T, Kovochich M, Liong M, Meng H, Kabehie S, George S, et al. Polyethyleneimine coating enhances the cellular uptake of mesoporous silica nanoparticles and allows safe delivery of siRNA and DNA constructs. ACS nano. 2009;3(10):3273-86.
104. Sampson HM, Robert R, Liao J, Matthes E, Carlile GW, Hanrahan JW, et al. Identification of a NBD1-binding pharmacological chaperone that corrects the trafficking defect of F508del-CFTR. Chemistry & biology. 2011;18(2):231-42.
105. Robert R, Carlile GW, Liao J, Balghi H, Lesimple P, Liu N, et al. Correction of the Delta phe508 cystic fibrosis transmembrane conductance regulator trafficking defect by the bioavailable compound glafenine. Molecular pharmacology. 2010;77(6):922-30.
106. Amsden B. Solute Diffusion within Hydrogels. Mechanisms and Models. Macromolecules. 1998;31(23):8382-95.
107. Woodley J. Bioadhesion: new possibilities for drug administration? Clinical pharmacokinetics. 2001;40(2):77-84.
108. Lelu S, Strand SP, Steine J, Davies Cde L. Effect of PEGylation on the diffusion and stability of chitosan-DNA polyplexes in collagen gels. Biomacromolecules. 2011;12(10):3656-65.

109. Suk J, Hanes JS, inventors; The Johns Hopkins University, assignee. Mucus penetrating gene carrier patent US 20130323313 A1.